Numerical analysis of the flow distribution within packed columns using an explicit approach

by
William George Joseph Theron

B.Eng. Mechanical (North-West University)

Student Number: 12900095

Dissertation submitted in partial fulfilment of the requirements for the degree
Master of Engineering in Nuclear Engineering
at the
School of Mechanical and Nuclear Engineering,
Potchefstroom Campus of the North-West University, South Africa.

Supervisor: Prof. C.G. du Toit

Potchefstroom

2011

Innovation through diversity

NORTH-WEST UNIVERSITY
YUNIBESITI YA BOKONE-BOPHIRIMA
NOORDWES-UNIVERSITEIT
POTCHEFSTROOM CAMPUS

Declaration

I, the undersigned, hereby declare that the work contained in this project is my own original work.

_____

William George Joseph Theron
Date: November 2011
Potchefstroom

Acknowledgements

I would like to thank the following people:

Jean le Clus-Theron

To my wonderful, considerate and tolerant wife, no words could ever describe your influence.

Professor Jat du Toit

Your meticulous attention to detail, never ending patience and steady uncomplicated guidance will never be forgotten.

Abrie Preller

Your sound advice ensured I was always heading in the right direction.

Friends and Family

Your ability to listen to my endless mumbling on the latest masters stumbling blocks and achievements will always be appreciated.

Abstract

Existing correlations developed to account for pressure drop and velocity distribution in packed beds are not ideal for beds with low aspect ratios. This study investigated a method to model flow distribution through packed columns by performing numerical analysis using an explicit approach. Fixed random packed beds for column-to-sphere diameter ratios of $1.39 \leq D/d \leq 4.93$ were generated with a discrete element method (DEM) code and validated using experimental data. Computational fluid dynamics (CFD) simulations were performed on the packings in the laminar, transitional and turbulent flow regimes and compared with results from the literature concerning porosity and pressure drop. The velocity distribution within the packed beds was also investigated. Various meshing methods at the sphere contact points were investigated with focus on both their efficiency and accuracy.

In addition to defining a method to model the flow distribution through packed columns, the study further aimed to validate the ability of STAR-CCM+® software to perform both the DEM and CFD simulations.

The DEM simulations were in agreement with the experimental data used and showed similar trends in the variation of the porosity over the lengths of the packings. The CFD simulations similarly compared well with the results obtained from the literature in terms of valid correlation ranges.

The combination of DEM to pack the columns and CFD to model the flow distribution proved to be an efficient and accurate method to model the flow distribution and associated phenomena through packed columns when considering an explicit approach. STAR-CCM+® provided a stable platform in which any column-to-sphere ratio packing could be modelled with relative ease. The explicit nature of the simulations ensured that the simulations were not bound to specific ranges.

Keywords: Random packed beds/columns, Low aspect ratio, Pressure drop, Porosity, Flow distribution, DEM, CFD, STAR-CCM+®.

Opsomming

Bestaande korrelasies wat ontwikkel is om drukverlies en snelheidsverspreiding in gepakte beddens in ag te neem, is nie ideaal by lae aspek verhoudings nie. Hierdie studie ondersoek 'n metode om die vloei veld deur gepakte kolomme te modelleer deur middel van 'n eksplisiete benadering numeriese analise. Vaste, onreëlmatige gepakte beddens vir kolom-tot-sfeer deursneëverhoudings van $1.39 \leq D/d \leq 4.93$ is gegenereer met behulp van 'n diskrete element metode (DEM) kode, en gevalideer deur van eksperimentele data gebruik te maak. Berekeningsvloeidinamika ("CFD") simulasies is gedoen op die pakkings in die laminêre, oorgangs- en turbulente vloeiregimes en vergelyk met resultate gevind in die literatuur, met betrekking tot porositeit en drukverlies. Die snelheidsdistribusie in die gepakte beddens is ook ondersoek. Verskeie rooster generasie metodes t.o.v. sfeer kontakpunte is ondersoek met die fokus op doeltreffendheid en akkuraatheid.

Behalwe om 'n metode te definieer om die vloeidistribusie deur gepakte kolomme te modelleer, het die studie verder ten doel gehad om die vermoë van STAR-CCM+® sagteware om beide die DEM en CFD simulasies te doen, te valideer. Die DEM simulasieresultate het ooreengestem met die eksperimentele data wat gebruik is, en vertoon soortgelyke tendense in die variasie van die porositeit oor die lengte van die pakkings. Die CFD simulasies het ook goed vergelyk met die resultate soos gevind in die literatuur, in terme van geldige korrelasie reikwydte.

Die kombinasie van DEM om die kolomme te pak, en CFD om die vloeiveld te modelleer, blyk 'n doeltreffende en akkurate metode te wees om die vloei verspreiding en geassosieerde verskynsels deur gepakte kolomme te modelleer, wanneer 'n eksplisiete benadering gevolg word. STAR-CCM+® bied 'n stabiele platform waarin enige kolom-tot-sfeer ratio pakking met relatiewe gemak gemodelleer kan word. Die eksplisiete aard van die simulasies verseker dat die simulasies nie tot 'n spesifieke omvang beperk word nie.

Sleutelwoorde: Onreëlmatige gepakte beddens/kolomme, lae aspek verhouding, drukverlies, porositeit, vloeidistribusie, DEM, CFD, STAR-CCM+®.

Table of Contents

List of Figures

List of Tables

Nomenclature

General

A	Area [m^2]
A_c	Cross-sectional area [m^2]
A_e	Empirically determined constant
A_w	Wall correction term
a	Contact area [m^2]
B_e	Empirically determined constant
B_w	Wall correction term
b	Bulk region
C_{fs}	Static friction coefficient
D	Column diameter [m]
d	Particle diameter [m]
d_c	Target cell size [m]
E	Young's Modulus
F	Force [N/m^2]
f_k	Darcy-Weisbach friction factor for pipe flow
G	Shear modulus
g	Gravitational constant
H	Height [m]
K	Elastic constant
L	Column length [m]
M	Mass [kg]
$\dot{m}$	Mass flow [kg/s]
N	Damping
P	Pressure [kPa]
R	Column radius [m]
r	Radial coordinate [m]
r_p	Particle distance from wall [m]
Re	Reynolds number
Re_{dp}	Particle Reynolds number
t_0	Rayleigh time step size [s]
t_1	Collision duration [s]
t_2	Geometric based time step size [s]
V	Volume [m^3]
V_{Rayleigh}	Rayleigh wave speed
v	Velocity [m/s]
y^+	Criterion for thickness of the wall cells
z	Normalized wall distance

Abbreviations

3D	Three-Dimensional
CFD	Computational Fluid Dynamics
CAD	Computer Aided Design
DEM	Discrete Element Method

HM	Hertz Mindlin
HTR	High Temperature Reactor
KTA	Kern Technisches Ausschuss
LBM	Lattice Boltzmann Method
LES	Large Eddy Simulation
NWU	North-West University
PMMA	Poly Methyl MethAcrylate
RANS	Reynolds-Averaged Navier-Stokes
RNG	Renormalisation Group
RSM	Reynolds Stress Model

Greek Letters

α	Aspect ratio
Δ	Change
ε	Porosity
δ	Packing density
μ	Viscosity
ρ	Density [kg/m^2]
ψ	Dimensionless pressure drop
ϕ	Friction coefficient
u	Poisson ratio
σ	Momentum
ξ	Overlap

Subscript

0	Superficial/Inlet/Initial
b	Bed
bl	Boundary layer
c	Inter-particle interaction
$crit$	Critical
eq	Equivalent
f	Face
g	Gravity
hom	Homogeneous
im	Impact
m	Modified
n	Normal
p	Particle
R	Radial
r	Resultant
s	Surface
t	Tangent
u	User-defined

Superscript

d	Damping

1 Introduction

1.1 Introduction

Packed beds/columns are widely used in the power, chemical and process industry. The purpose of packed beds varies between applications, which could involve nuclear packed bed reactors, catalytic reactors in process and chemical plants and thermal storage in renewable and conventional energy systems (Dreißigacker *et al*., 2010:1199). Regardless of the packed bed application, i.e. thermal absorption, extraction or catalytic reaction, the basic principle in all packed beds remains constant: a working fluid is passed through the bed of packed particles.

The design of a packed bed relies heavily on the pressure drop of the fluid flowing through the packed bed and pressure drop is sensitive to the porous structure of the packed bed (White & Tien, 1987:291). When designing a fluid system that incorporates a packed bed, it is customary for designers to assume that the distribution of flow is uniform over the diameter of the packed bed and porosity is equally distributed over the entire length of the bed (Di Felice & Gibilaro, 2004:3037). However, these assumptions are not valid for beds with low column diameter to particle diameter ratios (aspect ratio). At low and high aspect ratios the bed porosity varies sharply near the wall due to an interruption in packing. As a result the uniform velocity profile inside a packed bed can be severely distorted near the wall. The variation in porosity tends to have a larger influence on the packing structure as the aspect ratio of the bed is decreased (White & Tien, 1987:291; Du Toit, 2008:3073).

Several authors have attempted to correlate the pressure drop through packed beds and accurately take the wall effects into account for low aspect ratios (Eisfeld & Schnitzlein, 2001:4320). When low aspect ratio packings were considered, the experimental results were found to be more accurate than the correlations. The non-uniform variation in porosity at low aspect ratios affected the average porosity values used in the correlations and the correlated results showed deviation from experimental results.

Computational fluid dynamics (CFD) numerical analysis allows for accurate calculation of velocity profiles and pressure drops within packed columns by explicitly calculating the effect each sphere in the packing has on the pressure drop and flow distribution (Eppinger *et al*., 2011:324).

In order to perform the CFD simulation, a three-dimensional (3D) structure of the packed bed is required. The generation of such random packed beds are done by using the discrete element method (DEM) first described by Cundall and Strack (1979:47).

In this dissertation a methodology to accurately a perform numerical analysis of the flow distribution within packed columns is described. An explicit approach was adopted with specific focus on the generation of 3D packed beds using DEM. Calculation of flow distribution and pressure drop characteristics was done using CFD simulations. Figure 1-1 shows an example of the flow distribution in a packed column modelled in this study.

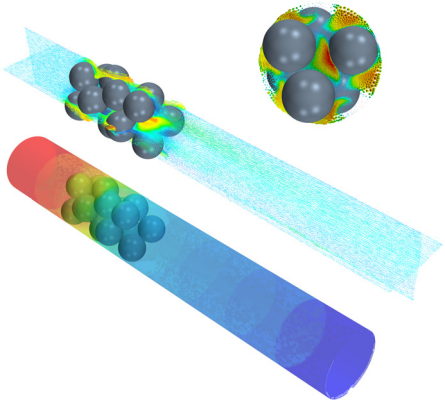

Figure 1-1. Flow distribution in a packed column.

1.2 Problem Statement

Existing correlations developed to account for pressure drop and velocity distribution in packed beds are not ideal for beds with low aspect ratios. With the increase in computational power in the recent years it is possible to effectively use DEM codes to randomly pack the small column-to-sphere diameter beds and generate multiple structural arrangements to be used by CFD codes for the flow distribution and pressure drop calculations. In addition, with the ability to automate the generation of multiple numerical beds and vary the flow conditions for each packing scenario, a thorough analysis of the flow distribution and pressure drop can be performed for low aspect ratio packed beds.

1.3 Objective

This study was aimed at performing the numerical analysis of the flow distribution within low aspect ratio packed columns using an explicit approach. The analysis allowed for the generation of packed beds using a DEM code and simulation of velocity profiles and pressure drops using CFD code. The study aimed to use a single platform to perform both the DEM and CFD simulations.

The ability of STAR-CCM+® software to accurately simulate packing and flow was investigated for this purpose. Validation of the bed packing was to be done by comparing the DEM generated beds with experimental data acquired in previous studies at the North-West University (NWU) and porosity variation correlations found in literature.

Eight sets of experimental packed column data were available and the various packing aspect ratios investigated are shown in Figure 1-2. Validation of the flow distribution and pressure drop was also done by comparing the CFD results to corresponding values predicted by correlations found in literature.

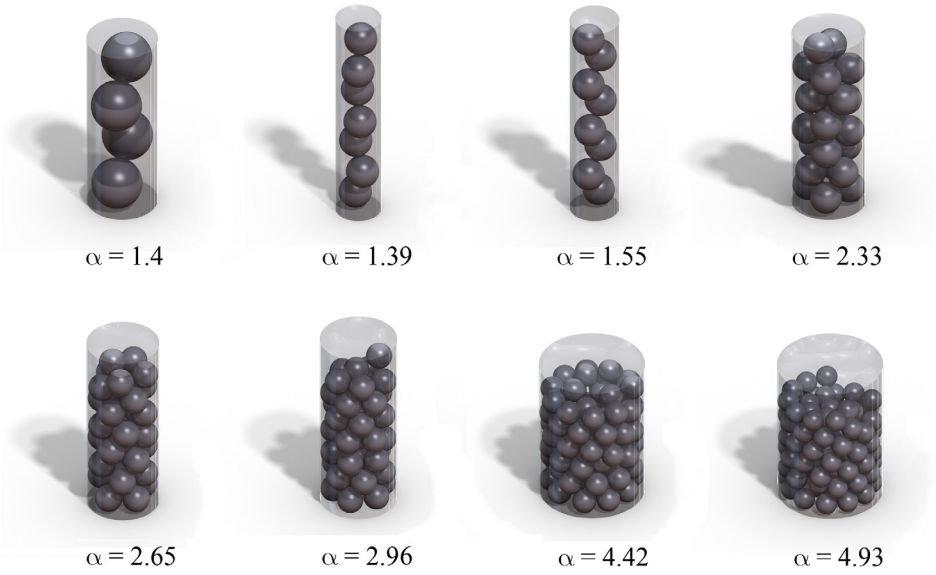

Figure 1-2. The various packed columns investigated in the study.

1.4 Outline of this Study

Chapter 1 serves as a general introduction to the study.

Chapter 2 initially presents a literature survey on general analysis of low aspect ratio packed beds. The study then progresses to determine influential factors in the numerical analysis of low aspect ratio packings and approaches and assumptions to be made with regards to the accurate calculation when using DEM and CFD models.

Chapter 3 presents a methodology to perform the analysis of a packed bed using numerical techniques.

Chapter 4 presents descriptions and validation of the results obtained using the DEM method, (discussed in Chapter 3), to generate packed beds while descriptions and validation of the results obtained using the CFD method are presented in Chapter 5

Chapter 6 of the dissertation provides concluding remarks and suggestions for future work.

2 Literature Survey

2.1 Introduction

The numerical analysis of the flow distribution and pressure drop over low aspect ratio packed columns using an explicit approach requires various methods of numerical calculation and simulation. The approach adopted in this study focused on the generation of packed beds using a DEM approach and the simulation of velocity profiles and pressure drops using CFD code. A comprehensive literature survey was performed to obtain a fundamental understanding of previous research. The survey highlighted the most influential factors in the analysis of packed beds.

The initial stages of the survey focused on the general analysis of low aspect ratio packed beds. This ensures all aspects of packed bed analysis are understood. The study then progressed to the influential factors. The study determined approaches and assumptions to be made with regards to accurate calculation when using DEM and CFD models.

2.2 Packed Bed Analysis Survey

2.2.1 Introduction

The packed bed analysis survey aimed to highlight previous research on packed bed analysis. The survey focused on previous numerical and experimental studies at low aspect ratio packing.

2.2.2 Low aspect ratio packed beds

2.2.2.1 When is a bed considered to have low aspect ratio?

Packed beds are considered to be at a low aspect ratio when the wall effects dominate the packing structure and the bed is packed in an inhomogeneous manner. The general consensus in literature is that wall effects are evident up to 5 particle diameters from the wall (Goodling *et al*., 1983:23). Therefore, any packed bed with an aspect ratio smaller than 10 can be included in the low aspect ratio range.

2.2.2.2 Previous studies on low aspect ratio beds

Various authors have published papers on low aspect ratio/low tube-to-sphere diameter packed beds. Winterberg and Tsotsas (2000:1084) found from a literature survey that the influence of the operating parameters Re (Reynolds number) and D/d_p (aspect ratio) and the physical phenomena of wall friction and flow maldistribution on the pressure drop of low aspect ratio packed beds are in conflict.

The assumption of homogeneous fluid velocity and void fraction distributions throughout a bed cannot be true near the container wall, where spheres tend to arrange themselves differently. When the wall region represents a small fraction of the whole, it is possible to ignore the inhomogeneity, however, at low aspect ratios the wall effects form a significant part of the whole and must be accounted for (Di Felice & Gibilaro, 2004:3037).

Winterberg and Tsotsas (2000:1084) researched the impact of aspect ratio on pressure drop in packed beds at low aspect ratios. They compared their calculated data to the homogeneous pressure drop (ΔP_{hom}) obtained by the Ergun equation for average bed porosity, $\bar{\varepsilon}$, and superficial velocity, $\bar{v}_0$. It was found that at aspect ratios $(\alpha > 10)$, pressure drops obtained were almost identical to ΔP_{hom} and for $(4 < \alpha < 10)$, significant deviations of up to 20% were found. Packed beds at very small aspect ratios $(\alpha < 4)$ were not even considered.

Cheng and Yuan (1997:1319) determined that at low aspect ratios the wall effect of the packed bed is important and should be accounted for carefully. They used a modified Ergun equation to predict the velocity distribution in low aspect ratio beds by introducing an effective tube diameter to ensure the pressure drop is predicted from the free flow space and the wetted area.

Eisfeld and Schnitzlein (2001:4321) performed a detailed analysis of 2300 experimental data points to determine the Reynolds number dependence on the wall effect. They compared the predictions of 24 published pressure drop correlations with available experimental data and found that the Reichelt (1972) approach of correcting the Ergun equation for the wall effect was the most promising.

De Klerk (2003:2022) found that packed beds exhibit damped oscillatory voidage variation in the near wall region. De Klerk demonstrated an improved radial bed voidage and average bed voidage prediction. He also noted that multiple stable packing configurations exist within the same packing mode, which complicates modelling at a small column-to-particle diameter ratio.

2.2.3 Packed bed numerical analysis

Two types of numerical approaches are defined in literature with regards to packed bed analysis. Firstly, packed beds are treated as pseudo-homogeneous structures where modified Navier-Stokes equations are applied in conjunction with Ergun pressure drop correlation to account for solid-fluid interaction. The second approach is to generate the actual 3D packed bed geometry and resolve the flow between the particles with the aid of CFD modelling (Atmakidis & Kenig, 2009:404).

The first approach, which uses a pseudo-homogeneous model equation, tends to lose accuracy at low aspect ratios where local phenomena dominates (Freund *et al*., 2003:903).

When considering the cross-section of a packed column at low aspect ratios where only a few spheres are used, the circumferential symmetry is not fulfilled. This establishes that even semi-empirical correlations that are extended to take into account axial and radial porosity, velocity and transport parameter variations, do not describe local phenomena in detail (Freund *et al*., 2003:903).

The second approach, which takes into account the actual packing structure, is better suited to low aspect ratio packed beds, due to the fact that no empirical correlations are required for the porosity distribution. According to Dixon and Nijemeisland (2001:5246) a spatially resolving 3D simulation is required to determine the local effects in packed beds at low aspect ratios.

The increase in computational power in recent years allows researchers to perform packing generation and fluid flow analysis in increasing detail, taking into account the 3D variation of the randomly packed beds and accounting for flow distribution and pressure drop, without the use of semi-empirical data (Freund *et al*., 2003:903).

2.2.3.1 Numerical generation of 3D packing

While various numerical methods exist to generate the 3D spherical packing, these methods are essentially of two types: deposition algorithms based on geometrical rules or dynamic simulation methods based on integration of Newton's laws of motion (Augier *et al*., 2010:1055).

Deposition models have been adopted by various authors and include sequential packing models by Mueller (1997:179) where identical spheres are sequentially packed on a base layer and the added spheres are placed to ensure they are stable under gravity. The Monte Carlo packing method was used by Freund *et al*. (2003:904) where the spherical packing was developed by random placement (raining) and a subsequent compression step. Caulkin *et al*. (2006:1178) developed an

approach to pack columns using a digital packing algorithm, Digipac. The Ballistic deposition method in combination with the Monte Carlo packing method is used by Atmakidis and Kenig (2009:405) where a large number of test particles were dropped into a bed and only the particle with the lowest position became part of the stack. Jafari *et al*. (2008:479) used a commercial grid generation tool GAMBIT 2.2 linked to a random number generator obtained by Matlab to position the spheres in a non-overlapping manner.

From the literature it is evident that deposition type simulations have been dominant in the numerical simulation of bed packing. Deposition models are considered fast methods to generate 3D spherical packings but tend to provide models that are mechanically unstable (Augier *et al*., 2010:1055).

Dynamic simulation methods include the discrete element method (DEM) initially developed by Cundall and Strack (1979:47) to determine the mechanical behaviour of assemblies of discrete elements in 1979. Kozicki and Donze´ (2009:786) noted that the DEM model takes into account contact interaction between elements (normal forces, tangential and rolling stiffness, local friction and non-dimensional plastic coefficient) and the mechanical response of the physical material (deformability, strength, dilatancy, strain localisation and other) to determine particle behaviour.

Based on a review of the literature it is evident that the dynamic simulation methods (DEM) allow authors to accurately generate randomly packed 3D columns. With the increase in computational power in recent years it is possible to effectively use a DEM code to randomly pack the small column-to-sphere diameter beds and generate multiple structural arrangements to be used by the CFD code for the flow distribution and pressure drop calculations.

In addition, with the ability to automate the generation of multiple numerical beds and vary the flow conditions for each packing scenario, a thorough analysis of flow distribution and pressure drop can be performed.

The DEM method is therefore a suitable numerical approach to simulate a 3D packed geometry. The general analysis map is shown in Figure 2-1.

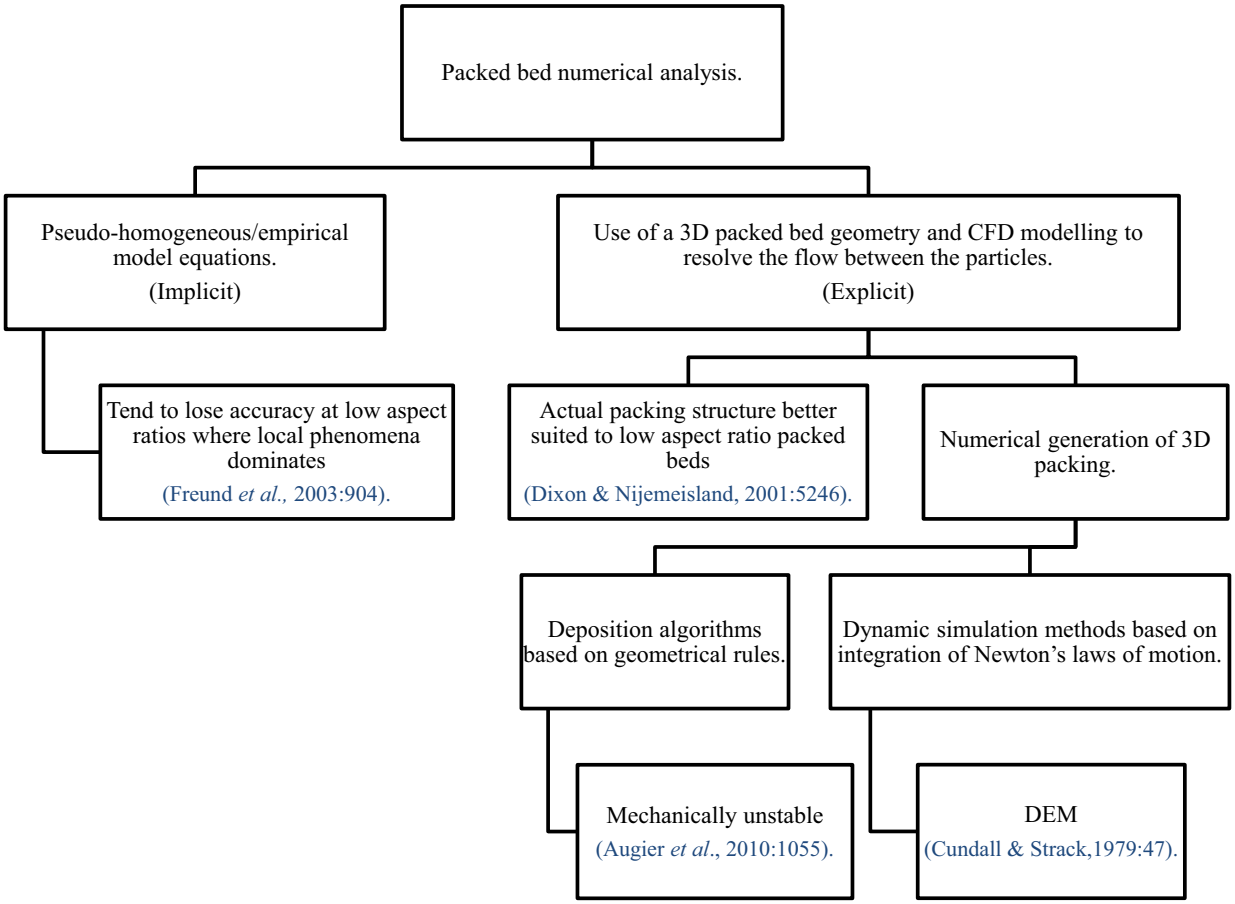

Figure 2-1. General analysis - packed bed numerical analysis.

2.2.3.2 Numerical calculation of flow characteristics

Two methods are generally used to determine the flow characteristics between spheres in packed columns. The methods include the lattice Boltzmann method (LBM) and Navier-Stokes equations applied to the voids between the spheres (Augier *et al*., 2010:1055).

Zeiser *et al.* (2001:1697) used the LBM to solve flow in a packed column. The studies were performed at a low aspect ratio ($\alpha = 3$) to ensure wall effects are dominant in their flow. LBM was also adopted by Freund *et al*. (2003:904) where flow characteristics and pressure drop in randomly packed columns were calculated and results were found to align with experimental data. However, there are still unresolved computational concerns with LBM due to its restrictions to a limited class of mesh, and other approaches to solving the Navier-Stokes equations are still appropriate.

The Navier-Stokes equations applied to the voids between the spheres were applied by Romkes *et al*. (2003:3) and the local velocity field studied for both structured and unstructured beds.

Most applications of CFD to packed beds are at low aspect ratios, this is attributed to the complex geometries associated with high aspect ratio beds and the associated problems of generating the geometries and discretising it as a mesh. Analysis of flow characteristics for low aspect ratio packed beds, using a commercial CFD finite volume code have been performed by the following authors, Guardo *et al.* (2005:1733); Jafari *et al.* (2008:476); Augier *et al*. (2010:1055) and Reddy and Joshi (2010:37).

2.3 Influential Factors at Low Aspect Ratios

Throughout the literature authors have identified various influential factors in packed bed analysis using an explicit approach. The literature survey focuses on the 5 categories that were found to be most prominent in previous research being packing, DEM and packed beds, porosity and pressure drop, CFD and packed beds, and flow distribution. Figure 2-2 summarises the categories and their relevant subsections.

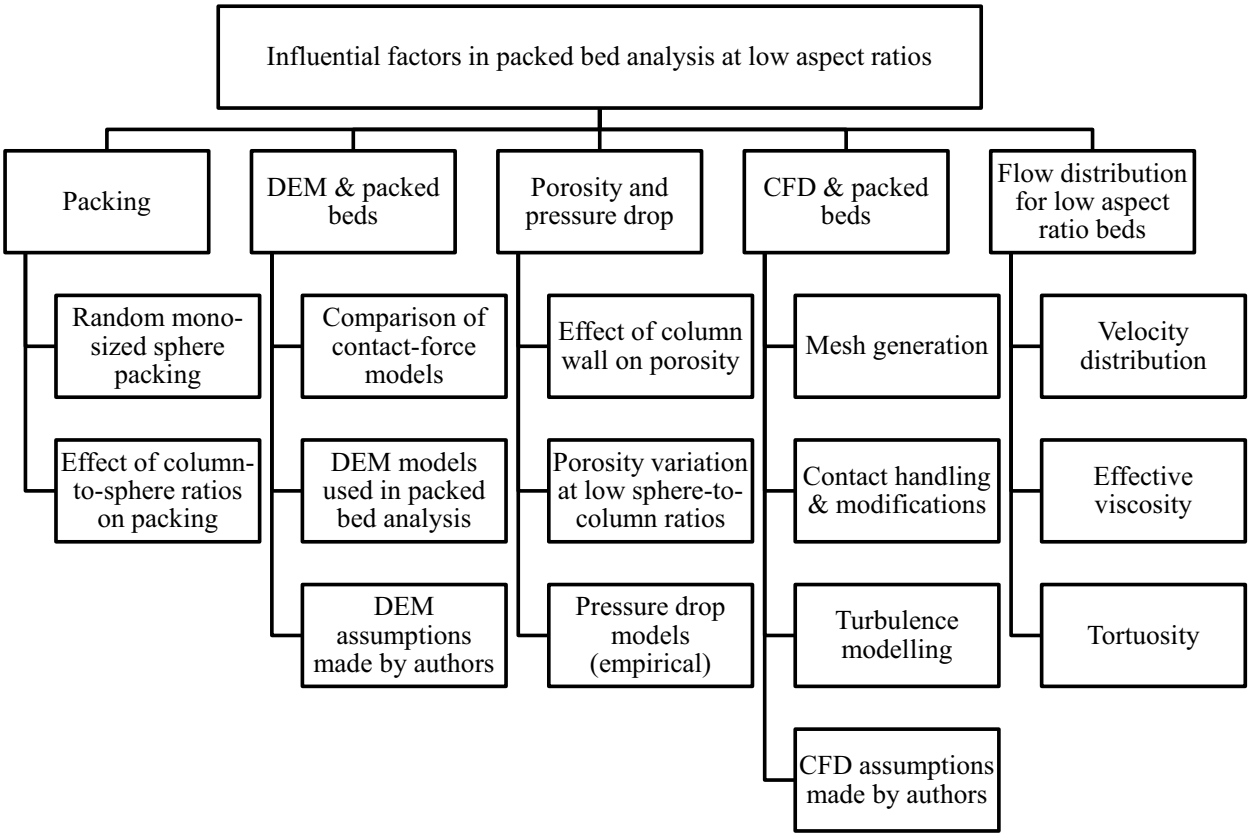

Figure 2-2. Influential factors in packed bed analysis at low aspect ratios.

2.4 Packing

2.4.1 Packing structures at low aspect ratios

Column-to-sphere ratio (aspect ratio) is the ratio of the containing column inner diameter to the diameter of the sphere particles:

$$\alpha = D / d_p \tag{2.1}$$

The column-to-sphere ratio can be considered as the most influential variable in the packing structure and porosity of packed columns. Sphere locations in packed columns are influenced by the column-to-sphere ratio due to the confining nature of the wall of the column, and are particularly influential in regions close to the wall (Govindarao *et al*., 1992:2105).

2.4.2 Theoretical assemblages of systematic packing

Granton and Fraser (1935:785) discussed the geometry and assembly of various discrete, ideal spheres. They described ordered packing by defining the angle of intersection, with the limiting angles between 60° and 90° as shown in Figure 2-3.

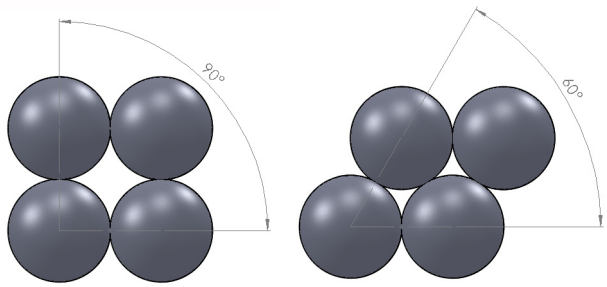

Figure 2-3. Limiting packing angles between 60° and 90°.

Gray (1968:43) noted that systematic or ordered packing generally will encounter two types of layers; square and simple rhombic, with three simple ways of stacking either the simple rhombic or square layers and 6 systematic packings options based on the simple layers (see Figure 2-4).

Granton and Fraser (1935:790) determined that for each type of packing there is a characteristic void fraction, which is given by the ratio of the volume of the complete unit void to the volume of the complete unit cell. The porosity and coordination for various systematic assemblages are given in Table 2-1.

Table 2-1. Systematic assemblages of spheres (Granton & Fraser, 1935:790).

	Porosity, percent	*Coordination number*
Cubic (case 1[a])	47.6	6
Ortho-rhombic (case 2,4)	39.5	8
Tetragonal (case 5)	30.2	10[b]
Rhombohedral (case 3,6)	26.0	12

a. See Figure 2-4

b. The coordination number is defined as the number of other particles that are in contact with the selected particle, also known as the kissing number.

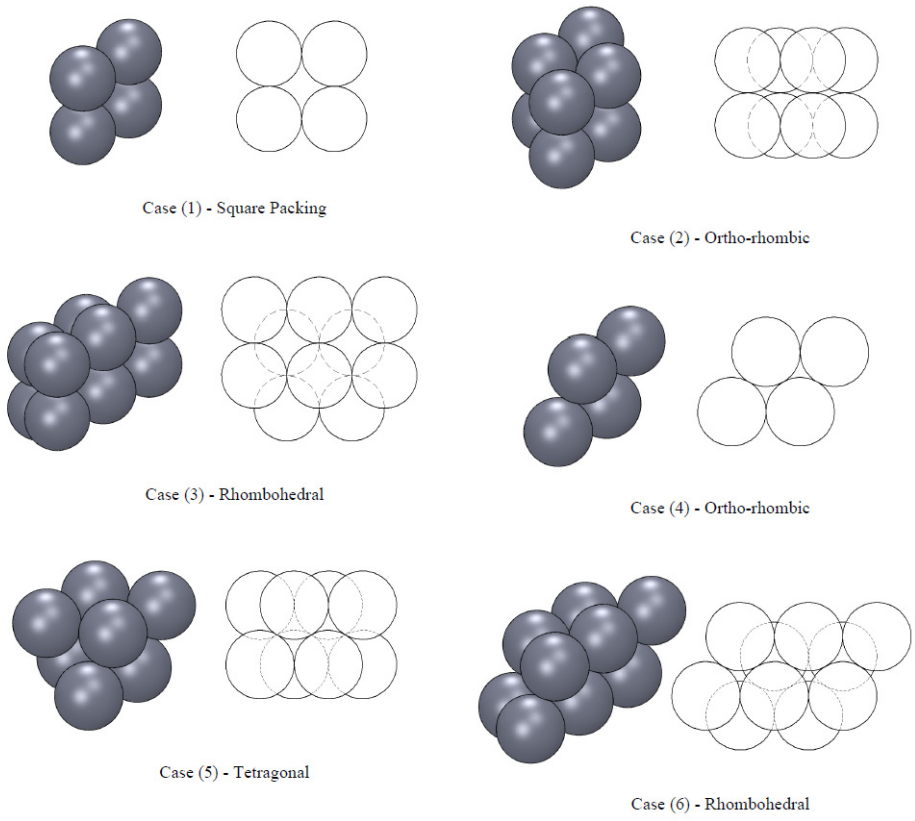

Figure 2-4. Square and rhombic packing schemes.

2.4.2.1 Structural characteristics at various low column-to-sphere ratios

Govindarao *et al*. (1992:2105) determined that 3 distinct types of packing behaviour can occur at low aspect ratios. The aspect ratios identified were firstly an aspect ratio of 2, the second between 1 and $1\frac{\sqrt{3}}{2}$, and the third between $1\frac{\sqrt{3}}{2}$ and 2.

It was determined that for the low aspect ratios it was possible to reproduce the packing of columns. The derived expressions and structures formed at the determined aspect ratios will be discussed next.

Columns of column-to-sphere ratio $(\alpha = 2)$

If we consider spheres of equal size dropped into a column one by one with the column diameter twice the diameter of the spheres and allow the spheres to settle before adding the next sphere, the first two spheres will settle on the floor and touch the wall. The sphere centres are at the same height and at a distance r_p from the walls. The next two spheres will settle in positions where they both rest on the first two spheres and touch the wall, this is repeated in the packing structure and all the spheres will rest on previously dropped spheres and touch the column wall. Because sufficient time is given for the spheres to come to rest the positions can be considered "stable" (see Figure 2-5(a)).

Columns of column-to-sphere ratio $\left(1 \le \alpha \le 1\frac{\sqrt{3}}{2}\right)$

In columns of column-to-sphere ratio $1 \le \alpha \le 1\frac{\sqrt{3}}{2}$ spheres arrange one over the other and each sphere will touch the column wall, thus the sphere centres will all lie at a distance r_p from the wall of the column (see Figure 2-5(b)).

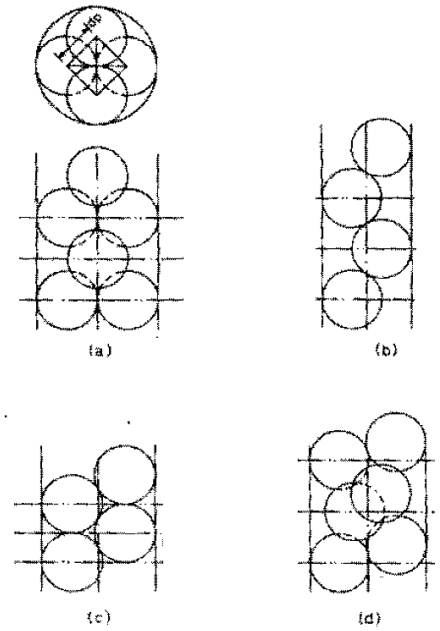

Figure 2-5. Low aspect ratio bed structures (Govindarao *et al*., 1992:2105).

Columns of column-to-sphere ratio $\left(\alpha = 1\frac{\sqrt{3}}{2}\right)$

When an aspect ratio is chosen to be $\alpha = 1\frac{\sqrt{3}}{2}$ the spheres will find a stable position so that the horizontal plane through the centre of a sphere is perpendicular to the vertical plane of the next sphere (see Figure 2-5(c)).

Columns of column-to-sphere ratio $\left(1\frac{\sqrt{3}}{2} \leq \alpha \leq 2\right)$

When an aspect ration is chosen to be $1\frac{\sqrt{3}}{2} \leq \alpha \leq 2$ the spheres will find a stable position so that the horizontal plane through the centre of a sphere is perpendicular to the vertical plane of the sphere in the layer above the sphere in contact (see Figure 2-5(d)).

Govindarao *et al*. (1992:2105) proved that the structure of packed beds at low aspect ratios shows periodicity and can be described in terms of unit cells. Therefore, the packing sections can be produced with characteristics similar to those of the overall bed.

The height of such a unit cell is seen to be half of the height of the bed, which shows periodicity in the location of the particles and is independent of the position of the base of the unit cell (see Figure 2-5).

Govindarao *et al*. (1992:2105) therefore proved the complete reproducibility of packing at 1ow aspect ratio beds. From the literature it was found that packing structures at certain aspect ratios can be reproduced and specific aspect ratios can be used to validate numerically generated bed packing structures.

2.5 Discrete Element Method (DEM)

2.5.1 Introduction to DEM

The discrete element method (DEM) is an explicit numerical model that dynamically approximates the mechanical behaviour of particles. The DEM model takes into account the force between particles during contact, which is calculated with mechanical elements such as springs and dashpots. A soft contact approach is adopted by which particles are allowed to overlap during contact. The particles displace independently from one another and interact only at contact points. Particles are assumed to be rigid bodies; therefore their deformation during contact is neglected. The three-dimensional dynamics equations used are based on the classical Newtonian approach for the second law of motion, forces and moments acting on each particle is determined for every time step (Kozicki and Donze´, 2009:786).

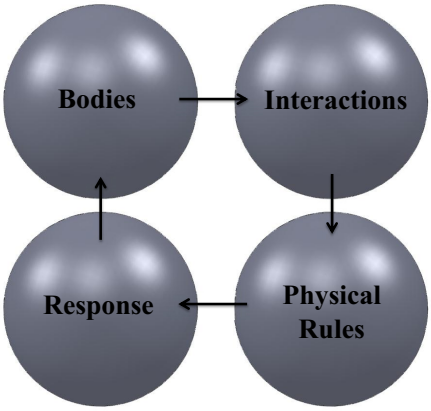

Figure 2-6. Simplified discrete element modelling (DEM) method.

If we consider the diagram shown in Figure 2-6, each particle/body will have a position, orientation, velocity and angular velocity. If there is an interaction with another object the body is subjected to physical rules such as the Newtonian second law of motion, forces and moments. The forces will change the body's response and in turn its position, orientation, velocity and angular velocity until interaction with another particle/body.

2.5.2 Previous research

Zhu *et al*. (2007:3378) presented a summary of the major theoretical developments in DEM up to mid-2006. They determined that extensive investigations under different packing/flow conditions at either macro or microscopic level by various investigators worldwide have increased over the last few years as seen in Figure 2-7. The steady incline of DEM research clearly indicates that DEM-based discrete particle simulation is accepted in industry and therefore can be assumed an effective way to generate packed beds.

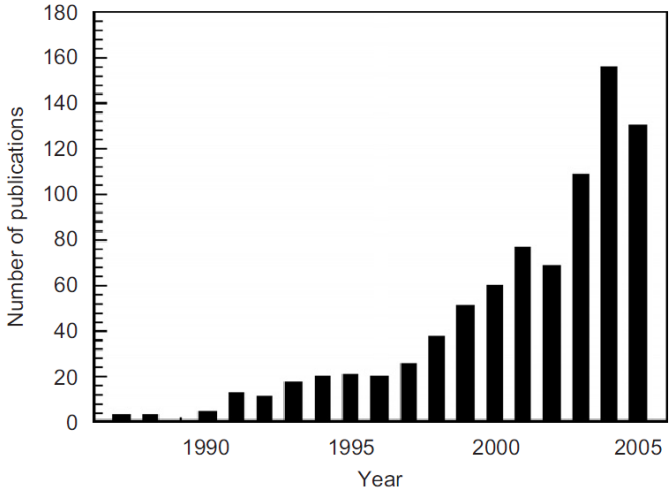

Figure 2-7. Publications related to discrete particle simulation (Zhu *et al*., 2007:3378).

The review of Zhu *et al*. (2007:3378) illustrates DEM development by highlighting three important aspects mainly related to the modelling of particle or particle–fluid flow. Zhu *et al*. (2007:3378) found that the theories underlying the DEM and models for calculating the contact forces between particles are better suited to numerical particle packing. Additional forces have been implemented in DEM simulation, which makes the DEM model more applicable to particulate research, including development of the CFD-DEM approach which can handle the particle–fluid interactions.

Kodam *et al*. (2010:5852) noted that most DEM models used for simulating the dynamics of particulate systems assume spherical particles. Spheres are typically used in DEM models because:

- Sphere characterization is simple, only a diameter is needed to describe a sphere.
- Contact detection between spheres is simple. Two spheres are in contact if the distance separating their centres is less than or equal to the sum of their radii.
- Contact force models for spheres are readily available in the literature. The Hertzian model is commonly used to determine the elastic normal force for contacts involving spheres.
- Contacts between spheres are modelled as single points of contact.

2.5.3 DEM and packed beds

Eppinger *et al*. (2011:324) generated a random packing of a low aspect ratio column by randomly initializing spherical monodisperse particles within the tubular fluid domain. The particles fell to the bottom of the tube due to gravity. A force balance was formulated and solved for each particle, and the gravity force and the interaction between particles and between particles and the tube wall was taken into account. Eppinger *et al*. (2011:324) deemed the DEM simulation to be completed when the velocity of each particle was virtually zero.

Theuerkauf *et al*. (2006:98) noted that DEM makes it possible to include particle properties which reflect on the porosity distribution as the packing structure of particles in a column depend mainly on the aspect ratio and the particle friction. It was found that the correct particle distribution was generated regardless of the aspect ratio. Various ball friction factors were simulated and Theuerkauf *et al*. (2006:98) found that the friction factor has an effect on the overall porosity of a packed column. The overall porosity was decreased when a lower friction factor was specified. The decrease in average porosity was due to lower frictional forces between the particles and a tighter packing could be achieved.

2.5.4 DEM contact force displacement models

2.5.4.1 Introduction

Various force displacement models are mentioned in literature, these models include; a linear spring–dashpot–slider system. More detailed contact force models based on the classical Hertz theory developed by Hertz (1882) as quoted by De Renzo and Di Maio (2004:525) for the normal direction, and simplifications of the model developed by Mindlin and Deresiewicz (1953) as quoted by De Renzo and Di Maio (2004:525) for the tangential direction. Contact models are considered to be either a linear model, or non-linear which include Hertz Mindlin and Deresiewicz no-slip model and the complete Hertz Mindlin and Deresiewicz model.

2.5.4.2 Linear model

Cundall and Strack (1979:47) initially proposed a parallel linear spring–dashpot model for the normal direction and a parallel linear spring–dashpot in series with a slider for the tangential direction. The linear spring–dashpot–slider system is considered the most intuitive and simple way of modelling mechanical relations. The linear model accounts for combinations of linear mechanical elements in series or parallel in order to represent the dynamic system with the appropriate characteristics. The spring accounts for elastic contribution to the response while the dashpot accounts for the dissipation due to plastic deformations.

The linear spring–dashpot model only accounts for frictional–elastic collisions, thus the material parameters for the definition of the model are the normal and tangential spring constants K_{n} and K_t and the friction coefficient ϕ. The force–displacement relations for the normal, F_n, and tangential, F_t, force calculations are (De Renzo & Di Maio, 2004:525):

$$F_n = -(K_n \cdot \xi_n) \tag{2.2}$$

$$F_t = -min(K_t \cdot |\xi_t|;\phi|F_n|)\frac{\xi_n}{\xi_t} \tag{2.3}$$

where ξ_n is the normal overlap and ξ_t the tangential overlap.

2.5.4.3 Non-linear models

The Hertz Mindlin and Deresiewicz no-slip model

Zhu *et al*. (2007:3378) described the Hertz Mindlin and Deresiewicz no-slip model as more complex than the linear model, although a theoretically sound model. The model uses the elastic theory of Hertz for the normal contact problem and the no-slip solution of the tangential contact problem as solved by Mindlin and Deresiewicz.

The complete Hertz Mindlin and Deresiewicz model

The complete theory of Hertz for the normal contact and Mindlin and Deresiewicz for the tangential problem is fairly complex in order to include all the possible combinations of normal and tangential displacement variations (De Renzo & Di Maio, 2004:525)

Zhu *et al*. (2007:3378) noted that due to its complexity, the complete Hertz Mindlin and Deresiewicz model is time-consuming for DEM simulations of granular flows often involving a large number of particles, and is therefore not so popular in the application of DEM.

2.5.4.4 Conclusion

De Renzo and Di Maio (2004:525) determined that the influence of different force–displacement models on the accuracy of the simulated collision process has not been investigated and reported extensively in literature. A comparison of three contact force models was therefore performed to establish the most accurate model in terms of packed columns.

It was found that regarding the values of the velocities at the end of a collision, no significant improvements can be attained using complex models. In terms of the evolution of the forces, velocities and displacements during the collision they noted that correct accounting for non-linearity in the contact model and micro-slip effects is of importance. Therefore, for systems sensitive to the actual force or displacement more accurate models such as the complete Mindlin and Deresiewicz model should be employed. STAR-CCM+® allows the option for the Hertz Mindlin and Deresiewicz no-slip model for DEM simulations and will be discussed next. The Hertz Mindlin and Deresiewicz no-slip model is referred to as the Hertz Mindlin no-slip contact model in STAR-CCM+® and will be named as such for the remainder of the study.

2.6 STAR-CCM+® Approach to DEM Modelling

The STAR-CCM+® modelling software approach to DEM modelling is handled as an extension to the Lagrangian modelling methodology to dense particulate flows. The distinct DEM characteristic is the introduction of inter-particle contact forces into equations of motion as illustrated in Figure 2-8.

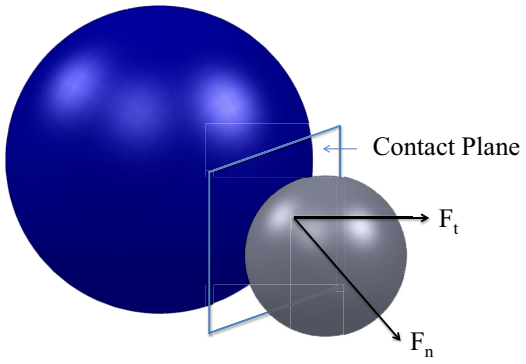

Figure 2-8. Inter-particle contact forces.

The DEM model in STAR-CCM+® uses a classical mechanics method and is based on the soft-particle formulation where particles are allowed to develop an overlap (dashpot) which take into account viscous damping and repulsive forces pushing particles apart.

2.6.1 STAR-CCM+® DEM model

The DEM theory used in STAR-CCM+® will be noted and described in this section. The section will ensure the models are understood on a fundamental level.

2.6.1.1 Momentum balance for a DEM particle

STAR-CCM+® defines the momentum balance of a material particle as the sum of the gravitational force, user defined force and a the force representing inter-particle interaction due to particle contacts with other particles and with mesh boundaries:

$$F_{\mathrm{r}} = F_{\mathrm{g}} + F_{\mathrm{u}} + F_{c} \tag{2.4}$$

where F_{r} is the resultant forces acting on the particle, F_{g} is the gravitational forces, F_{u} is user defined forces and F_{c} is inter-particle interaction forces:

$$F_c = \sum_{neighbour\ particles} F_{contact} + \sum_{neighbour\ boundaries} F_{contact} \tag{2.5}$$

The DEM particle equations of motion also incorporate angular momentum conservation equations. However, due to the static end state of the packings considered in this study, the angular momentum will not be described in detail.

2.6.1.2 Hertz Mindlin no-slip contact model

The Hertz Mindlin no-slip contact model is the default model used in STAR-CCM+® due to its accurate and efficient force calculation. Contact force formulation in DEM is typically a variant of the spring-dashpot model. The spring generates a repulsive force pushing particles apart and the dashpot represents viscous damping and allows simulation of collision types other than those that are perfectly elastic. The forces at the point of contact are modelled as a pair of spring-dashpot oscillators, one representing the normal direction and the other the tangential direction of force with respect to the contact plane normal vector (CD-ADAPCO, 2011:3450).

The forces between two spheres, A and B, are described by the following set of equations in STAR-CCM+®:

$$F_c = F_n + F_t \tag{2.6}$$

where F_n is the normal and F_t is a tangential force component.

The normal direction is defined by the normal force:

$$F_n = -K_n \xi_n - N_n v_n \tag{2.7}$$

where K_n is the normal spring stiffness and results from the equivalent properties of the two materials and N_n is the normal damping. v_n is the velocity in the normal direction and ξ_n the overlap in the normal direction.

$$K_n = \frac{4}{3} E_{eq} \sqrt{d_n r_{eq}} \tag{2.8}$$

where the equivalent Young's Modulus E_{eq} and the equivalent radius r_{eq} are defined as:

$$\frac{1}{E_{eq}} = \frac{(1-u_i^2)}{E_i} + \frac{(1-u_j^2)}{E_j} \tag{2.9}$$

$$\frac{1}{r_{eq}} = \frac{1}{r_i} + \frac{1}{r_j} \tag{2.10}$$

with E_i , u_i , r_i and E_j , u_j , r_j the Young's Modulus, Poisson Ratio and radius of each sphere in contact.

The normal damping N_n is defined as:

$$N_n = \sqrt{(5K_n M_{eq})}N_n^d \tag{2.11}$$

where the equivalent mass M_{eq} is defined as:

$$\frac{1}{M_{eq}} = \frac{1}{M_i} + \frac{1}{M_j} \tag{2.12}$$

The STAR-CCM+® Hertz Mindlin no-slip contact model similarly takes into account the tangential force, spring stiffness and damping as a function of the Young's Modulus, Poisson Ratio and radius of each sphere, with the addition of an equivalent shear modulus G_{eq} taken into account for the tangential spring stiffness and a static friction coefficient C_{fs} for the tangential force.

Therefore, the contact forces in both the normal and tangential directions are a function of the radius, Young's Modulus, Poisson Ratio and the mass of each of the spheres in contact. The calculated contact force is proportional to the overlap, as well as to the particle material and geometric properties.

Particle-to-wall collisions use similar formulas as particle-to-particle collisions. The wall radius and mass are assumed to be infinite, therefore the equivalent radius r_{eq} is reduced to r_{p} and equivalent mass M_{eq} to M_{particle}.

STAR-CCM+® assumes the tangential force to be non-linear and detail micro-slip tracking is replaced by an analytical expression. It was found that the analytical expression resulted in code that is computationally efficient and accurate (CD-ADAPCO, 2011:3452).

2.7 Porosity

2.7.1 Introduction to porosity

Porosity is defined as the ratio between the void volume and the total volume, also known as the void fraction (Liu *et al*., 1999:438). It is also defined as one minus the packing density δ and is the most basic parameter for characterizing the microstructure in a porous matrix. Porosity is given as follows:

$$\varepsilon = 1 - \delta \tag{2.13}$$

$$\varepsilon = \frac{V_{Void}}{V_{Total}} = 1 - \frac{\Sigma A_{Solid}}{A_{Total}} \tag{2.14}$$

2.7.2 Porosity variation

2.7.2.1 Radial porosity variation

The influence of the variation of the porosity in packed beds is considered of great importance in the calculation of the pressure drop, flow and heat transfer characteristics in packed beds. Various researchers have set out to determine radial voidage variation of packed beds in the bulk and near-wall region experimentally (Benenati & Brosilow, 1962:359; Goodling *et al*.,1983:23).

Experiments to determine packing structures and porosity variation were first performed by Roblee *et al.* (1958:460) who measured the radial variation in porosity in the near wall region experimentally. Roblee *et al.* (1958:460) achieved this by packing cardboard cylinders with cork spheres and filling the void space with molten wax. Sections of the solidified wax were cut out and analysed to determine the fraction of voids (wax) for each section. It was found that the bed porosity showed a damped oscillatory behaviour in the near wall region, and approached a constant value 4 to 5 particle diameters from the wall.

Benenati and Brosilow (1962:359) performed porosity experiments by filling a container with uniformly sized lead spheres and then filled the void space with epoxy resin. The cured container was machined into sections and analysed by determining the weight loss. Porosity behaviour similar to findings of Roblee *et al*. (1958:460) and Goodling *et al*. (1983:23) were found.

Goodling *et al*. (1983:23) filled a cylinder with polystyrene spheres. An epoxy mixed with finely ground iron was then used to fill the spaces between the spheres. The hardened column was then

cut into thin annular rings and the radial porosity for each ring was determined. Goodling *et al.* (1983:23) concluded that the radial porosity takes on the value of unity at the cylinder wall and then oscillates with a damped amplitude towards the mean bulk porosity near the bed centre. The experiments showed that the effect of the wall on the porosity can be detected up to a distance of 5 sphere diameters from the wall, similar to the results of Roblee *et al.* (1958:460). The variation in radial porosity determined by various authors was compiled by De Klerk (2003:2022) and is shown in Figure 2-9. The porosity shows damped oscillatory behaviour as the distance is increased from the column wall.

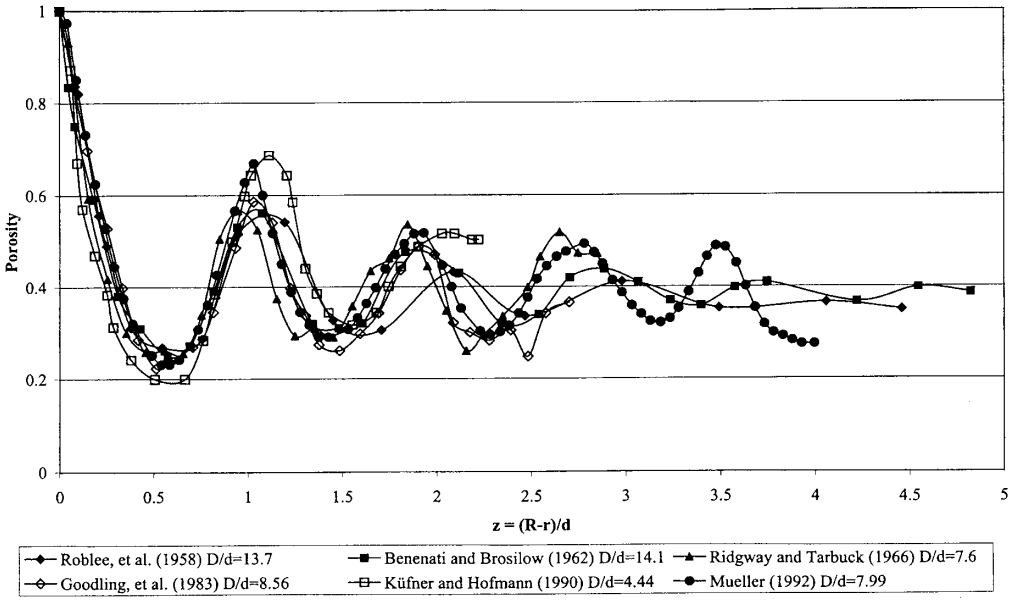

Figure 2-9. Radial porosity variation, De Klerk (2003:2022).

2.7.2.2 Axial porosity variation

Zho and Yu (1995:1505) studied the dependence of the bulk porosity on d_p/H under loose and dense randomly packed conditions, and they found a variation in the bulk porosity between $0.395 < \varepsilon_b \leq 0.46$ in dense randomly packed case when $0.05 < d_p/H \leq 0.4$. The results showed that the bulk porosity of both the dense and loose randomly packed beds start to increase when $dp/H >$ 0.05 (as quoted by Van Antwerpen *et al.* (2010:1806).

Zho and Yu (1995:1505) proposed a formula to define the minimum height at which the change in porosity due to packing height of the column (end-effect) has a negligible effect:

$$\frac{H_{crit}}{D} = 90.29\left(\frac{d_p}{D}\right)^{1.41} \tag{2.15}$$

Experimental data and correlations of the porosity variation in the axial direction is not common in the literature. The axial variation can be considered important as it is the variation of porosity in the direction of flow.

2.7.3 Effect of column wall on porosity

Spheres packed randomly in a column with large particle-to-column diameter ratios extend over three distinct regions: the wall region, the near wall region and the bulk packing region. The packing structure in the wall region is changed due to the presence of the wall (see Figure 2-10).

Packed beds of uniform spheres show a damping in oscillations of porosity in the near wall region. There is a possibility of multiple stable packing configurations for a specific packing mode (column-to-particle diameter ratio). This is especially prevalent at small column-to-particle diameter ratios. Due to the multiple stable packing configurations in randomly packed beds, there exists multiple possible average bed voidage and correspondingly different radial porosity distributions which have an effect on the predictive ability of bed porosity models. Models reported in the literature fail to relate the voidage variation in the near wall region to the average bed porosity and the change in average of the voidage oscillations. The reported literature also neglects to take into account deviations from the expected sinusoidal behaviour caused by the voidage variation in the near wall region. The development of a radial porosity model that improves the prediction of the radial bed voidage ε_R and average bed voidage $\bar{\varepsilon}$ shows that there is no need for a separate average bed voidage model, and further improvement in modelling can be achieved by taking into account deviations from the sinusoidal form of the radial bed voidage variation (De Klerk, 2003:2022).

2.7.4 Porosity variation as a function of column-to-sphere ratio

The influence of the column-to-particle diameter ratio on the voidage of a packed bed can be calculated from the radial porosity variation.

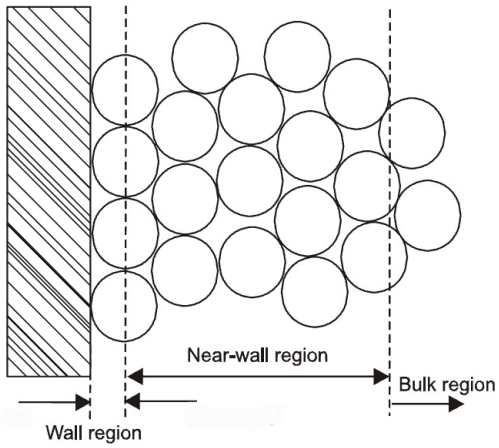

Figure 2-10. Regions in large aspect ratio columns (Van Antwerpen, *et al.* 2010:1804).

However, researchers have also investigated the relationship experimentally. Carman (1973:150) experimentally determined a parabola shaped voidage variation in a 'densely' packed column with particle-to-column diameter ratios in the region of $1 \leq D/d_p \leq 2$. An exponential decline in the parabola shaped voidage was observed in the region $2 \leq D/d_p \leq 10$. Constant voidage values were found at larger particle-to-column diameter ratios.

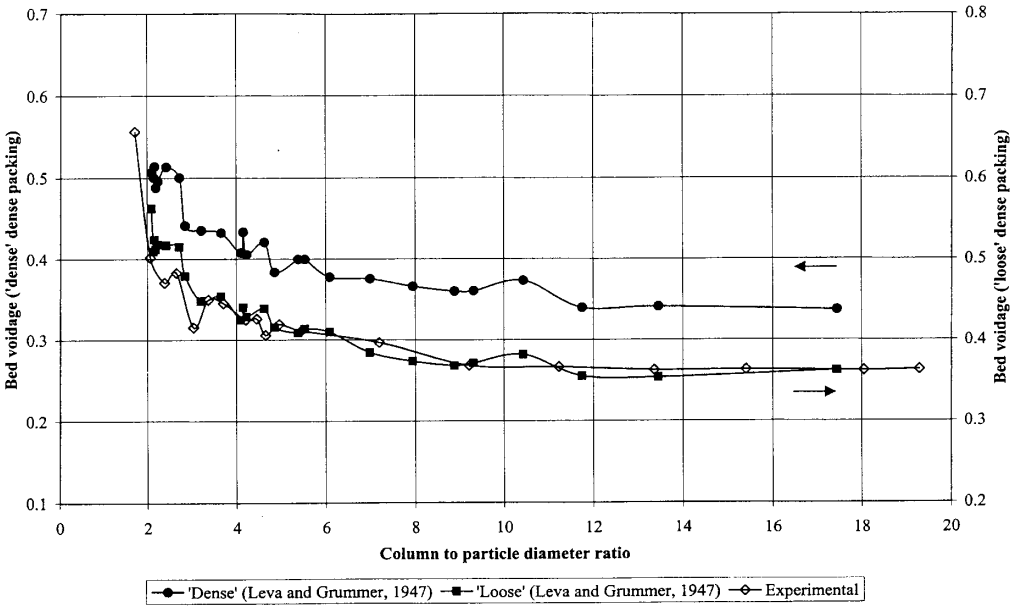

Figure 2-11. Average bed porosity variation (De Klerk, 2003:2025).

Leva and Grummer (1947) (*in*: De Klerk, 2003:2025) determined a parabola shaped voidage variation in 'loose' and 'densely' packed steel pipes experimentally, noting a difference of around 4% between the loose and dense packing. A linear relationship was found between the inverse ratio of the particle-to-column diameter and the bed voidage (see Figure 2-11).

De Klerk (2003:2028) noted that at small column-to-particle diameter ratios, typically less than 10 the effect of voidage variation becomes more prominent. De Klerk (2003:2028), determined the existence of multiple stable packing configurations within the same packing mode to be prevalent at small column-to-particle diameter ratios.

De Klerk (2003:2028) found the radial bed porosity models reported in the literature to be lacking in their ability to describe the influence of column-to-particle diameter on porosity. De Klerk (2003:2028) developed a radial porosity model to redress some of these shortcomings subsequently and improved radial bed voidage ε_R and average bed voidage $\bar{\varepsilon}$ prediction were demonstrated. It was also shown that there is no need for a separate average bed voidage model, apart from its computational simplicity in calculations requiring only the average bed porosity.

2.7.5 Porosity variation at low column-to-sphere ratios

Table 2-2 indicates bed voidage values at low column-to-particle diameter ratios calculated experimentally by De Klerk (2003:2024) (see Figure 2-11).

Table 2-2. Bed voidage at different aspect ratios, De Klerk (2003:2024).

Aspect Ratio	*Porosity*
1.7	0.657
2	0.502
2.4	0.471
2.6	0.483
3	0.416
3.3	0.45
3.7	0.445
4.2	0.425
4.4	0.426
4.6	0.406
4.9	0.419

The standard correlation for predicting the overall void fraction in a packed bed of spheres was developed by Dixon (1988:707), and is described as follows:

$$\varepsilon = 0.4 + 0.05\frac{d_p}{D} + 0.412\left(\frac{d_p}{D}\right)^2 \tag{2.16}$$

Cheng (2011:261) noted that the average velocity increased when the bed aspect ratio was reduced and that different packing configurations lead to the porosity variation for the given aspect ratio. As seen in Figure 2-12, Cheng plotted various measurements of porosity, together with relevant formulas found in literature. Using the obtained data Cheng proposed the following correlation to describe the relationship between ε and the bed's aspect ratio (D/d_p) empirically.

$$\varepsilon = (\varepsilon_1^{-3} + \varepsilon_2^{-3})^{-1/3} \tag{2.17}$$

where ε_1 is an asymptote for small D/d,

$$\varepsilon_1 = 0.8\left(\frac{D - d_p}{d_p}\right)^{0.27} \tag{2.18}$$

and ε_2 approximates the D/d_p dependence for large D/d_p,

$$\varepsilon_2 = 0.38\left[1 + \left(\frac{d_p}{D - d_p}\right)^{1.9}\right] \tag{2.19}$$

Cheng (2011:261) also stated that the porosity in the near wall region, say, $D/d_p < 2$ may strongly depending on channel shape and the location of the peak porosity may vary.

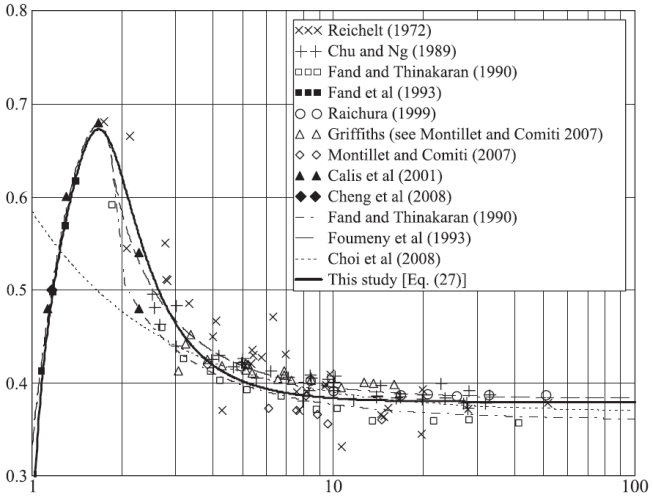

Figure 2-12. Variation of porosity with D/d_p (Cheng, 2011:261).

2.7.6 Porosity modelling approaches

2.7.6.1 Discrete approach (explicit)

The discrete approach takes voids and the particles into account explicitly. Any point $\vec{x}$ in the packed bed is either in a void or a particle (Du Toit, 2008:3073).

The porosity at the point is then given as:

$$\varepsilon(\vec{x}) = \begin{cases} 0, \textit{for the point in particle} \\ 1, \textit{for the point in a void} \end{cases} \tag{2.20}$$

Mueller (1992:69) identified that several sequential packing models are required to numerically construct packed beds of identical spheres in cylindrical containers. Mueller's numerical models ensure newly added spheres are placed on a base layer of spheres in the cylindrical container at a vertical location stable under gravity, therefore ensuring the sphere is either in contact with 2 spheres and the container wall (wall sphere), or three spheres in the container packing (inner sphere). The numerical model developed by Mueller determines the particular procedure by which the wall or inner spheres are added to the beds.

The centre coordinates of the spheres calculated by Mueller's sequential models are used to determine the packed container overall void fraction and radial void fraction. Muller generated beds with $D/dp > 3$ and verified the numerically generated beds with experimental data.

2.7.6.2 Continuum approach (implicit)

The commonly used continuum approach will typically employ Reynolds-averaged Navier-Stokes (RANS) codes where the effect of the spheres on velocities and temperatures are modelled. The continuum approach models pores and spheres implicitly, therefore not taking into account the detail of the flow around the spheres (Du Toit, 2008:3073).

Using the continuum approach at any point $\vec{x}$ in the packed bed, the porosity or void fraction is given as:

$$\varepsilon(\vec{x}) = f(\vec{x}) \; with \; 0 \leq f(\vec{x}) \leq 1 \tag{2.21}$$

2.8 Computational Fluid Dynamics (CFD)

2.8.1 Introduction to CFD

Computational fluid dynamics or CFD is the analysis of systems involving fluid flow, heat transfer and associated phenomena by means of a computer based simulation (Versteeg & Malalasakera, 1995:1). The increase of computational performance in recent years makes the simulation of packed beds with three-dimensional CFD time and cost effective. CFD applications to model fluid flow in a porous matrix are based on the numerical solution of the Navier-Stokes equations.

2.8.2 CFD and packed beds

CFD allows for the simulation of a packed bed in a completely explicit manner, taking into account the position of each sphere and its relative influence on the flow distribution and pressure drop in a packed bed. Various authors have used CFD simulation to model flow distribution in packed beds; Nijemeisland and Dixon (2001:231); Calis *et al*. (2001:1713); Romkes *et al*. (2003:3); Guardo *et al.* (2005:1733); Lee *et al*., (2007:2185); Wang-Kee In and Hassan (2008:2) and Atmakidis and Kenig (2009:404) simulated the flow distribution through structured sphere packings. McLaughlin *et al*. (2008:3); Reddy and Joshi (2008:444); Reddy and Joshi (2010:37); Atmakidis and Kenig (2009:404) and Eppinger *et al.* (2011:324) simulated the flow distribution through random sphere packings.

Logtenberg *et al.* (1999:7) used CFD to simulate 10 solid spheres in a tube with a tube-to-particle diameter ratio of 2.43, that included both particle-to-particle and also wall-to-particle contacts. Simulations were reported with heat generation from the spheres. Calis *et al*. (2001:1713) used a commercial CFD code (CFX-5.3) to predict the pressure drop characteristics of packed beds of spheres that have an aspect ratio of 1 to 2 with an average error of about 10%. The packed bed contained only 16 particles and three million cells were required to perform accurate simulations. To quote Calis *et al*. (2001:1713):

> *"It is anticipated that within five years from now the simulation of a packed bed containing a few hundred particles will be considered a 'standard' problem in terms of memory and calculation time requirements."*

Reddy and Joshi (2008:444) performed a CFD simulation of the single phase pressure drop in fixed and expanded beds at an aspect ratio of 5 and having 151 particles arranged in 8 layers. The sim-

ulations were performed in the creeping, transition and turbulent flow regimes, the Reynolds number ($d_p V_L \rho_L / \mu_L$) was varied from 0.1 to 10,000. Reddy and Joshi (2008:444) found that the deviations from Ergun's equation, due to the wall effects which are important in $D/d_p < 10$ beds, were well explained by the CFD simulations.

An increase in the pressure drop was observed due to the wall friction in the creeping flow, whereas, in turbulent regime, a decrease in the pressure drop was observed due to the channeling near the wall. Energy balance has been established through the CFD predicted values of energy dissipation rates (viscous as well as turbulent) (Reddy & Joshi, 2008:444).

Guo and Dai (2010:293) performed CFD simulations to investigate and analyse the local flow and heat transfer in a 120-sphere random packed bed. Detailed temperature field information was obtained. Inhomogeneity of flow and heat transfer due to the non-uniform distribution of void fraction were discussed and analysed.

Eppinger *et al.* (2011:324) performed CFD simulations for aspect ratios of $3 \leq D/d_p \leq 10$ in the laminar, transitional and turbulent flow regime which were compared with results from literature concerning porosity and pressure drop. The simulations were performed by generating a random fixed bed with a DEM-code. The fluid domain was meshed with the commercial CFD code STAR-CCM+® with the complete simulation process automated, ensuring large amounts of data could be obtained in a short period.

From the literature it is evident that the increase in computational performance in recent years, has steadily pushed the boundaries and limitations in the simulation of packed beds using CFD codes.

The various key modelling issues noted by; Eppinger *et al.* (2011:324), Guo and Dai (2010:293), and Reddy and Joshi (2008:444) are:

- Contact points;
- Mesh generation;
- Transition from a laminar to a turbulent flow regime; and
- Turbulence models.

The approaches adopted by various authors to overcome the above-mentioned modelling issues will be discussed next.

2.8.3 Contact points

The complex geometries created due to the packing structure of the beds produce various modelling issues that need to be addressed to ensure that high quality computational meshes are created, to in turn ensure accurate and time efficient simulations.

A crucial point for the mesh generation is the cell quality at contact points. These cells are either highly skewed, which could lead to convergence problems during the calculation, or the mesh is highly refined in this area, which increases the number of cells and as a direct consequence the computational time (Eppinger *et al*., 2011:324).

Various techniques of contact handling were used throughout the literature to ensure reliable numerical simulations. Calis *et al*. (2001:1713) and Nijemeisland and Dixon (2001:231) showed that by introducing a gap at the point of contact between spheres, mesh generation quality is increased. The gap is created by reducing the spheres to 99% of their size after generation of the packed beds. These authors confirmed that the fluid velocity in the created gaps is practically zero. Romkes *et al*. (2003:3); Reddy and Joshi (2008:444); Reddy and Joshi (2010:37); Atmakidis and Kenig (2009:404) and Augier *et al.* (2010:1059) also shrank spheres by 1% or 2%. Shrinking the spheres removes the contact points and cells are generated between the spheres. However, the shrinking of the spheres reduces the solid fraction and therefore the porosity. In a subsequent step, porosity and pressure drop were corrected.

Guardo *et al.* (2005:1733) suggested an increase in the size of the spheres. The increase in sphere size changes the contact points to contact lines or areas and the skewness of the cells is reduced. This method also needs a subsequent correction of the values for porosity and pressure drop.

McLaughlin *et al.* (2008:3) and Reyneke (2009:38) bridged the spheres with small cylinders if the distance between the particles fell below a predefined value.Wang-Kee In and Hassan (2008:2) employed direct area contacts by reducing the pitch between the spheres. These methods also avoided highly skewed cells or a large number of cells and it was shown that macroscopic flow properties such as the pressure drop were not influenced by the addition of the small cylinders at contact points. No information was provided concerning the influence on porosity.

Eppinger *et al.* (2011:324) created gaps at the contact points by flattening the particles locally in the contact region as soon as the minimum distance between two surfaces fell below an adequate and predefined value. The gap between the particles allowed the generation of fluid cells. Due to

the fact that the velocity near the contact points was very low, the number of cells in the gap were also kept low, see Figure 2-13.

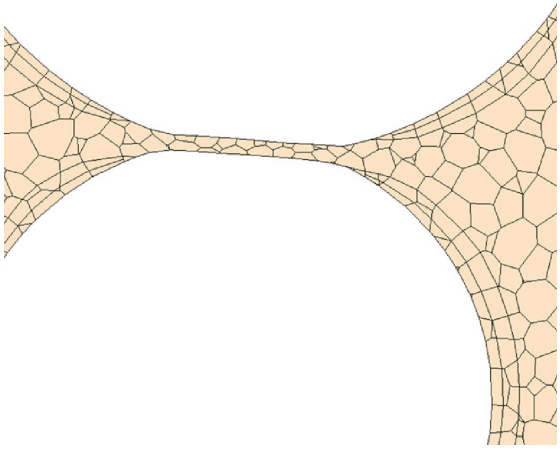

Figure 2-13. Artificial gap between two spheres (Eppinger *et al.*, 2011:326).

From the literature it is clear that the most practiced method of contact point correction is the reduction in sphere size. The gap allows a computational mesh containing less nodes/elements and is less resource intensive. The method however reduces the solid fraction and therefore the porosity and pressure drop must be corrected. This can be overcome by using the method of flattening the particles locally in the contact region or by bridging the spheres with small cylinders, thus minimizing the effect on porosity and overall characteristics of the packed bed.

Lee *et al*. (2007:2194) simulated the effects of the treatment of the contact between pebbles in a packed bed. Numerous differences in the flow fields and heat transfer were found in cases using the gap approximation. Dissimilar distributions were found in local heat transfer as well as in the flow regime. The modelling of the direct contact resulted in the generation of additional hot spots on the pebble surface where the local temperatures were significantly higher than those of the other regions. Large vortices were generated in the vicinity of the contact regions, due to the blockage of the coolant flow, and this finally caused a decrease of the local heat transfer in these regions. Lee *et al*. (2007:2194) noted that when applying a gap approximation to a packed bed, the results were meaningful enough by themselves from the viewpoint of the pure flow effect on the packed bed geometry.

From the results of the study by Lee *et al*. (2007:2194), it is evident that the treatment of the contacts among the pebbles with approximated gaps may give inaccurate information about the local flow fields and heat transfer.

2.8.4 Mesh generation

Calis *et al*. (2001:1713) and Dixon *et al*. (2011:1174) both implemented layers of prism cells on the column walls and spheres and improved the mesh generation quality by specifying a fixed size on the surfaces of the spheres and specifying a growth rate which controls the rate at which the mesh size increases from the sphere surfaces. The optimum mesh size was then determined during a grid-independence study.

The momentum boundary layer was estimated from the relation (Dixon *et al*., 2011:1174):

$$\frac{\sigma_{bl}}{d_p} = 1.13\,Re^{-0.5} \tag{2.22}$$

Reddy and Joshi (2008:444) described unstructured tetrahedral mesh generation of packed beds as a complex task due to triangulation, in which elements are created to resolve sphere-to-sphere and sphere-to-wall contact points. Reddy and Joshi (2008:444) found that the triangle faces of the tetrahedral degenerate at the contact points. They overcame the issue by specifying a minimum angle allowed in triangulation. Reddy and Joshi (2008:444) considered a high quality mesh to have a skewness of < 0.7.

2.8.4.1 Thin Mesher

Preller (2011) performed tests on the thin mesher available in STAR-CCM+® and its influence on mesh density. The tests ranged between 0.2 mm and 1.5 mm cell surface sizes. The results obtained by Preller showed that by specifying two prism layers, the ratio between the number of cells and skewed cell volume was at its most efficient. When specifying a minimum surface size of 0.75 mm with two prism layers Preller found that the number of skewed cells was reduced by 4.5 times compared to a normal polyhedral mesh. It was also noted that a normal polyhedral mesh would require 8.5 times more cells in the contact region to achieve the same volume of skewed cells compared to the thin mesher with two prism layers. Figure 2-14 shows the volume of skewed cells vs. the size of the mesh generated by Preller.

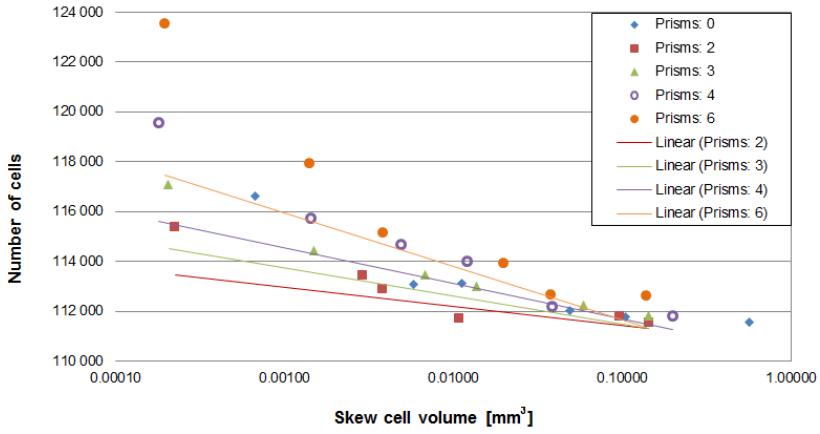

Figure 2-14. The volume of skew cells vs. the size of the mesh generated (Preller, 2011).

2.8.5 Turbulence modelling

Turbulence creates disorder and an irregular flow field and typically occurs when high velocity gradients are present in fluids. Turbulence is diffusive, dissipative and has high Reynolds numbers (CD-ADAPCO, 2011:2539).

The following basic approaches to modelling turbulence in packed beds are found in the literature:

- Models that provide closure of the Reynolds-averaged Navier-Stokes (RANS) equations:
    - Spalart-Allmaras model (One-equation model);
    - k - ε type models (Two-equation models); and
    - k - ω type models (Two-equation models).
- Large eddy simulation (LES).

2.8.5.1 Wall functions

High velocity gradients are present in the near wall region and generally require excessive mesh refinement. The refined mesh can greatly increase computational time. An alternative to mesh refinement is to use wall functions. The thickness of the wall cells is expressed in the value of y^+, which in the case of standard wall functions should preferably be between 30 and 300 or at least between 10 and 1000 to produce accurate results (Calis *et al.*, 2001:1717). Meeting the y^+criterion everywhere on the sphere surface is difficult due to large deviations of the local velocity near the solid surfaces because of stagnant zones near the points of contact between spheres. Calis *et al.* (2001:1717) noted that the flow should be well developed in order for the standard wall model to

be valid. However, this is most likely not fully met in the case of a packed bed. These factors will introduce a systematic error in the simulated pressure drop characteristics that is hard to initially assess.

2.8.5.2 Turbulence models used for packed beds

In turbulence modelling (RANS) the large and small scale turbulent structures are modelled so that the mesh refinement that is required for direct numerical simulation is not needed. Averaging the governing equations includes the following flow variables: time, ensemble, spatial and mass averages.

Calis *et al*. (2001:1717) used the k - ε (because it is the most widely used turbulence model) and Reynolds stress (RSM); (because isotropic turbulence, assumed in the k - ε model, may not be valid in the considered geometries) turbulence models to model turbulence in structured beds. The simulated Re_{dp} ranged up to 5 x 10^4.The y^+ criteria for wall functions and y^+ values ranged from 4.4 at Re_{dp} = 1 x 10^3 to 440 Re_{dp} = 1 x 10^5. The RSM turbulence models yielded only slightly different pressure drop results from the k - ε turbulence model. The difference was considered too small to justify the extra computational demand of the RSM model.

Guardo *et al.* (2005:1733) investigated the influence of various turbulence models on the wall-to-fluid heat transfer in a packed bed. They noted that it is of paramount importance to determine the most adequate turbulence models in packed bed simulations. Table 2-3 shows the summarised RANS turbulence models used in their study. The study used a column with a homogeneous packing of 44 spheres in 4 layers. The simulations were performed in a Reynolds range from Re_{dp} = 1 x 10^2 to Re_{dp} = 1 x 10^3.

Guardo *et al.* (2005:1733) found the y^+ values obtained by their mesh were in the range of 0.2 < y^+ < 20 making the mesh inadequate for the application of wall functions. All the models correlated well with the theoretical pressure drop proposed by the Ergun (1952) equation. It was found that the results obtained with the Spalart-Allmaras turbulence model were better aligned than the two-equation RANS models. The results obtained in the transition regime and low Re numbers were found to be inaccurate and showed slower convergence times when turbulence models were used.

CD-ADAPCO (2011:2539) notes that the Spalart-Allmaras models for RANS equations are not suited to accommodate flows that are dominated by free-shear layers, flows where complex recirculation occurs (particularly with heat transfer), or natural convection.

Table 2-3. Turbulence models referenced by Guardo *et al*. (2005:1733).

Model:	*One-equation models*	*Two-equation models*			
	Spalart–Allmaras	*Standard k - ε*	*RNG k - ε*	*Realizable k - ε*	*Standard k - ω*
Reference as quoted by Guardo *et al*. (2005:1733)	Spalart and Allmaras (1992)	Launder and Spalding (1974)	Choudhury *et al*. (1993)	Shih *et al*. (1995)	Wilcox (1998)
Features:	Uses a differential partial equation for the turbulent velocity scale. The turbulent quantity modelled is the effective viscosity.	Uses one differential equation for the turbulent velocity scale and another for the turbulent length scale. The variables modelled are the turbulent kinetic energy, k, and the rate of dissipation of turbulent kinetic energy.	This model is derived from the instantaneous Navier–Stokes equations, using the "renormalisation group" (RNG) methods. This results in a model with constants different from those in the standard k - ε model, and additional terms in the transport equations.	The term "realizable" means that the model satisfies certain mathematical constraints on the normal stresses, consistent with the physics of turbulent flows. It adopts a new eddy-viscosity formula and a new model equation for dissipation (ε).	This model is based on model transport equations for the turbulence kinetic energy *(k)* and the specific dissipation rate *(ω)*, which can also be thought of as the ratio of ε to k. Production terms have been added to the model equations.

McLaughlin *et al*. (2008:6) and Wang-Kee In and Hassan (2008:3) used the standard k - ω and shear-stress transport k - ω models for packed bed turbulence. The simulated pressure drop, for both the turbulence models aligned with the theoretical pressure drop and fell within the error bounds of the pressure drop correlation. McLaughlin *et al*. (2008:7) noted that both the standard k - ω and shear-stress transport k - ω turbulence models are suitable for pressure drop simulations in packed beds.

Preller (2011) performed a study on the influence of the various turbulence models on packed beds and their relation to pressure drop through the packing. Preller's study outcome was used as the determining factor to which turbulence model was most applicable in this study.

From the literature, it is evident that the majority of RANS turbulence models are accurate enough when used to model pressure drop through packed beds (Comparison between pressures obtained from simulations based on RANS turbulence models and pressure drops predicted using correlations compared well). General consensus is that resource intensive models offer little improvement in accuracy over the simpler models.

2.9 Pressure Drop

The design of a packed bed structure relies heavily on the calculation of pressure drop through packed beds (Du Toit, 2008:3073). Due to the importance of pressure drop through packed beds, studies over many decades have been carried out on the bed porosity due to the packing structure and the related pressure drop.

The first differential equation developed to describe the flow distribution inside a porous medium bounded by rigid walls was done by Brinkman (*in*: Vortmeyer & Schuster, 1983:1692). Brinkman developed the differential equation by extending Darcy's law to account for the viscous forces near the walls. The Brinkman equation governs the flow inside a porus medium.

Blake (1922) (*in*: Ergun, 1952:90)established a pressure drop calculation method that makes use of the hydraulic diameter concept. Blake suggested that the dimensionless groups f_k and Re_m should be used to characterize the pressure loss due to the particulate system for various mass-flow rates.

f_k is recognized as the Darcy-Weisbach friction factor for pipe flow and Re_m the modified Reynolds number, where both terms are calculated by using the hydraulic diameter of a packed bed of spheres in terms of the average porosity $\bar{\varepsilon}$. The model assumes an average porosity and a uniform velocity profile are used throughout.

The general form of the friction factor developed by Blake is given as:

$$\phi = \frac{A_e}{\frac{Re_{dp}}{(1-\bar{\varepsilon})}} + \frac{B_e}{\left[\frac{Re_{dp}}{(1-\bar{\varepsilon})}\right]^{2-n}} \tag{2.23}$$

where values of A_e and B_e are empirically determined constants.

Eisfeld and Schnitzlein (2001:4321) give the particle Reynolds number Re_{dp} as:

$$Re_{dp} = \frac{\rho_0 v_0 d_p}{\mu_0} \tag{2.24}$$

for $Re_{dp} < 10$ flow is laminar, for $10 < Re_{dp} < 300$ flow is in the transition region and for $Re_{dp} > 300$ flow is turbulent. (Ziolkowska & Ziolkowski, 1988, as quoted by Eisfeld and Schnitzlein, 2001:4321).

Van der Walt (2006:18) noted two variations on the general form of the friction factor developed by Blake. Firstly, the constant n can be taken as 2, as originally proposed by Reynolds (as quoted by Ergun, 1952:91). This is generally known as the Ergun-type equation, which is most frequently encountered in the literature and is the most common variation. The second variation is where 1.9

$< n <$ 1.95, as proposed by Carman (1937), and is therefore generally known as the Carman-type equation.

2.9.1 Carman-type equations

The KTA equation was developed by a German research group to calculate the pressure drop through high temperature reactor (HTR) pebble bed cores over a very large range of Reynolds numbers (Kern Technisches Ausschuss, KTA, 1981, as quoted by Van der Walt, 2006:18).The KTA equation is a Carman type equation.

Van der Walt (2006:18) noted that the following assumptions were made when the KTA equation was developed

1. The influence of the walls on the pressure drop must be negligible. Based on various experimental investigations of various authors, the research team chose data points at bed-to-particle diameter ratios and Reynolds numbers where the influence of the walls was negligible. By plotting the bed-to-particle diameter ratio to the Reynolds number they were able to draw a curve which indicates the lower limit of the range for which the influence of the walls is negligible. The theoretical basis for this curve is, however, not clear from the KTA report.

2. The bed length was larger than 4 particle diameters.

3. Only correlations developed for unstructured (randomly packed) beds were investigated.

4. Only experiments with particles larger than 1 mm diameter were considered.

2.9.2 Ergun type equations

Correlations to predict overall void fraction for use in global prediction of pressure drop such as the Ergun equation, depend on the fluid properties, porosity (fractional void volume), orientation, size, shape and surface of the particles. Ergun (1952:89) developed an empirical correlation to predict the pressure loss per unit bed length of a packed bed. In his investigation he found that the pressure loss is simultaneously caused by both kinetic and viscous energy losses. Ergun discovered that these energy losses strongly depend on the porosity of the bed, with the viscous energy loss being proportional to $\left(1-\bar{\varepsilon}\right)^2/\bar{\varepsilon}^3$ while the kinetic energy loss is proportional to $\left(1-\bar{\varepsilon}\right)/\bar{\varepsilon}^3$.

The Ergun equation combines the Kozeny-Carman Equation, valid for laminar flow, and the Burke-Plumber Equation, valid for turbulent flow (Ergun, 1952:89).

$$\frac{\Delta P}{H} g = \frac{150(1-\varepsilon)^2}{\varepsilon^3} \frac{\mu v_0}{d_p^2} + 1.75 \frac{1-\varepsilon}{\varepsilon^3} \frac{\dot{m} v_0}{d_p} \tag{2.25}$$

The terms in the Ergun equation are defined as follows: ΔP, is the pressure drop over the bed, H is the height of the packing material, g is the gravitational constant, ε is the void fraction, μ is the fluid viscosity, v_0 is the superficial velocity measured at average pressure, d_p is the effective particle diameter and $\dot{m}$ is the mass flow rate of fluid. Ergun's correlation was derived at modified Reynolds numbers $\mathrm{Re}_m < 10^3$. The Reynolds number is a dimensionless quantity which is used to determine whether fluid flow is laminar or turbulent.

Eisfeld and Schnitzlein (2001:4321) performed a detailed analysis of investigations into pressure drop and the influence of the container walls which lead to a detailed analysis of more than 2300 experimental data points. Observation showed that the variation in flow behaviour at the wall region was caused by the counteracting effects of the wall friction and the increased porosity near external boundaries. Comparison of 24 predictions determined through published pressure drop correlations with available experimental data showed that correction of the Ergun equation for the wall effect, known as the Reichelt's approach (Reichelt, 1972:1068), was the most promising for Reynolds numbers of $0.01 \leq \mathrm{Re} \leq 17635$, tube-to-particle diameter ratios of $1.624 \leq D/d \leq 250$, and a mean voidage of $0.330 \leq \varepsilon \leq 0.882$. Improvement in existing correlations for spheres, cylinders, and for all types of particles independent of their shape were acquired for different types of packings by fitting the coefficients of the equation to the database developed from the 2300 experimental data points.

Van der Walt (2006:18) noted that the correlation of Reichelt (1972) predicts a significant influence of the walls on the pressure drop for bed-to-particle diameter ratios lower than 10, contrary to the assumption made in the KTA correlation.

In Figure 2-15 Eisfeld and Schnitzlein (2001:4321) gave the ratio of pressure drop of a finite packing, $\Delta p_f = \Delta p(D/d_p)$ to pressure drop of an infinite packing $\Delta p_{\mathrm{inf}} = \Delta p(D/d_p \rightarrow \infty)$ versus aspect ratio, according to the Reichelt dimensionless pressure drop (Equation (2.24)) at a mean void fraction of $\varepsilon = 0.4$.

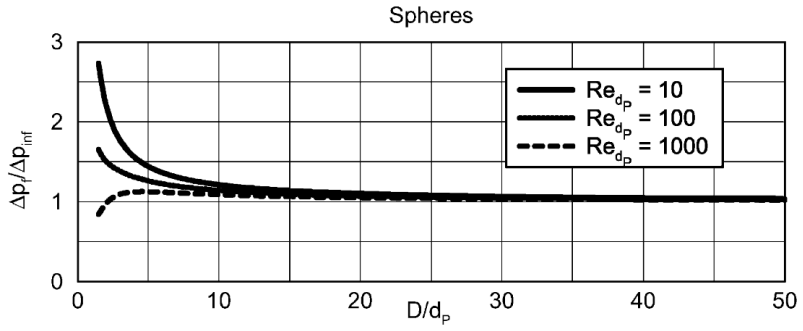

Figure 2-15. $\Delta p_f/\Delta p_{\text{inf}}$ v.s α, Eisfeld and Schnitzlein (2001:4321)

From Figure 2-15 it is clear that the influence of the particle Reynolds number Re_{dp} on the pressure drop is increased exponentially at low aspect ratios ($\alpha < 10$) when the wall effects are dominant in the packing, at $Re_{dp} > 1000$ the effects are the opposite.

2.10 Velocity Distribution

Reyneke (2009:38) noted that velocity distribution through a randomly packed bed depends on; the porosity distribution of the bed, the Reynolds number, particle diameter to inner cylinder radius ratio, and the length of the bed.

As noted in Section 2.7.3 porosity in packed beds vary sharply in the near-wall regions. White and Tien (1987:291) found that the increase in porosity at the wall region distorts the velocity distribution causing higher velocities at the near-wall regions. This is known as the flow-channelling phenomenon. The effect of the wall on the packing structure and the influence of the variation in porosity on the velocity distribution is shown in Figure 2-16.

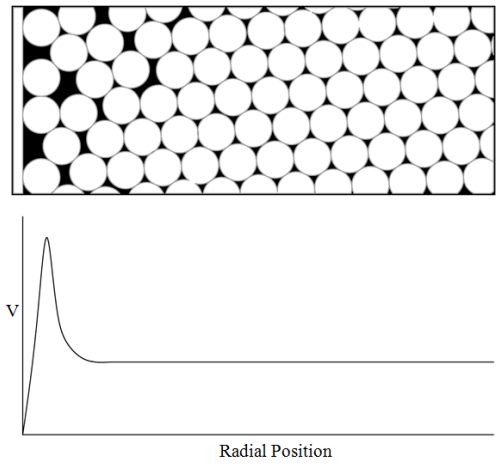

Figure 2-16. Velocity distribution due to wall interface (Reyneke, 2009:38).

Eppinger *et al.* (2011:324) investigated the velocity distributions for a range of low aspect ratio packed columns. They found that for all investigated particle Reynolds numbers ($1 < Re_{dp} < 1000$) and all aspect ratios ($1 < \alpha < 8$) the highest velocities were found in the near wall region (highest porosity). They also found that at an aspect ratio of eight remarkably high velocities were found at the middle axis due to a channel formed by the packing. The simulated circumferential-averaged axial velocity profile by Eppinger *et al.* (2011:324) is shown in Figure 2-17.

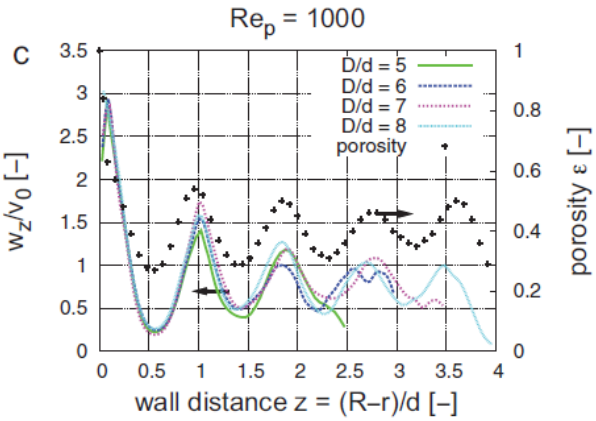

Figure 2-17. Circumferential-averaged axial velocity profiles (Eppinger *et al.*, 2011:329).

2.11 Conclusion

The literature survey aimed to provide a fundamental understanding of previous research. The initial stages of the survey focused on the general analysis of low aspect ratio packed beds. The study found that multiple authors had investigated low aspect ratio packed beds. It was found that DEM allowed authors to generate mechanically stable randomly packed 3D beds and with the increase in computational power in recent years it was possible to effectively use DEM and CFD codes.

Influential factors at low aspect ratios were then investigated, the factors were: packing, DEM, porosity, CFD and flow distribution. It was found that multiple reproducible packing arrangements were possible at low aspect ratios. It was also noted that within specific ranges the reproducibility of packing arrangements was lost.

The DEM research confirmed that DEM is an appropriate tool for simulation of packed bed arrangements. The Hertz Mindlin and Deresiewicz no-slip model, which uses a classical mechanics method and is based on the soft-particle formulation where particles are allowed to develop an overlap (dashpot) taking into account viscous damping and repulsive forces pushing particles

apart, is best suited to simulate packed beds. The model was also noted to be available in STAR-CCM+®.

The porosity research found that radial porosity variation was well documented in the literature and that porosity variation in the axial direction was rarely mentioned. At low aspect ratio packings the variation in the axial direction was found to be of importance as noted in Section 2.7.3.

The CFD literature study showed that low aspect ratio packings were predominant in literature as the CFD meshing and simulation was resource-intensive and the complex geometries associated with packed beds increased exponentially as the number of particles were increased. The contact points, mesh and turbulence models were deemed to be critical to the accuracy of the simulations.

The pressure drop study found that the that correction of the Ergun equation for the wall effect, known as the Reichelt's approach (Reichelt, 1972:1068), was the most promising correlation to correlate pressure drop for Reynolds numbers of $0.01 \leq Re \leq 17635$, tube-to-particle diameter ratios of $1.624 \leq D/d \leq 250$, and a mean voidage of $0.330 \leq \varepsilon \leq 0.882$.

The velocity distribution literature survey found that an increase in porosity at the wall region distorts the velocity distribution causing higher velocities at the near-wall regions (flow-channelling).

The literature survey therefore provided a a fundamental understanding of previous research and highlighted the most influential factors in the analysis of packed beds. The next chapter will define a methodology to setup both DEM and CFD simulations in STAR-CCM+®.

3 Method

3.1 Introduction

The method chapter will summarise, describe and discuss the methods and steps required to perform the hydraulic analysis of a packed bed using numerical techniques. STAR-CCM+® was chosen as the core code to perform the analysis due to its ability to simulate both the packing of a cylinder and the associated flow field and pressure drop. The general methodology outline is shown in Figure 3-1.

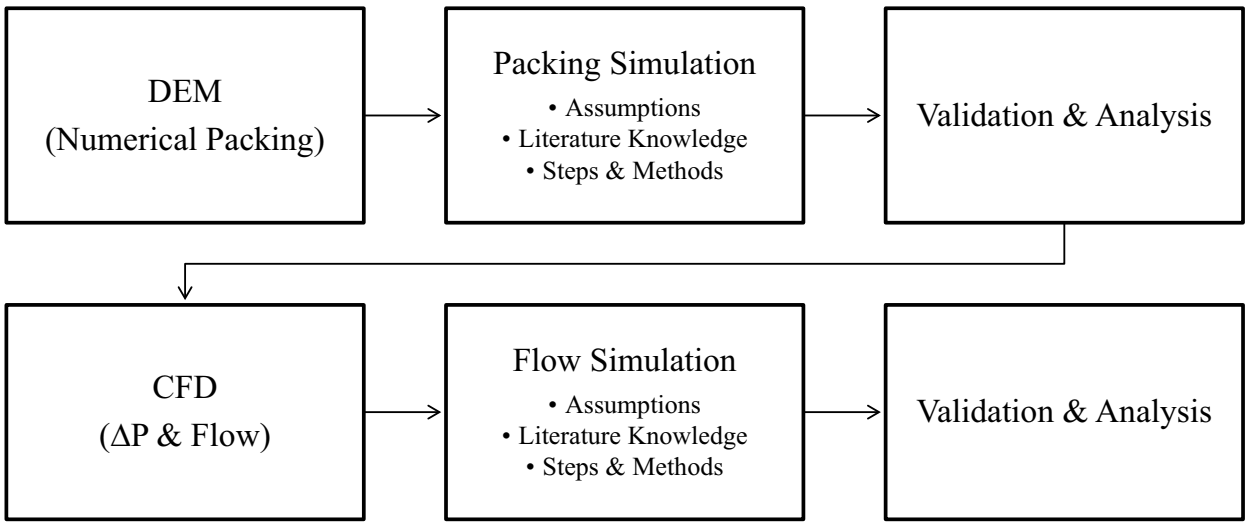

Figure 3-1. Methodology

The study followed a logical order with each successive step building on results from the previous.

3.2 DEM Setup

The accurate numerical simulation of particle packing in a cylinder using the DEM method in STAR-CCM+® depended greatly on the simulation setup.

This section will discuss the general setup steps required to ensure accurate simulation of a packing consisting of uniform spherical particles in a column.

The setup of a DEM numerical model in STAR-CCM+® required the following steps:

- A base CAD (Computer Aided Design) model to define the column boundaries;
- Assigned regions;
- Definition of the surface and volume mesh;
- Contact model (Hertz Mindlin);
- Material and geometric properties (column and spheres);
- Reference values (gravity);
- Injector specifications;
- Solver parameters and stopping criteria; and
- Result visualisation and extraction.

The critical steps will be discussed with regard to packing columns with uniform sized spherical particles and take into account knowledge and assumptions presented in the literature survey.

3.2.1 CAD model

The first step required the column geometry to be defined in STAR-CCM+®. This was done by importing a model prepared previously in Solid Works® 3D CAD 2011. The CAD model was defined as a solid cylinder with its diameter equivalent to the inner diameter of the experimental setup by Roslee (2009), and the column height was determined by the number of particles in the packing. To ensure the column was able to hold the defined number of particles, the column specified height H was 2 particle diameters longer than the expected packing height determined in the experimental setup.

> **Note:** When the parasolid (*.x_t) was exported from the CAD model, the resolution was set to a maximum value, this ensured the imported geometry surfaces were closed, manifold and triangulated with near equal sized triangles.

3.2.2 Assigned regions

Discretisation of the CAD model was done by splitting the column surfaces into parts; namely wall, inlet, and base and assigning parts to regions. The mesh could then be generated for the assigned regions.

3.2.3 Surface and volume mesh

A surface mesh consists of faces (triangles) and vertices that discretise the geometry of the individual regions that are used for the volume mesh generation.

A volume mesh is created from an enclosing surface. The core volume mesh can contain either trimmed, polyhedral or tetrahedral type cells for each mesh region, determined via the selection of mesh models. When considering a mesh for a DEM simulation, the fluid solution is not of particular importance, therefore a relatively coarse mesh can be used, with a base size generally one quarter the size of the defined particles. For DEM simulations, the surface re-mesher and polyhedral volume mesher were used.

3.2.4 Physics models

The DEM Model in STAR-CCM+® is activated by selecting the Lagrangian multiphase and implicit unsteady model, which will be discussed next.

3.2.4.1 Lagrangian multiphase model

A Lagrangian multiphase model indicates a Lagrangian/Eulerian framework for multiphase simulation (CD-ADAPCO, 2011:2439).

Conservation of mass, momentum and energy is taken into account in the model. The flow of particles is governed by the momentum conservation equation, and convective heat transfer is governed by the energy conservation equation. Specific models include a mass conservation equation to account for the change in mass due to evaporation or condensation within particles.

Defining a Lagrangian multiphase model requires the initial conditions of each particle, namely how and where they are introduced into the simulation, to be defined. This is done by the injectors.

If the flow of the continuous phase is laminar, a parcel/particle released from a point at a given instance will follow a smooth, unique trajectory. i.e. the motion is deterministic. On the other hand, parcels introduced into a turbulent carrier flow will each have their own random path due to interaction with the fluctuating turbulent velocity field.

DEM particles are handled differently from Lagrangian particles, for a Lagrangian phase (material and massless particle types) the parcel can represent many particles at once or a fraction of a particle only. For DEM particles the parcel always represents a single particle. This should be noted

when setting up a particle injector as the Lagrangian injectors are used to initialise the DEM particles.

3.2.4.2 Implicit unsteady model

The implicit unsteady model in STAR-CCM+® is a time model and it is the only unsteady model available with the Segregated Flow and Segregated Fluid Energy models. It uses the Implicit Unsteady Solver of which the primary function is to calculate and control the update at each physical time for the calculation. It also controls the time-step size.

3.2.4.3 Additional physics model specification

In addition to the compulsory physics models required for DEM simulation, additional models were selected that are dependent on the materials and properties of the experiments performed. The following are dependent on the simulation characteristics:

- Material group, i.e. gas flow, liquid flow;
- Equation of State, i.e. constant density, ideal gas; and
- Viscous Regime, i.e. laminar, inviscid.

3.2.5 Contact model

As discussed in Section 2.5.4 the Hertz Mindlin no-slip contact model was used to model the sphere packing.

3.2.6 Material and geometric properties

Both the spheres and the column walls were simulated with properties of Poly Methyl Methacrylate (PMMA), commonly known as acrylic glass. The material properties are similar to the material used in the experimental studies done by Roslee (2009). The material properties are shown in Table 3-1.

Table 3-1. PMMA material properties.

Mass density	1190 kg/m^3
Young's modulus	2500 MPa
Poisson ratio	0.37

3.2.7 Particle injection

The initial conditions of each particle, namely how and where they are introduced into the simulation, are defined by injectors. An injector setup for DEM particles is based on the Lagrangian methodology mentioned in Section 3.2.4.1 and represents parcels as a single particle.

When setting up an injector, the particles are injected into the system stress-free to ensure the overlap assumptions of the contact model are not violated. The flow rate of particles is therefore limited to a finite maximum value that depends on particle diameter, injection velocity and distribution, as well as the unsteady iteration time.

A surface injector is used to initialise the spherical particles. The rate at which the spheres are dropped into the column is defined by the mass or mass flow rate of each sphere (parcel). The defined mass flow is scaled by A_f/A_s, where A_f is the area of the face through which the sphere enters and A_s is the total area of the surface injector.

When defining a particle injector for a packed column, the injector is set up to create spheres at the inlet surface. The spheres were injected at a mass flow rate that ensures a single sphere is dropped every second, therefore the mass flow rate is calculated as a function of the sphere radius [r] and density [ρ].

$$\dot{m} = \frac{4}{3}\rho\pi r^3 \tag{3.1}$$

3.2.8 Particle interactions

Particle interactions are defined by specifying a phase pair, which consists of a first and second phase. The first phase selects the interacting Lagrangian phase (e.g. sphere-to-sphere), the second phase selects the second interacting Lagrangian phase which can include a Lagrangian phase, boundary type, or specific boundary (e.g sphere-to-wall).

3.2.9 Solver parameters & stopping criteria

3.2.9.1 Time Scale

The DEM simulation is of a transient/dynamic nature, therefore a solver time-step and elapsed time was set.

To ensure time independence is achieved the maximum time-step allowed for a DEM particle is constrained by the assumption that the force acting on a particle is only affected by the particle's immediate neighbours during a single time-step duration. The time-step is therefore limited by the time it takes the Rayleigh wave to propagate across the surface of the sphere to the opposite pole (Johnson, 1985:4).

In all materials there is an ultimate wave speed. This is called the Rayleigh wave speed and is dependent on the mobility of particles in the material. Sound in a material travels at the Rayleigh wave speed. Until the early 1990's it was theorized that the maximum propagation speed for cracks in a material should be the Rayleigh wave speed. This makes sense because the Rayleigh wave speed depends on particle mobility, and cracks of course also depend on particle mobility.

This means our cracks should be able to approach the speed of sound in the material. The Rayleigh wave speed in a material is calculated by the equation:

$$V_{\text{Rayleigh}} = \sqrt{\frac{E}{\rho}} \tag{3.2}$$

where E is Young's modulus of elasticity and ρ is the density of the material. The calculated Rayleigh wave speed for our PMMA is 1614 m/s. The time step size is given as:

$$t_0 = \pi \frac{R_p}{V_{\text{Rayleigh}}} \tag{3.3}$$

The Rayleigh wave velocity depends on material properties. An additional factor that needs to be taken into account is the duration of impact of two perfectly elastic spheres:

$$t_1 = 2.94\left(\frac{5\sqrt{2\pi\rho}}{4}\frac{1-v^2}{E}\right)^{\frac{2}{5}} \frac{R}{5\sqrt{v_{im}}} \tag{3.4}$$

In order to resolve the collisions, a minimum of 10 time-steps is required for collision resolution (Johnson, 1985:8).

The final restriction on a DEM particle time-step is geometric in nature. It is based on the assumption that particles should not move too far within the time-step. This prevents missing contacts

between DEM particles, particles and walls. Therefore, each particle is constrained such that it takes at least 10 time-steps for the particle to move the full length of the radius.

$$t_2 = \left(\frac{r}{v_p}\right) \tag{3.5}$$

The final particle time-step is determined as a minimum of t_0, t_1 and t_2. In practice t_0 is typically the limiting factor while t_1 and t_2 only constrain particles that are moving fast, or the material's Young's Modulus is set very low in order to accelerate the simulation (Johnson, 1985:8).

To ensure accuracy and quick solution time (low processing times) a time step of 0.01 seconds was defined in this study, with an elapsed time long enough to ensure a stable packing was achieved. The simulation was considered complete when all the particle velocities were below $1e^{-4}$ m/s.

3.2.9.2 Coupled implicit solver

No fluid flow effect was taken into account in the DEM simulation, therefore the coupled implicit solver was frozen.

3.2.10 Result visualisation & extraction

The column packing is visualized through a scalar scene. The scene is setup to display the velocity of each particle. Once all the particles are dropped and the velocity of each particle is virtually zero $V < 1e^{-4}$ m/s, the simulation is considered to have reached a steady state (see Figure 3-2).

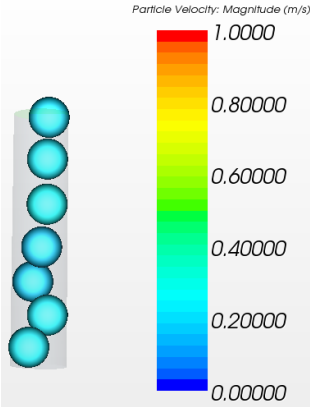

Figure 3-2. Scalar scene displaying the particle velocity

The centre position of each sphere given in X,Y,Z cartesian coordinates were extracted when the DEM simulation was completed. CAD beds were generated in Solid Works® 3D CAD 2011, using the sphere centre positions. A cavity of the packed spheres was created in Solid Works® 3D CAD

2011 as seen in Figure 3-3 and exported back to STAR-CCM+® as a surface mesh for further flow analysis.

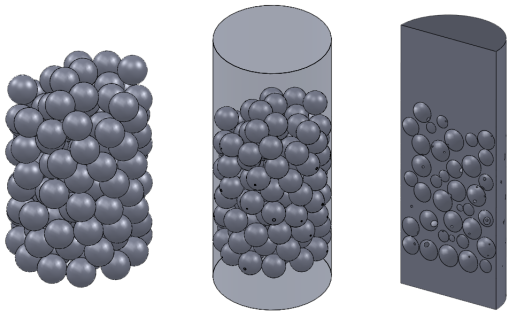

Figure 3-3. Particle positions imported into Solid Works® 3D CAD 2011.

3.3 DEM Validation

3.3.1 Introduction

Porosity is defined in Chapter 2 as the ratio between the void volume and the total volume, also known as the void fraction (Liu *et al*., 1999:438). The resulting porosity of the DEM packed bed is dependent on the surface roughness, the manner of packing and the column aspect ratio.

3.3.2 Validation of bed porosity

The DEM validation was done by comparing the global bed and axial porosity distribution with results obtained from the literature and experimental data. The radial porosity is less important in low aspect ratio beds due to the small column diameters.

The axial porosity variation of the numerically generated beds were extracted using an axial porosity code developed by Du Toit (2008). The code uses an area-based porosity calculation by creating individual cross sections that determine the surface area occupied by void spaces and solid particles in the axial direction of the packed column. The axial porosity $\varepsilon(z)$ at level z is given as:

$$\varepsilon(z) = 1 - \frac{\Sigma A_{iz}}{A_c} \tag{3.6}$$

where A_c is the cross-sectional area of the cylinder at level z and A_{iz} the area of the cross section of the sphere i in the plane z given as:

$$A_{iz} = \pi[r_p^2 - (z_i - z)^2] \quad \text{for} \quad |z_i - z| < r_p \tag{3.7}$$

where r_p is the radius of the spheres.

The empirically derived formula by Cheng (2011:261) which describes the relationship between $\bar{\varepsilon}$ and the beds aspect ratio (D/d_p) was used to validate the packing.

3.4 CFD Setup

3.4.1 Introduction

The analysis of pressure drop can be considered a fluid–particle interaction problem, where the spherical packed columns generated by the DEM method are imported into a computational fluid dynamics code and the analysis of the fluid interaction with the packed spheres is determined using predetermined physics models.

The accurate numerical simulation of pressure drop and velocity distribution in STAR-CCM+® depended greatly on the simulation setup.

This section will discuss general setup and steps required to ensure accurate simulation of pressure drop through packed spherical particles in a column.

The setup of a CFD numerical model in STAR-CCM+® required the following:

- A base CAD model to define the column boundaries and spherical particles;
- Assigned regions (spilt boundary by patch);
- Assigned boundary conditions;
- Defined surface and volume mesh;
- Defined physics models;
- Reference values;
- Initial conditions;
- Solver parameters and stopping criteria; and
- Result visualisation and extraction.

The critical steps will be discussed with regard to pressure drop through packed columns with uniform sized spherical particles and take into account knowledge and assumptions presented in the literature survey.

3.4.2 Assumptions

The following assumptions were made and the distribution and pressure drop through packed columns were analysed accordingly:

- Uniform diameter spherical particles;
- Small column diameter to sphere diameter;
- No heat transfer to be modelled;
- Isothermal and incompressible flow;
- Laminar, transition and turbulent flow;
- Spheres surfaces and inner column wall defined as ‘no-slip’;
- Outlet defined as ‘pressure outlet’; and
- Constant profile at ‘velocity inlet’.

3.4.3 CAD model

To ensure the influence of the boundary conditions at the inlet and outlet are minimized the column was extended by extruding the inlet by 3 particle diameters and the outlet by 10 particle diameters before it was imported into STAR-CCM+® as a surface mesh, as shown in Figure 3-4.

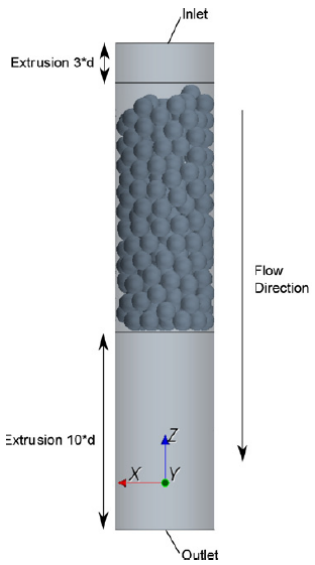

Figure 3-4. Packed bed geometry variation (Eppinger *et al.*, 2011:326).

3.4.4 Assigned regions

Discretisation of the CAD model was done by splitting the column surfaces into parts; wall, inlet, outlet and spheres and assigning parts to regions. The mesh could then be generated for the

assigned regions. It is also important to note that a part must be assigned to a region before its surfaces can be assigned a boundary.

3.4.5 Boundary conditions

3.4.5.1 Inlet Boundary

The inlet boundary was specified as a velocity inlet. The constant profile inlet velocity was specified as a function of the particle Reynolds number Re_{dp} and five Re_{dp} numbers were simulated for each case, one laminar (Re_{dp} = 1), one in transition region (Re_{dp} = 100) and three in the turbulent region (Re_{dp} = 500, 1000, 1500).

3.4.5.2 Outlet Boundary

The outlet boundary was specified at 100 kPa absolute for all simulations.

3.4.5.3 Wall

The wall boundary was modelled as a non-slip boundary.

3.4.5.4 Spheres

The spheres were modelled as a single non-slip boundary. The spheres were also defined with a specific mesh size as shown in Table 3-2.

3.4.6 Mesh generation

The volume mesh was based on the surface mesh and consisted of polyhedrons. When generating a mesh for a flow simulation, the mesh quality is of extreme importance, particularly in the near wall region when turbulent flow is considered. The mesh should have an appropriate resolution, therefore a mesh designed for both accuracy and simulation time should be used.

Meshing of packed beds was discussed in Section 2.8.4. From the literature survey it was concluded that introducing a gap by reducing the spheres to 99% of their size after generation of the packed beds will increase meshing quality at contact points and ensure reliable numerical simulations. The influence of the thin mesher in STAR-CCM+® on contact treatment and mesh dependence was not found in literature and was thus tested. The thin mesher creates a volume mesh for thin regions and is typically used for thin geometries where the solid material thickness needs to

be adequately captured with good quality cells. To ensure high quality mesh, a skewness < 0.7 is required.

A similar study on numerical modelling of flow through packed beds of uniform spheres was performed in conjunction to this study at the North-West University by Preller (2011). The study by Preller involved detailed analysis of contact treatment, meshing density and turbulence modelling. The results obtained by Preller were noted in this study and used as guidance to achieve appropriate mesh density and accurate flow results in this study. Preller's results were compared with the literature and assumptions discussed in Chapter 3. Where applicable tests were performed to confirm the chosen methods.

3.4.6.1 Contact Treatment

The introduction of a gap by reducing the spheres to 99% of their size was deemed sufficient to increase meshing quality at contact points when using a polyhedral mesher and ensured reliable numerical simulations as discussed in Section 2.8.3. Tests were performed by Preller (2011) on the influence of the thin mesh contact treatment and its ability to account for sphere contacts without a gap approximation. The tests were performed using the thin mesher in conjunction with the built in STAR-CCM®cell quality remediation model (the cell quality remediation model enables solutions to be obtained over bad cells by modifying the gradients over the cells). Results obtained by Preller (2011) showed almost identical results for pressure drop and velocity distribution between 100% sphere size (thin mesher) and a 0.7 % reduction in sphere size (polyhedral mesher). The contact treatment methods adopted by Preller (2011) are validated in Chapter 5.

Table 3-2. Surface and volume mesh parameters (mesh independence).

Base size	140 mm column	4 mm
	44 mm column	1.25 mm
Spheres surface size	28.4 mm spheres	Min = 0.375 mm, Target = 0.625 mm
	31.678 mm spheres	Min = 0.375 mm, Target = 0.625 mm
	60 mm spheres	Min = 0.75 mm, Target = 1.25 mm
Wall boundary surface size		4 mm / 1.25 mm (Relative to base)
Surface growth rate		1.3
Number of surface layers		2
Mesher		Thin

3.4.6.2 Mesh Independency

To achieve mesh independence the mesh resolution was determined by varying the parameters until their effect on the pressure drop was negligible. Correct simulation of mesh density ensures efficient and accurate simulation of flow phenomena. Preller (2011) performed comprehensive mesh independency studies for turbulent flow through packed beds. The results obtained by Preller (2011) were used in this study. Mesh independence was achieved with parameters given in Table 3-2.

3.4.7 Turbulence model

Various turbulence models were discussed in Section 2.8.5. The literature survey concluded that the majority of RANS turbulence models are accurate enough when used to model pressure drop through packed beds (results fall within acceptable bands when compared to correlations). General consensus was that resource intensive models offer little improvement in accuracy over the simpler models, for this reason the realisable k - ε turbulence model was used due to is ability to account for strong adverse pressure gradients, separation and recirculation which may occur in packed columns. The realisable k - ε turbulence model was also considered less computationally expensive than the RANS and LES turbulence models.

Preller (2011) performed a study on the effect the various turbulence models available in STAR-CCM+® have on pressure drop through a packed bed. The particle Reynolds number was specified at Re_{dp} = 3426 and a dense random packing of spheres was used for the simulation as seen in Table 3-3. Preller's results were compared with the pressure drop predicted by the KTA equation discussed in Section 2.9.1 and can be seen in Table 3-3.

Table 3-3. Turbulence model predicted pressure drop and deviation (Preller, 2010).

Case	*Turbulence Model*	*Pressure Drop [Pa]*	*Deviation from KTA [%]*
1	Realizable k - ε	44.2805	5.858254
2	Standard k - ω	43.0962	8.376175
4	Spalart-Allmaras model	42.1183	10.45516
6	KTA Correlation	47.0360	0

From the results in Table 3-3 it is evident that the Realizable k - ε is the most accurate of the RANS turbulence models.

3.4.8 Initial conditions

To ensure the simulation converges in the quickest time possible the initial values for the pressure outlet and velocity inlet were specified.

3.4.9 Solver parameters and stopping criteria

The simulation was considered complete when the residual values of all the solvers showed no variation and a residual value below $1e^{-4}$ and a steady state solution was achieved.

3.5 CFD Validation

3.5.1 Validation of pressure drop

The correlation proposed by Reichelt (1972:1069) with the modifications by Eisfeld and Schnitzlein (2001:4321) is an Ergun-type correlation. Section 2.9.2 noted that the Reichelt equation for pressure drop is the best suited pressure drop equation for low aspect ratio packed beds and were used to validate the pressure drop through columns. The Reichelt correlation is based on the method proposed by Metha and Hawley (1969) (*in*: Eisfeld & Schnitzlein, 2001:4321) . The method includes the column walls in the hydraulic diameter calculations.

The Reichelt dimensionless pressure drop with modifications by Eisfeld and Schnitzlein (2001:4321) is given as follows:

$$\psi = \frac{K_1 A_w^2 (1-\varepsilon)^2}{Re_{dp}} \frac{}{\varepsilon^3} + \frac{A_w}{B_w} \frac{1-\varepsilon}{\varepsilon^3} \tag{3.8}$$

with the wall correction terms:

$$A_w = 1 + \frac{2}{3(D/d_p)(1-\bar{\varepsilon})^2} \tag{3.9}$$

$$B_w = \left[k_1 \left(\frac{d_p}{D} \right)^2 + k_2 \right] \tag{3.10}$$

Where K_1, k_1 and k_2 are coefficients that were fitted to the experimental database developed by Eisfeld and Schnitzlein (2001:4321). When based on spherical particles the values for the coefficients are: K_1 = 154, k_1=1.15 and k_2= 0.87. The dimensionless pressure drop is given as:

$$\psi = \frac{\Delta P}{\rho_0 v_0^2} \frac{d_p}{L} \tag{3.11}$$

The Reichelt pressure drop correlation is valid for Reynolds numbers between $0.001 < Re_p < 17635$, average bed porosity between $0.330 < \varepsilon < 0.882$ and aspect ratios between $1.642 < \alpha < 250$.

3.6 Conclusion

A summarized methodology to setting up and validating both DEM and CFD simulations in STAR-CCM+® was described and discussed. The methodology outline demonstrated by Figure 3-1 was followed and various key aspects with regard to setup and validation were noted.

The method chapter determined that when setting up a DEM simulation in STAR-CCM+® various inputs were required: a base CAD model to define the column boundaries, assigned regions, definition of the surface and volume mesh, contact model (Hertz Mindlin), material and geometric properties (column and spheres), reference values (gravity), injector specifications, solver parameters and stopping criteria, and result visualisation and extraction. The material was defined as PMMA and the minimum time step to account for the Rayleigh wave speed was determined.

Validation of the DEM simulations was discussed and experimental results from Roslee (2009) and the empirically derived formula by Cheng (2011:261) which describes the relationship between $\bar{\varepsilon}$ and the beds aspect ratio (D/d_p) were used to validate the packing. The general setup and steps required to ensure accurate simulation of pressure drop through packed spherical particles in a column using CFD simulation in STAR-CCM+® was discussed and a methodology determined. The CAD model boundaries, mesh generation, contact treatment, mesh independency and turbulence models were discussed. The Realizable k - ε was found to be the most suitable of the RANS turbulence models.

Validation of the CFD simulations was discussed and Reichelt's approach (Reichelt, 1972:1068), was the most promising correlation to correlate pressure drop for Reynolds numbers of $0.01 \leq Re \leq 17635$, tube-to-particle diameter ratios of $1.624 \leq D/d \leq 250$, and a mean voidage of $0.330 \leq \varepsilon \leq 0.882$.

A methodology to setting up and validating both DEM and CFD simulations in STAR-CCM+® was described and discussed. The next chapter will discuss results and validate DEM and CFD simulations in STAR-CCM+®.

4 DEM Simulations & Validation

4.1 Introduction

The DEM simulations and validation chapter will summarise, describe and attempt to validate the results obtained using the DEM method discussed in Chapter 3.

4.2 Data Origin

In previous studies on porosity variation of packed columns performed at the North-West University by Roslee (2009), sphere positions for various small column-to-sphere ratio packed beds were obtained through x-ray tomography.

Table 4-1. Aspect ratios obtained from sphere and column combinations.

Experiment Number	*Sphere Diameter*	*Column Inner Diameter*	*Packing Height*	*Aspect Ratio*	*Number of Spheres*
	(mm)	*(mm)*	*(mm)*	*(D/d_p)*	
1	31.678	44	188	1.389	7
2	60	84	181	1.4	4
3	28.4	44	184	1.549	8
4	60	140	194	2.333	15
5	31.678	84	165	2.652	32
6	28.4	84	181	2.958	51
7	31.678	140	179	4.419	102
8	28.4	140	185	4.929	140

Using the geometrical conditions of the experiments performed by Roslee (2009), eight experimental packed column data sets were available. By basing the numerical simulations on the experimental component geometries, the experimental data was used to validate and benchmark the numerical packing simulations performed in this study. In addition, the numerical results were also compared with other experimental and numerical data found in the literature.

The sets obtained by Roslee (2009) were defined by the homogeneous particle size and the inner diameter of the column. The experiments consisted of sphere diameters of 28.4 mm, 31.678 mm and 60 mm and columns with inner diameters of 44 mm, 84 mm and 140 mm. Combinations of the various sphere and column sizes produced a range of eight aspect ratios that the study focused on, see Table 4-1.

Roslee (2009) found that the experimental data obtained through x-ray tomography provided acceptable approximations of the sphere positions.

As shown in Table 4-1, the aspect ratios range from 1.389 to 4.929. Three DEM simulations were performed for each aspect ratio and the results and validation will be discussed next. All the DEM simulations used the assumptions mentioned in Section 3.2.

4.3 Porosity Results & DEM Validation

4.3.1 Introduction

As discussed in Section 3.3.2 the variation of the porosity in the axial direction of the numerically generated beds was extracted by using an axial porosity code developed by Du Toit (2008).

4.3.2 Porosity at aspect ratio of 1.39

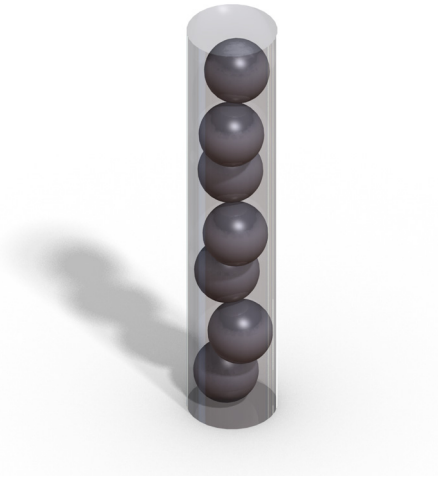

Figure 4-1. 3D representation of packing at an aspect ratio of 1.39.

Figure 4-1 provides a 3D representation of the first packing with the aspect ratio of 1.39. Figure 4-2 shows the axial porosity distribution for the particular packing. The results of three DEM simulations were compared with the experimental results obtained by Roslee (2009). All three DEM

simulations were performed with the exact same geometrical conditions. A random time and position injector was specified to ensure the spheres were dropped into the column at different times and positions on the inlet plane. The random injectors ensured that, once settled, none of the beds produced the same center coordinates for the spheres.

All the DEM simulations were set up using the method described in Section 3.2. Therefore, the method will not be described again and only the results of the various simulation cases will be discussed.

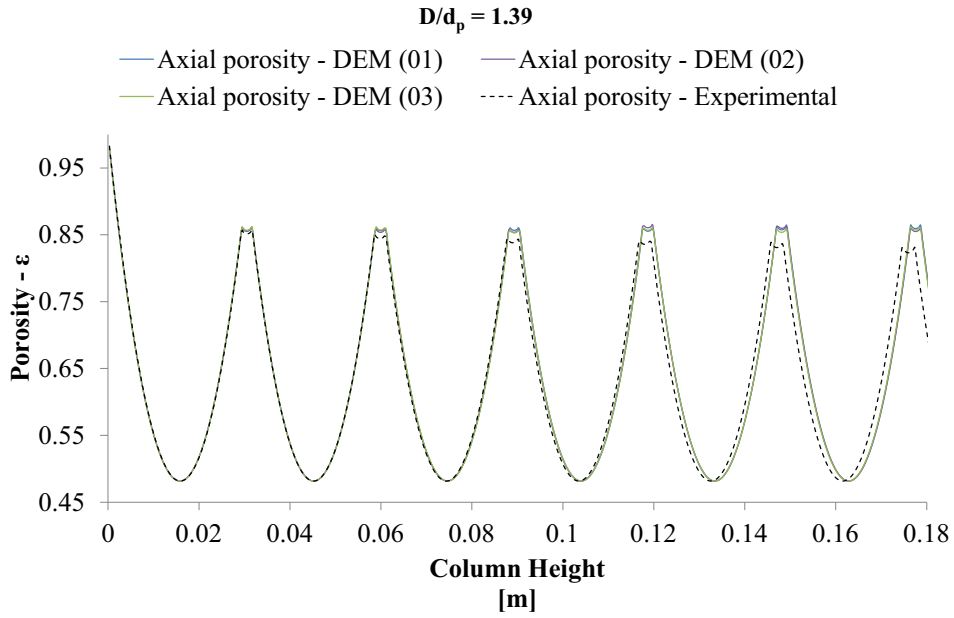

Figure 4-2. Axial porosity at aspect ratio of 1.39.

The axial porosity variation for all three of the DEM simulations is evident from Figure 4-2 and the experimental results showed a similar variation. The maximum difference between the DEM simulation and the experimental data in porosity is 0.09826 which is considered to be very low, from this it can be concluded that the packing at a ratio of 1.39 shows a constancy and can therefore be considered a structured packing. The difference in amplitude between the DEM and experimental simulation could also be due to the inaccuracies in the measuring techniques used in the experiments.

The repeatability in packing found at an aspect ratio of 1.39 is noted by Govindarao, *et al.* (1992:2105), who proved that the structure of packed beds at low aspect ratios shows periodicity.

As noted in Section 2.4.1, packings of aspect ratio $1 \leq \alpha \leq 1\frac{\sqrt{3}}{2}$ are structured and arrange spheres one over the other with each sphere touching the column wall. Thus the sphere centers will all be

located at a distance r_p from the wall of the column. The results obtained for a packing at an aspect ratio of 1.39 showed a similar structure to that seen in Figure 4-1.

4.3.3 Average bed porosity at aspect ratio of 1.39

The average porosity of the DEM simulations at an aspect ratio of 1.39 was determined by averaging the axial porosity variation in the beds. The average porosity was calculated from the bottom of the packing to one sphere diameter from the top of the packing. As noted in Section 3.3, the height of the packing should be reduced by one sphere diameter to minimize the effects of the loosened structure in the upper part of the packing (Eppinger, *et al*. 2011:325).

The average porosity of all the DEM simulations at an aspect ratio of 1.39 was found to be:

$$\bar{\varepsilon}_{1.39\,DEM} \approx 0.633 \tag{4.1}$$

By using Equation (2.17) derived by Cheng (2011:261), which defined the relationship between ε and the beds low aspect ratios (D/d_p), the calculated ε for an aspect ratio of 1.39 is:

$$\bar{\varepsilon}_{1.39\,Cheng} = 0.6174 \tag{4.2}$$

Equation (2.16) derived by Dixon (1988:707) is not valid for an aspect ratio of 1.39.

4.3.4 Porosity at aspect ratio of 1.4

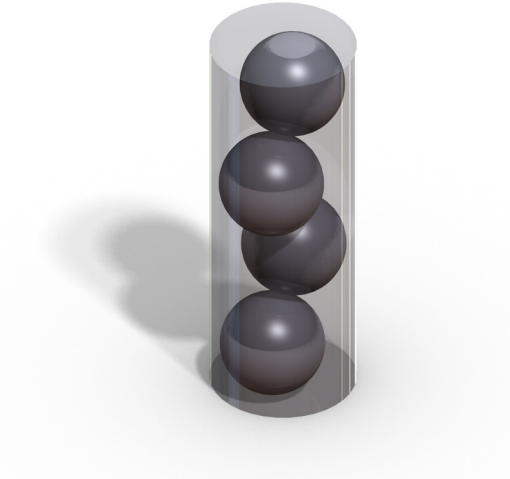

Figure 4-3. 3D representation of packing at an aspect ratio of 1.4.

Figure 4-3 gives a 3D representation of the second packing with an aspect ratio of 1.4. Figure 4-4 shows the axial porosity distribution at an aspect ratio of 1.4 for the particular case.

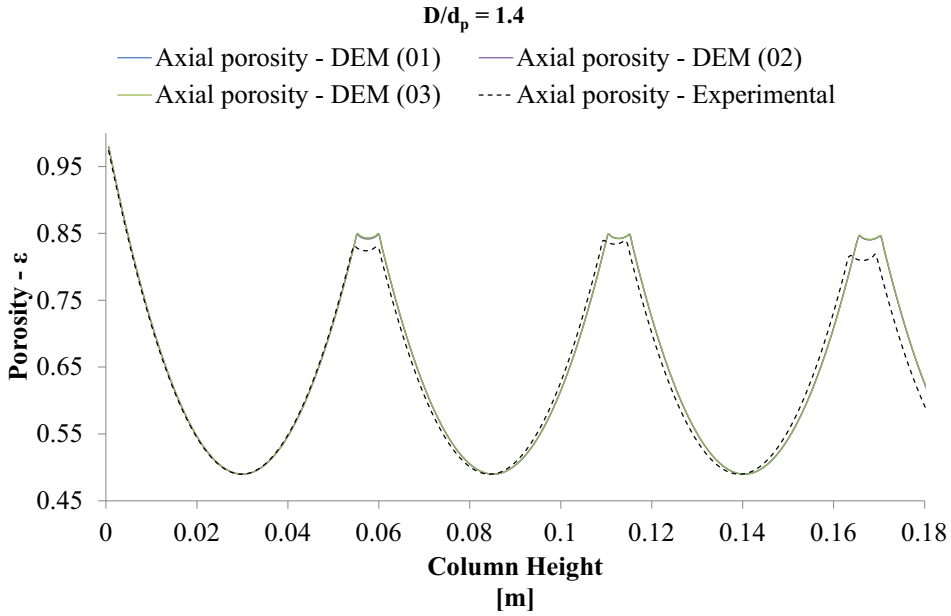

Figure 4-4. Axial porosity at aspect ratio of 1.4

Similar to the packing at an aspect ratio of 1.39, the packing at an aspect ratio of 1.4 was structured and showed similar variation for all three simulations, as seen in Figure 4-4. The maximum difference between all the DEM simulations and the experimental data in axial porosity was 0.056447 which again was very low. The experimental results did however vary slightly at the first and third peaks in Figure 4-4. Again, the slight variation in amplitude could be from experimental measuring inaccuracies. This could be interpreted as measuring errors in the experiments. The results were still within acceptable tolerance ranges and the DEM packing at an aspect ratio of 1.4 was considered accurate.

The structured packing found at an aspect ratio of 1.4 was also in the aspect ratio range of $1 \leq \alpha \leq 1\frac{\sqrt{3}}{2}$, as noted by Govindarao *et al*. (1992:2105).

4.3.5 Average bed porosity at aspect ratio of 1.4

The average porosity of all the DEM simulations at an aspect ratio of 1.4 was found to be:

$$\bar{\varepsilon}_{1.4\,DEM} \approx 0.6425 \tag{4.3}$$

By using Equation (2.17) derived by Cheng (2011:261), the calculated ε for an aspect ratio of 1.4 was:

$$\bar{\varepsilon}_{1.4\,Cheng} = 0.6216 \tag{4.4}$$

Equation (2.16) derived by Dixon (1988:707) is not valid for an aspect ratio of 1.4.

4.3.6 Porosity at aspect ratio of 1.55

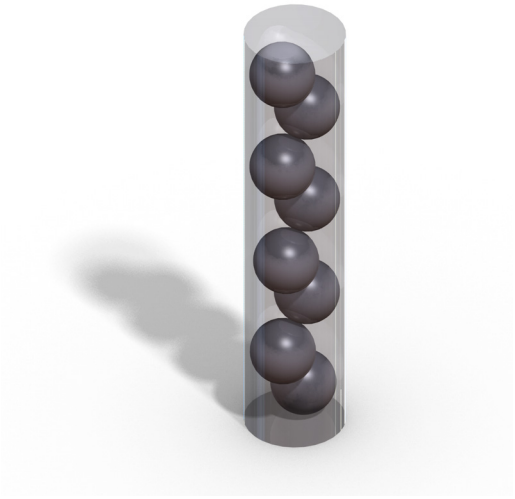

Figure 4-5. 3D representation of packing at an aspect ratio of 1.55.

Figure 4-5 gives a 3D representation of the third packing with an aspect ratio of 1.55. Figure 4-6 shows the axial porosity distribution for the particular case.

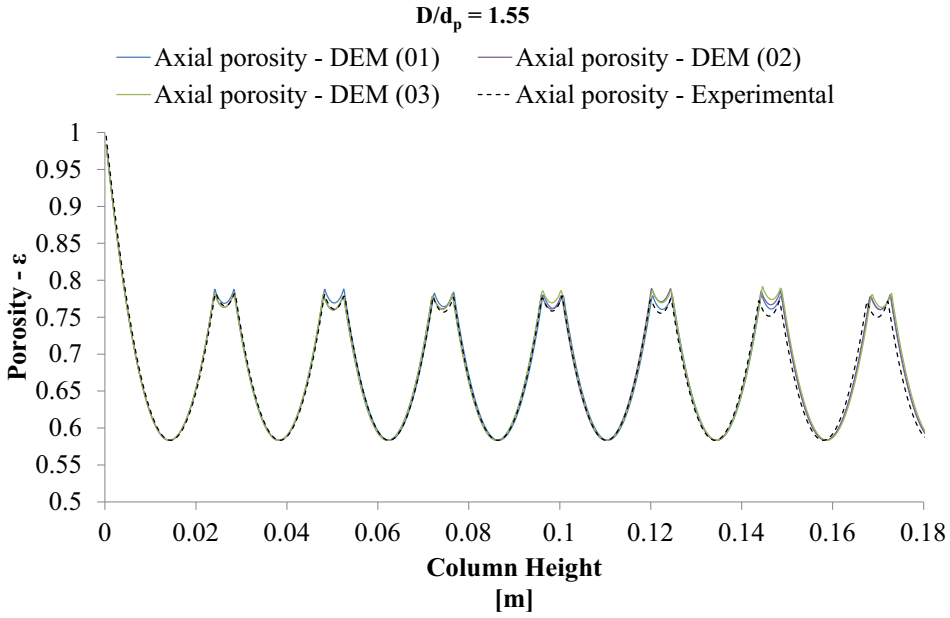

Figure 4-6. Axial porosity at aspect ratio of 1.55.

Similar to the packing at aspect ratios of 1.39 and 1.4 respectively, the packing for an aspect ratio of 1.55 was structured and showed similar variation for all three simulations, as seen in Figure 4-6. The maximum difference between all the DEM simulations and the experimental data in axial porosity was 0.040641, which again was very low. Therefore, the results were within acceptable tolerance ranges and the DEM packing at an aspect ratio of 1.55 was considered accurate.

The structured packing found at an aspect ratio of 1.55 was also in the aspect ratio range of $1 \leq \alpha \leq 1\frac{\sqrt{3}}{2}$, as noted by Govindarao *et al*. (1992:2105).

4.3.7 Average bed porosity at aspect ratio of 1.55

The average porosity of all of the DEM simulations at an aspect ratio of 1.55 was found to be:

$$\bar{\varepsilon}_{1.55\,DEM} \approx 0.666 \tag{4.5}$$

By using Equation (2.17), derived by Cheng (2011:261) the calculated ε at an aspect ratio of 1.55 was:

$$\bar{\varepsilon}_{1.55\,Cheng} = 0.677 \tag{4.6}$$

Equation (2.16) derived by Dixon (1988:707) was not valid for an aspect ratio of 1.55.

4.3.8 Porosity at aspect ratio of 2.33

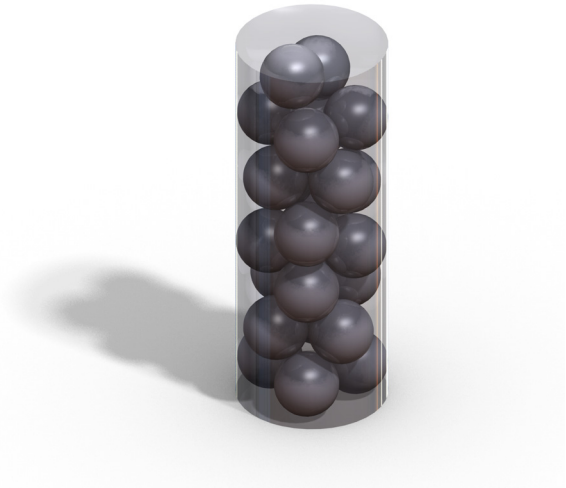

Figure 4-7. 3D representation of packing at an aspect ratio of 2.33.

Figure 4-7 gives a 3D representation of the fourth packing with aspect ratio of 2.33. Figure 4-8 shows the axial porosity distribution for the particular case.

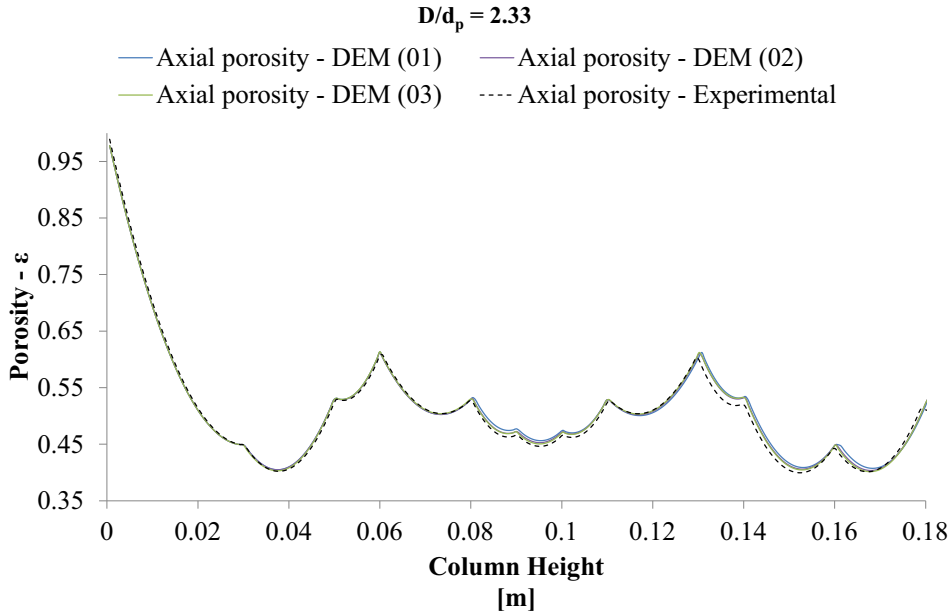

Figure 4-8. Axial porosity at aspect ratio of 2.33.

Similar to the packing at aspect ratios of 1.39, 1.4 and 1.55 respectively, the packing at an aspect ratio of 2.33 was structured and showed similar variation for all three simulations as seen in Figure 4-8. The maximum difference between all of the DEM simulations and the experimental data in axial porosity was 0.026302 which again was very low. Therefore, the results were within acceptable tolerance ranges and the DEM packing at an aspect ratio of 2.33 was considered accurate.

4.3.9 Average bed porosity at aspect ratio of 2.33

The average porosity of all of the DEM simulations at an aspect ratio of 2.33 was found to be:

$$\bar{\varepsilon}_{2.33\,DEM} \approx 0.513 \tag{4.7}$$

By using Equation (2.16) derived by Dixon (1988:707), the calculated ε at an aspect ratio of 2.33 was:

$$\bar{\varepsilon}_{2.33\,Dixon} = 0.497 \tag{4.8}$$

By using Equation (2.17) derived by Cheng (2011:261), the calculated ε at an aspect ratio of 2.33 was:

$$\bar{\varepsilon}_{2.33\,Cheng} = 0.545 \tag{4.9}$$

4.3.10 Porosity at aspect ratio of 2.65

Figure 4-9. 3D representation of packing at an aspect ratio of 2.65.

Figure 4-9 provides a 3D representation of the fifth packing with an aspect ratio of 2.65. Figure 4-10 shows the axial porosity distribution for the particular case.

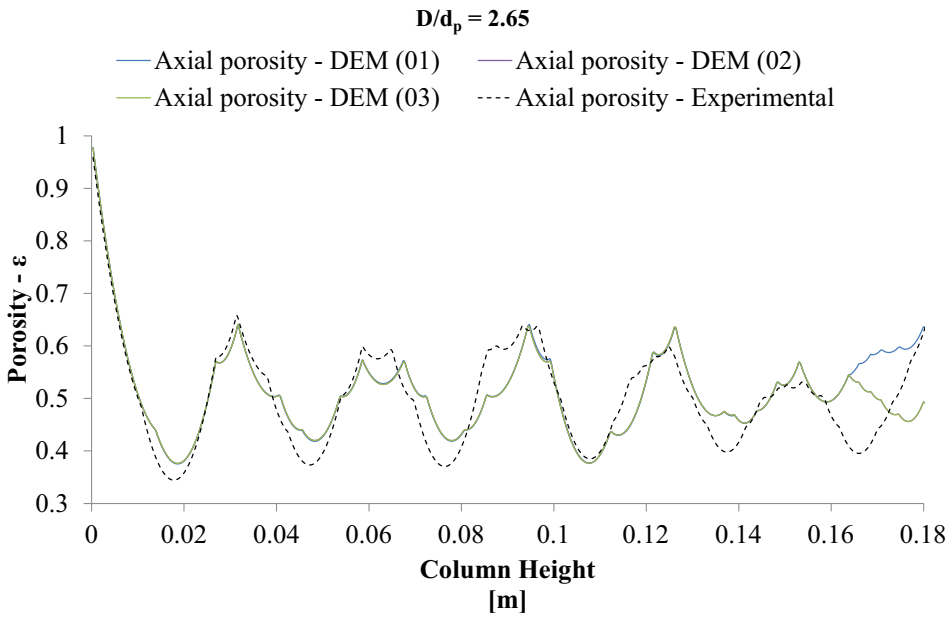

Figure 4-10. Axial porosity at aspect ratio of 2.65.

The packing at an aspect ratio of 2.65 showed a similar structure in all three of the DEM simulations. There was, however, larger deviations in comparison with the experimental results than was seen at the lower aspect ratios. The methods used to extract sphere positions of the spheres in the

experiment tended to be more tedious as the number of spheres increased, which could lead to larger deviation between experimental and DEM results, as seen in Figure 4-10. The porosity variation, however, showed a similar trend to the experimental results.

4.3.11 Average bed porosity at aspect ratio of 2.65

The average porosity of all of the DEM simulations at an aspect ratio of 2.65 was found to be:

$$\bar{\varepsilon}_{2.65\,DEM} \approx 0.508 \tag{4.10}$$

By using Equation (2.16) derived by Dixon (1988:707), the calculated ε at an aspect ratio of 2.65 was:

$$\bar{\varepsilon}_{2.65\,Dixon} = 0.478 \tag{4.11}$$

By using Equation (2.17) derived by Cheng (2011:261), the calculated ε at an aspect ratio of 2.65 was:

$$\bar{\varepsilon}_{2.65\,Cheng} = 0.497 \tag{4.12}$$

4.3.12 Porosity at aspect ratio of 2.96

Figure 4-11. 3D representation of packing at an aspect ratio of 2.96.

Figure 4-11 provides a 3D representation of the sixth packing at with aspect ratio of 2.96. Figure 4-12 shows the axial porosity distribution for the particular case.

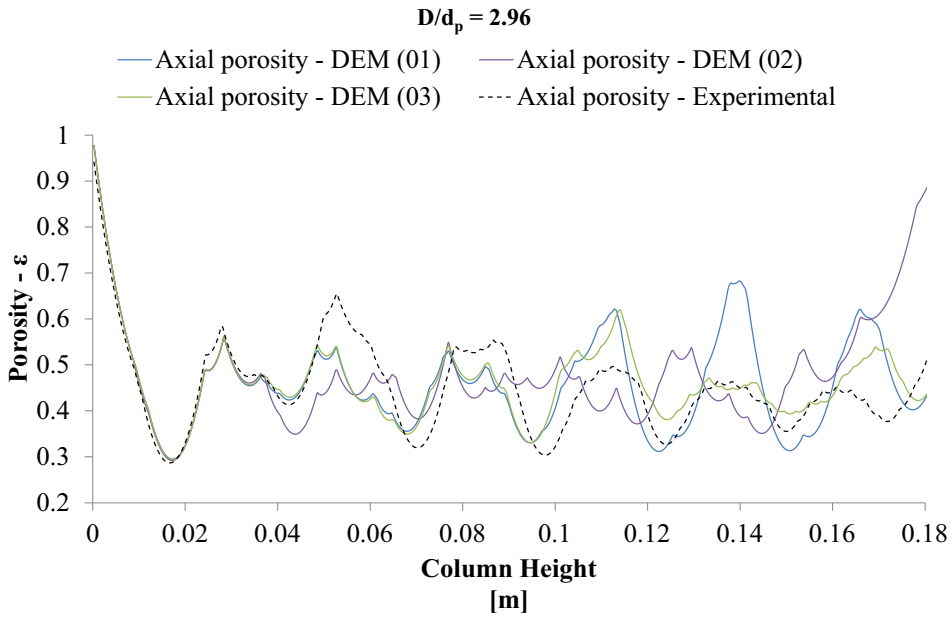

Figure 4-12. Axial porosity at aspect ratio of 2.96.

The packing at an aspect ratio of 2.96 showed a similar porosity variation in all three DEM simulations and experimental results up to a height of 0.04 [m]. Larger variations in axial porosity were found at heights above 0.04 [m]. The joint effect of the bottom and confining wall is generally observed at conditions H/d_p < 5 and 2<D/d_p<10. The effect is noticed in the 2.96 aspect ratio packing structure. The packing at an aspect ratio of 2.96 therefore produced a random packing. The porosity variation, however, showed a similar trend to the experimental results with regard to the average bed porosity (discussed in Section 4.3.13).

4.3.13 Average bed porosity at aspect ratio of 2.96

The average porosity of all the DEM simulations at an aspect ratio of 2.96 was found to be:

$$\bar{\varepsilon}_{2.96\,DEM} \approx 0.466 \tag{4.13}$$

By using Equation (2.16) derived by Dixon (1988:707), the calculated ε at an aspect ratio of 2.96 was:

$$\bar{\varepsilon}_{2.96\,Dixon} = 0.464 \tag{4.14}$$

By using Equation (2.17) derived by Cheng (2011:261), the calculated ε at an aspect ratio of 2.96 was:

$$\bar{\varepsilon}_{2.96\,Cheng} = 0.467 \tag{4.15}$$

4.3.14 Porosity at aspect ratio of 4.42

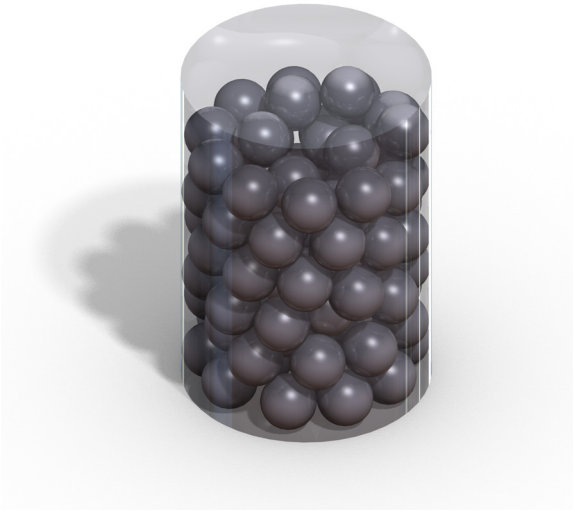

Figure 4-13. 3D representation of packing at an aspect ratio of 4.42.

Figure 4-13 provides a 3D representation of the seventh packing with an aspect ratio of 4.42. Figure 4-14 shows the axial porosity distribution for the particular case.

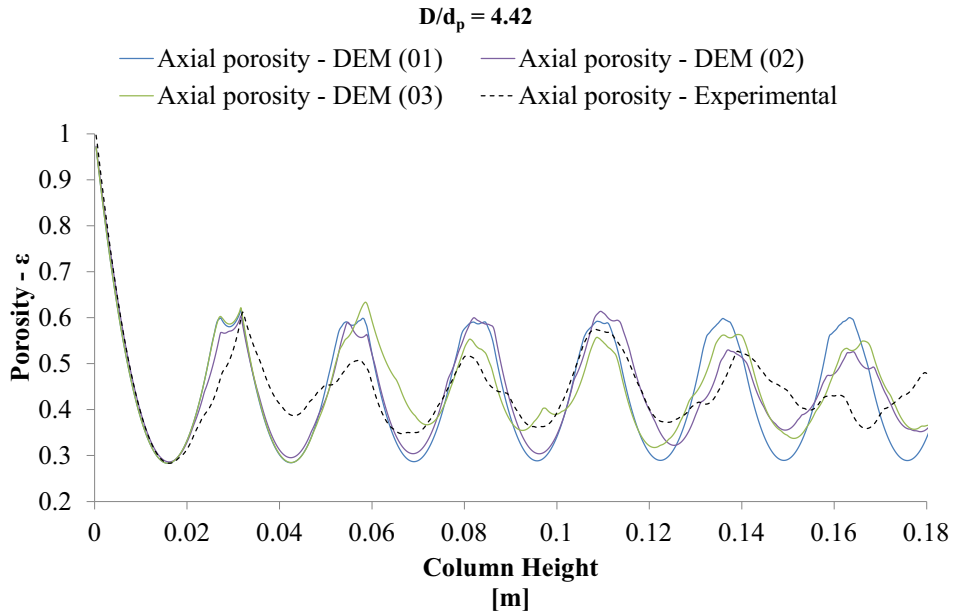

Figure 4-14. Axial porosity at aspect ratio of 4.42.

The packing at an aspect ratio of 4.42 showed a similar trend in porosity variation in all three DEM simulations. Once again the joint effect of the bottom and confining wall was observed. The packing at an aspect ratio of 4.42 therefore produced a random packing. The porosity variation, how-

ever, showed a similar trend to the experimental results with regard to the average bed porosity (discussed in Section 4.3.15).

4.3.15 Average bed porosity at aspect ratio of 4.42

The average porosity of all the DEM simulations at an aspect ratio of 4.42 was found to be:

$$\bar{\varepsilon}_{4.42\,DEM} \approx 0.442 \tag{4.16}$$

By using Equation (2.16) derived by Dixon (1988:707), the calculated ε at an aspect ratio of 4.42 was:

$$\bar{\varepsilon}_{4.42\,Dixon} = 0.432 \tag{4.17}$$

By using Equation (2.17) derived by Cheng (2011:261), the calculated ε at an aspect ratio of 4.42 was:

$$\bar{\varepsilon}_{4.42\,Cheng} = 0.41 \tag{4.18}$$

4.3.16 Porosity at aspect ratio of 4.93

Figure 4-15. 3D representation of packing at an aspect ratio of 4.93.

Figure 4-15 gives a 3D representation of the eighth packing with an aspect ratio of 4.93. Figure 4-16 shows the axial porosity distribution for this particular case.

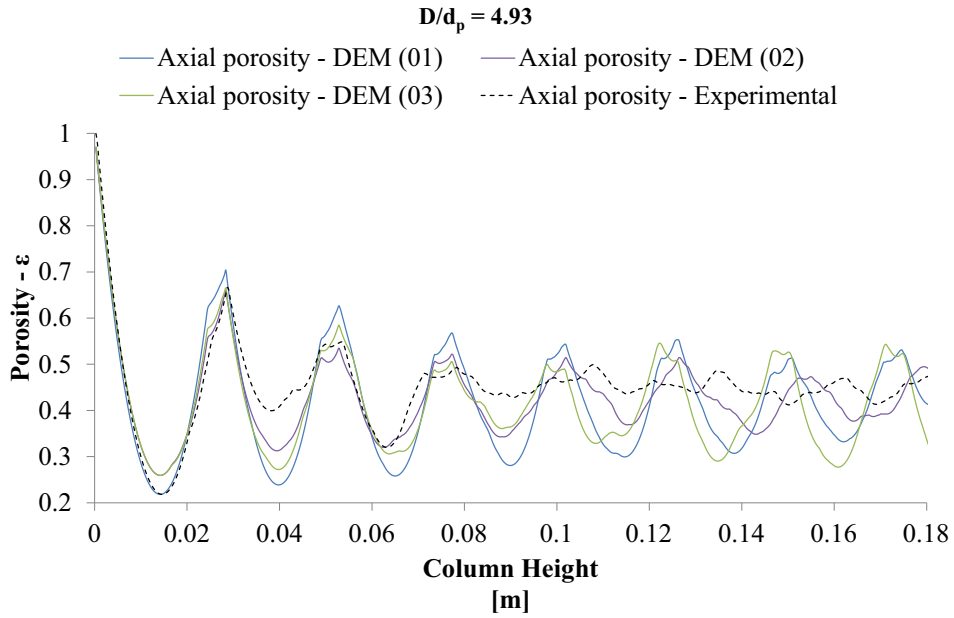

Figure 4-16. Axial porosity at aspect ratio of 4.93.

The packing at an aspect ratio of 4.93 showed a similar trends in porosity variation in all three DEM simulations. Once again the joint effect of the bottom and confining wall was observed. The packing at an aspect ratio of 4.93 therefore produced a random packing. The porosity variation, however, showed a similar trend to the experimental results with regard to the average bed porosity (discussed in Section 4.3.17).

4.3.17 Average bed porosity at aspect ratio of 4.93

The average porosity of all the DEM simulations at an aspect ratio of 4.93 was found to be:

$$\bar{\varepsilon}_{4.93\,DEM} \approx 0.421 \tag{4.19}$$

By using Equation (2.16) derived by Dixon (1988:707), the calculated ε at an aspect ratio of 4.93 is:

$$\bar{\varepsilon}_{4.93\,Dixon} = 0.427 \tag{4.20}$$

By using Equation (2.17) derived by Cheng (2011:261), the calculated ε at an aspect ratio of 4.93 is:

$$\bar{\varepsilon}_{4.93\,Cheng} = 0.402 \tag{4.21}$$

4.3.18 Average bed porosity at various aspect ratios

As noted by De Klerk (2003:2022), due to the multiple stable packing configurations in randomly packed beds, an anomalous average bed voidage and correspondingly different porosity distributions exist which have an effect on the predictive ability of bed porosity models. The global porosity distribution of the packed beds analised in this study shows consistency at low aspect ratios as shown in Figure 4-17. It can therefore be concluded that the average porosity is an effective means to validate results obtained by a DEM code.

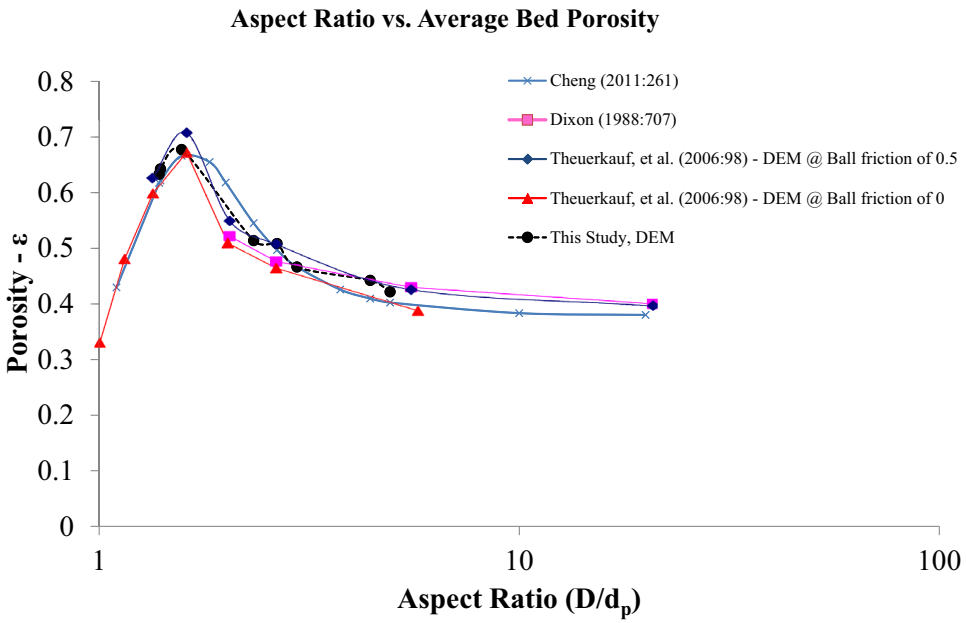

Figure 4-17. Average bed porosity vs. aspect ratio.

The overall porosity variations were also compared with the results from the study performed by Theuerkauf *et al*. (2006:98), on the influence of ball friction on the overall porosity, as shown in Figure 4-17. The DEM results achieved by Theuerkauf *et al*. (2006:98) showed a decrease in porosity at lower friction factors. A ball friction factor of 0.2 was specified for all the DEM simulations performed in this study for low aspect ratio cases.

A trend was also seen when the global porosity found in the DEM simulations were compared to global porosity derived from correlations by Dixon (1988:707) and Cheng (2011:261).

4.4 Conclusion

The DEM simulations and validation chapter summarised, described and validated the results obtained using the DEM method discussed in Chapter 3.

The simulations were performed for eight packed column aspect ratios. The results showed that for the first four aspect ratio packings (α = 1.39, 1.4, 1.55 and 2.33) a reproducible packing structure was formed. The DEM simulations and the experimental data with regard to axial variation in porosity showed similar variation and slight deviations which could be accounted for as measuring errors during the experimental data extraction. The DEM results for the first four simulations were therefore considered accurate.

The larger aspect ratios (α = 2.65, 2.96, 4.42 and 4.93) produced random packing structures and the axial porosity variation showed a similar trend when comparing the DEM axial porosity variation results to the axial porosity variation found in the experimental data. The joint effect of the bottom and confining wall was observed at these aspect ratios. The DEM results for the last four simulations were therefore also considered accurate.

The overall porosity variations were compared with the results from the studies performed by Theuerkauf *et al*. (2006:98) and correlations by Dixon (1988:707) and Cheng (2011:261). The DEM results achieved by the authors showed similar variation in porosity at various aspect ratios. A similar trend was seen when the global porosity found in the DEM simulations were compared to the experimental results and global porosity derived from correlations.

The use of the Discrete Element Method (DEM) to determine sphere positions for calculation of axial porosity distribution and overall porosity produced results which strongly correlated with experimental data and algorithms developed by Dixon (1988:707) and Cheng (2011:261). DEM could therefore be considered a reliable tool to producing 3D structures of the packed beds for CFD simulations and other purposes. The next chapter will discuss results and validate the CFD simulations performed in STAR-CCM+®.

5 CFD Simulations & Validation

5.1 Introduction

The CFD simulations and validation chapter will summarise, describe and attempt to validate the results obtained using the CFD method discussed in Chapter 3.

5.2 Contact Treatment & Meshing Validation

5.2.1 Introduction

Various methods of contact treatment were highlighted in the literature survey and method chapters. Six test cases were simulated to determine the best combination of meshing method and contact treatment. The considered meshing methods and contact combinations are shown in Table 5-1.

Table 5-1. Contact treatment and meshing cases.

	100% Sphere Size	*99% Sphere Size*	*Polyhedral Mesher*	*Thin Mesher*	*Prism Mesher*	*Surface Re-mesher*
Case 1	•		•			•
Case 2	•			•		•
Case 3	•		•	•		•
Case 4	•		•		•	•
Case 5	•		•	•	•	•
Case 6		•	•			•

The packing at an aspect ratio of 1.4 was used to validate the methods. The pressure drop was modelled for steady state flow using air as an ideal gas. The realisable k - ε turbulence model was used to model the turbulent nature of the flow field. The pressure drop and mesh quality were analyzed in all the cases and the most suitable method was determined.

5.2.2 Meshing model and contact treatment

5.2.2.1 Mesh setup

The minimum and target surface sizes for the boundaries and sphere surfaces used in the test cases were based on the mesh independency results established in Section 3.4.6.2. Six test cases were set up to determine the most accurate and efficient contact treatment and meshing model. The generic mesh input values for the contact treatment cases are given in Table 5-2.

Table 5-2. Mesh parameters for contact treatment cases.

	Meshing Values
Base size ($d_p/d_c = 15$)	4 mm
Spheres surface size Min = ($d_p/d_c = 80$), Max = ($d_p/d_c = 48$)	Min = 0.75 mm, Target = 1.25 mm
Wall boundary surface size ($d_p/d_c = 15$)	4 mm
Surface growth rate / Stretching	1.3
Thin mesh layers / prism layers	2

5.2.2.2 Boundary conditions

The boundaries were specified as shown in Figure 5-1, with the velocity inlet and the pressure outlet specified at a distance of three and ten times the diameter of the spheres from the top and bottom of the packing. The reference pressure was specified as standard atmospheric pressure which is 101.326 kPa. The relative pressure on the outlet was set at 0 kPa since the total pressure would be the sum of the reference and relative pressures. The velocity at the inlet was specified as 0.383 m/s with a corresponding particle Reynolds number of 1500 and a static temperature of 26.85°C was specified.

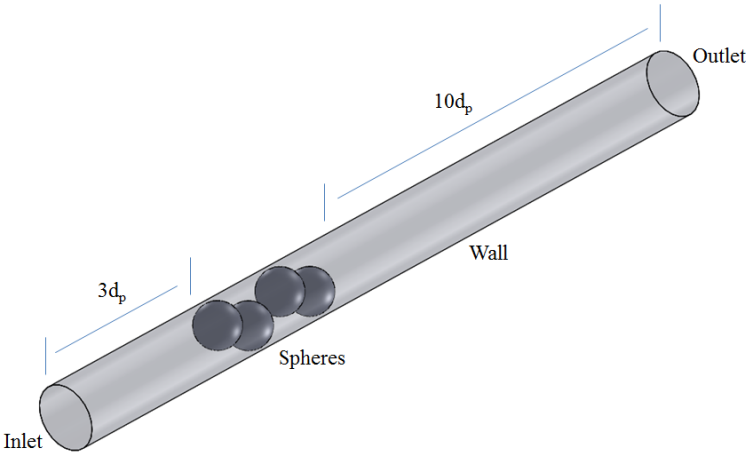

Figure 5-1. Surface mesh boundary conditions.

5.2.3 Results and Discussion

Table 5-3. Mesh quality results

	Skewed Cell Volume [mm^3] (volume of cells with skewness > 0.7)	*Number of Cells*	*Close Proximity Faces*
Case 1	18.5	356159	1476
Case 2	0.003	294158	1472
Case 3	17.1	355798	1477
Case 4	23.6	473071	1476
Case 5	23.4	473063	1476
Case 6	0	266098	0

5.2.3.1 Mesh quality

Table 5-3 summarises the mesh quality of all the cases. Case 6 showed the best quality with no skewed cells above 0.7 and the least number of cells (less resource intensive). Case 2, however, also had a very low skewed cell volume and low number of cells. Case 2 was meshed using the thin mesher and 100% of the sphere size, the mesh skewness was the best of all the cases with 100% of the sphere size modelled.

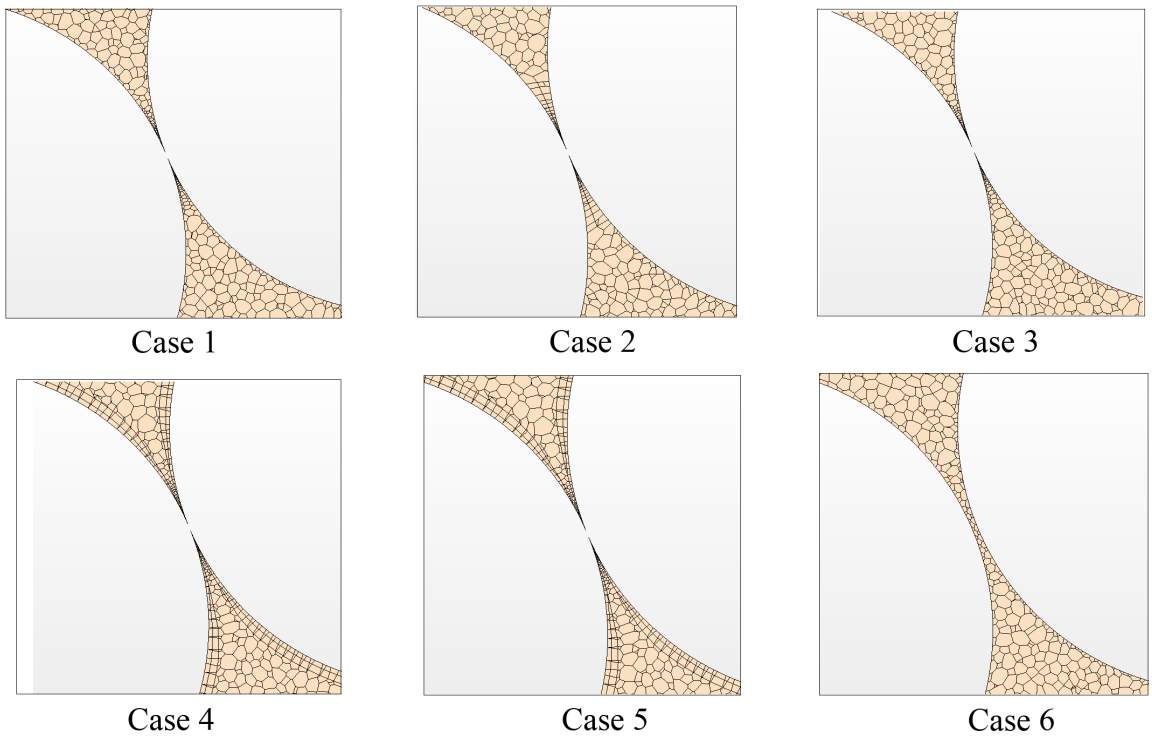

Figure 5-2. Mesh structure at contact points.

As discussed in Section 2.8.3, when contact points were treated as pebbles with approximated gaps or sphere reduction the results yielded inaccurate information about the local flow fields and heat

transfer. Therefore the pressure drop over the spheres were compared for the 3 best cases and the most suitable method determined. The mesh structure generated at the contact points in each of the six cases is shown in Figure 5-2.

5.2.3.2 Pressure drop and flow distribution

The pressure drop over the packing was simulated at a Reynolds number of 1500 which is in the turbulent flow region. The pressure drop for each case was calculated and the results are shown in Table 5-4.

Table 5-4. Simulated pressure drop for test cases.

	Simulated Pressure Drop [Pa]
Case 1	1.6
Case 2	1.6
Case 3	1.6
Case 4	1.6
Case 5	1.6
Case 6	1.4

From the results it is clear that there is very little variation in pressure drop for the first five cases. Case 6 showed a decrease in pressure drop due to the sphere sizes being decreased to 99%, thus increasing the bed porosity. From the results we could conclude that the pressure drop was not affected by the type of mesher used and the mesh with the best quality at 100% sphere size should be used in the simulations.

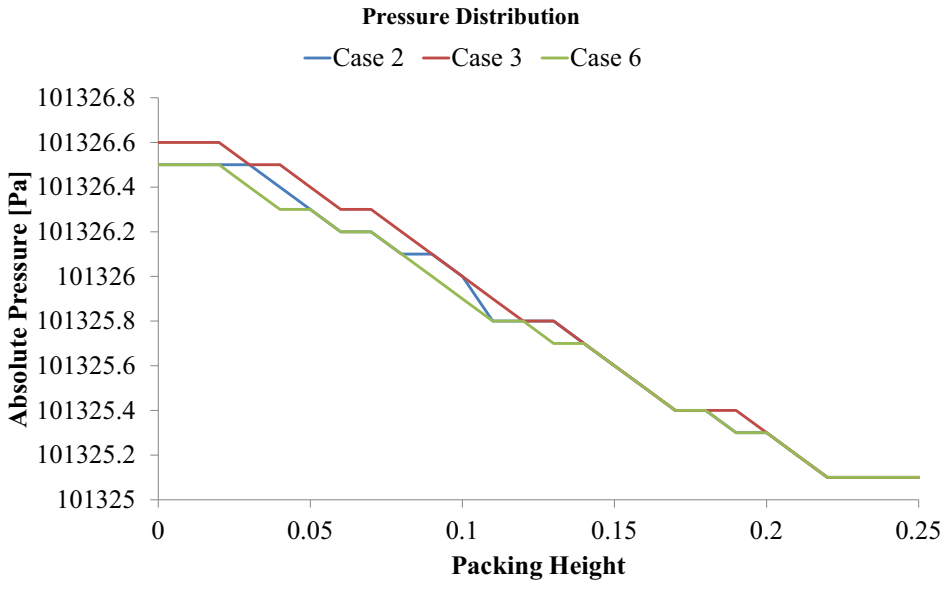

Figure 5-3. Case 2,3 and 6 pressure variation over height.

Case 2, 3 and 6 had the lowest number of cells and lowest skewed volume. These three cases were compared in terms of pressure drop and velocity distribution. Figure 5-4 shows the pressure distribution simulated for Case 2, 3 and 6. The three cases show similar variation in pressure. The pressure variation over the length of the columns is given in Figure 5-3.

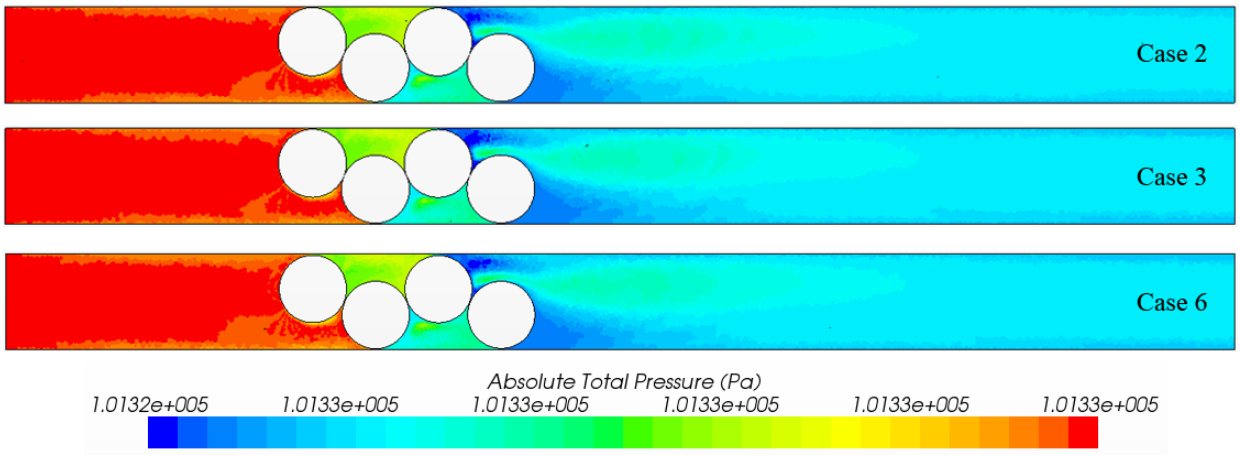

Figure 5-4. Case 2,3 and 6 pressure distribution.

Figure 5-5 shows the velocity distribution simulated for Case 2, 3 and 6. The three cases showed similar variation in velocity and a slight increase in velocity at the wall regions as expected. Once again no notable difference is shown in the velocity distribution.

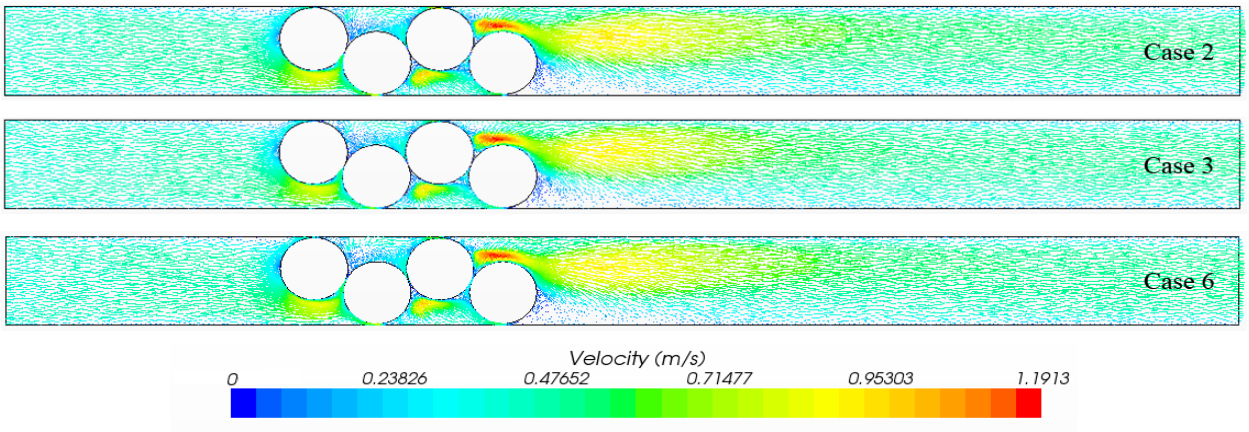

Figure 5-5. Case 2,3 and 6 velocity distribution.

5.2.4 Conclusion

The thin mesher produced the lowest number of cells and best quality at 100% sphere size. The pressure drop and velocity distribution was also similar for all the cases. The thin mesher is therefore the best choice when aiming for simulation efficiency and accuracy.

5.3 Pressure Drop & Velocity Distribution

The pressure drop and velocity distribution were analysed for three of the low aspect ratio packed columns. The cases considered were the packings with aspect ratios of 1.39, 2.33 and 4.3. The three aspect ratios were chosen because they each have a different sphere size (Validate d_p/d_c) and unique packing structures. Table 5-5 presents the dimensions and properties of the considered cases.

The simulated pressure drop was validated using the correlation derived by Eisfeld and Schnitzlein (2001:4321) with the adapted parameters for friction coefficient of Reichelt's correlation as discussed in Section 2.9. The pressure drop correlation is given by Equation (3.8). The correlation validity, however, will only be applicable to the 2.33 and 4.3 aspect ratios. The minimum packing height was not mentioned by Eisfeld and Schnitzlein (2001:4321). The packing heights will correspond to the DEM simulations. The packing at an aspect ratio of 4.93 will, however, only be simulated with 75 particles due to the exponential increase in mesh cells when the number of spheres are increased.

Table 5-5. CFD simulation data.

Simulation Number	*Sphere Diameter*	*Column Inner Diameter*	*Simulated Packing Height*	*Aspect Ratio*	*Packing Height Ratio*	*Number of Spheres*
	(mm)	*(mm)*	*(mm)*	*(D/d_p)*	*(H/d_p)*	
1	31.678	44	192	1.389	6.06	7
2	60	140	210	2.333	3.5	15
3	28.4	140	101	4.929	3.56	75

5.3.1 Flow at aspect ratio of 1.39

5.3.1.1 Simulation overview

The simulation was set up using the method described in Section 3.4 only basic inputs and the results of the various simulation cases will be discussed.

The pressure drop through packed spheres at an aspect ratio of 1.39 was modelled for steady state flow using air as an ideal gas. The inlet and outlet boundaries were specified at a static temperature of 26.85°C. A uniform inlet velocity was specified at the inlet boundary and atmospheric pressure of 101.325 kPa at the outlet.

The mesh conditions are given in Table 3-2 with a base size of 1.25 mm and sphere surface sizes defined at a target of 0.625 mm and minimum of 0.375 mm. Unstructured polyhedral cells were generated in the primary flow domain and structured prism cells at the contact regions. The thin mesher was used and 662671 cells were generated. The realisable k - ε turbulence model was used for turbulent simulations.

The pressure drop and velocity distribution were analysed for laminar, transition and turbulent flow and the particle Reynolds numbers simulated were; 1 - laminar, 100 - transition, 500, 1000, 1500 - turbulent.

5.3.1.2 Pressure drop

The plane average pressure drop was extracted over various lengths of the packing to determine the accuracy of the simulation. The Eisfeld and Schnitzlein (2001:4321) correlation determines the pressure drop from the average bed porosity. As noticed in the DEM simulation the porosity can vary dramatically between the bottom and top of the packing. The pressure drop was therefore extracted and compared over four different length: bottom of the packing to the top, centre of the bottom sphere to the centre of the top sphere, one sphere diameter from the bottom to one sphere diameter from the top, and from the bottom of the packing to one sphere diameter from the top. The ranges are shown in Figure 5-6.

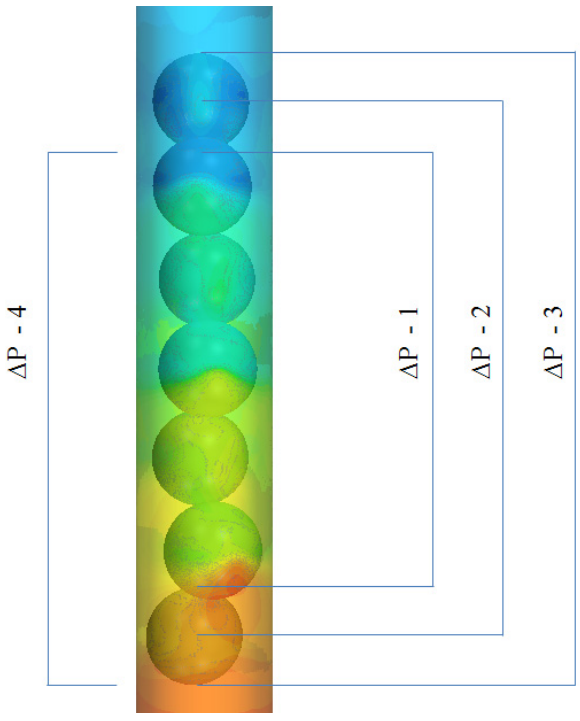

Figure 5-6. Pressure ranges extracted from CFD simulations, α = 1.39.

The Eisfeld and Schnitzlein (2001:4321) correlation required an average porosity $\bar{\varepsilon}$. The value for average porosity was obtained in the DEM simulation and calculated as 0.633 at an aspect ratio of 1.39. Particle Reynolds number Re_{dp} was varied to account for the flow regimes discussed previously. The column inner diameter D and sphere diameter d_p is given in Table 5-5. The four pressure drop regions and their respective lengths are given in Table 5-6.

Table 5-6. Pressure drop ranges, α = 1.39.

Case	*Length [mm]*
ΔP - 1	144.672
ΔP - 2	176.35
ΔP - 3	208.1
ΔP - 4	176.35

5.3.1.3 Pressure drop results

The pressure drop over the laminar, transition and turbulent ranges are given in Figure 5-7. The Eisfeld and Schnitzlein (2001:4321) pressure drop correlation was not valid for an aspect ratio of 1.39. The expected deviation between the simulated results and the correlation is seen in Figure 5-7. The normalised root mean square deviation over the pressure ranges given in Table 5-6 was 13.37%. The results showed an increase in deviation as the particle Reynolds number was increased. Comparison between the simulated and correlated pressure drop at a length of 176.35 mm is shown in Figure 5-7.

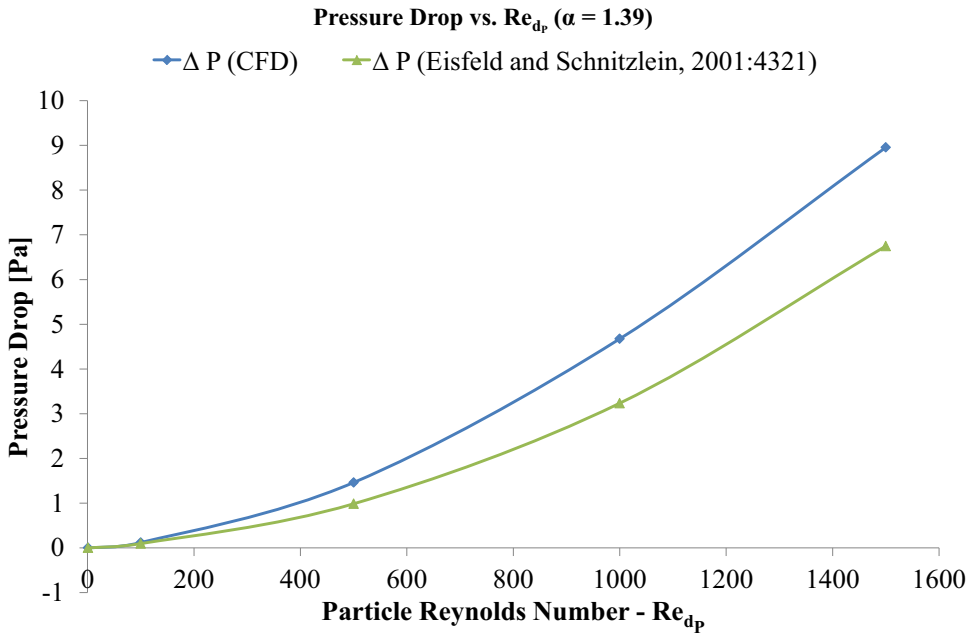

Figure 5-7. Pressure drop versus particle Reynolds number at α = 1.39.

5.3.1.4 Velocity distribution

Similar to the findings by Eppinger *et al.* (2011:324) the velocity distribution for a range of low aspect ratio packed columns showed an increase in any channels formed within the packing. The channels caused an increase in porosity and hence an increase in velocity. The channels formed at $\alpha = 1.39$ are shown in Figure 5-8.

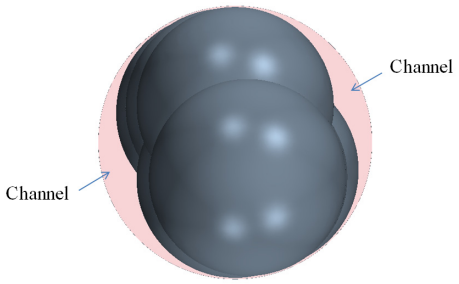

Figure 5-8. Channels formed at $\alpha = 1.39$.

The velocity distribution is shown in Figure 5-9. The maximum velocities occur within the channels. Figure 5-9 shows the velocity distribution at $Re_p = 1000$. A similar variation in velocity was found in the laminar, transition and turbulent regions.

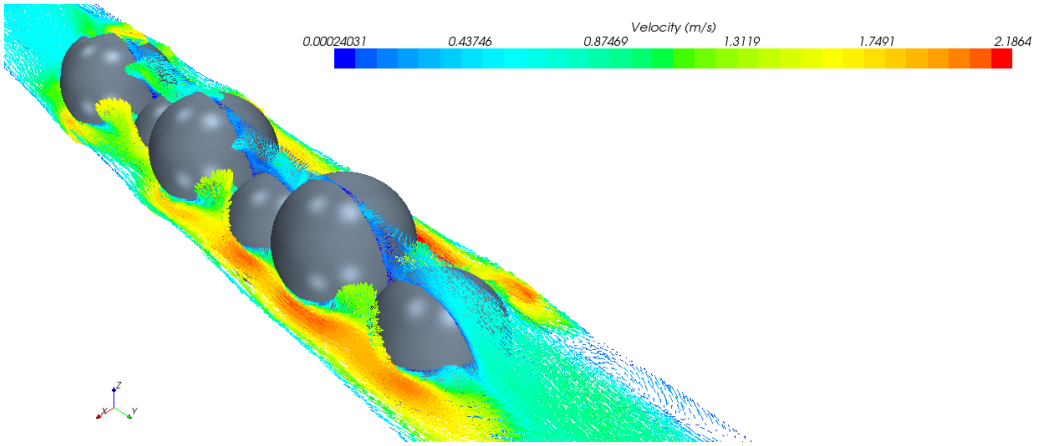

Figure 5-9. Velocity distribution at $\alpha = 1.39$.

5.3.2 Flow at aspect ratio of 2.33

5.3.2.1 Simulation overview

Similar to the simulation at an aspect ratio of 1.39 the simulation was set up using the method described in Section 3.4. The pressure drop through packed spheres at an aspect ratio of 2.33 was also modelled for steady state flow using air as an ideal gas. The inlet and outlet boundaries were specified at a static temperature of 26.85°C. A uniform inlet velocity was specified at the inlet boundary and atmospheric pressure of 101.325 kPa at the outlet.

The mesh conditions are given in Table 3-2 with a base size of 4 mm and sphere surface sizes defined at a target of 1.25 mm and maximum of 0.75 mm. Unstructured polyhedral cells were generated in the primary flow domain and structured prism cells at the contact regions. The thin mesher was used and 723801 cells were generated. The realisable k - ε turbulence model was used for turbulent simulations.

The pressure drop and velocity distribution were analised for laminar, transition and turbulent flow and the particle Reynolds numbers simulated were; 1 - laminar, 100 - transition, 500, 1000, 1500 - turbulent.

5.3.2.2 Pressure drop

Similar to the results for the aspect ratio of 1.39 the pressure drop was extracted over various lengths of the packing to determine the accuracy of the simulation. The ranges are shown in Figure 5-10.

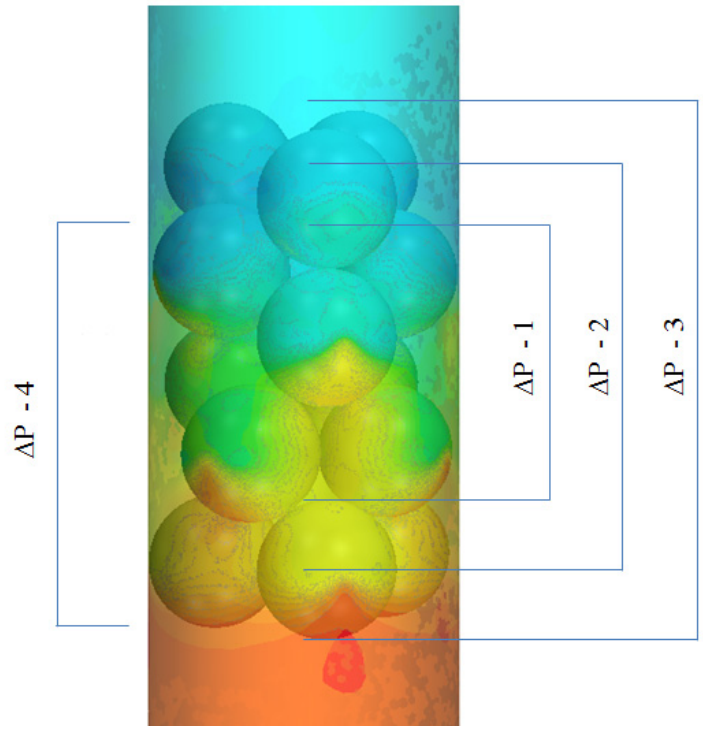

Figure 5-10. Pressure ranges extracted from CFD simulations, α = 2.33.

The average porosity $\bar{\varepsilon}$, used in the Eisfeld and Schnitzlein (2001:4321) correlation was obtained in the DEM simulation and calculated as 0.513 for a aspect ratio of 2.33. Particle Reynolds number Re_{dp} was varied to account for the flow regimes discussed previously. The column inner diameter D and sphere diameter d_p are given in Table 5-5. The four pressure drop regions and their respective lengths are given in Table 5-7.

Table 5-7. Pressure drop ranges, $\alpha = 2.33$.

Case	*Length [mm]*
ΔP - 1	120.4
ΔP - 2	180.4
ΔP - 3	240.4
ΔP - 4	180.4

5.3.2.3 Pressure drop results

The pressure drop over the laminar, transition and turbulent ranges are given in Figure 5-11. The Eisfeld and Schnitzlein (2001:4321) pressure drop correlation is valid for an aspect ratio of 2.33. The agreement between the simulated results and the correlation is evident from Figure 5-11. The normalised root mean square deviation over the pressure ranges given in Table 5-7 is 4%. The results showed a similar variation in pressure drop as the particle Reynolds number was increased.Comparison between the simulated and correlated pressure drop at a length of 180.4 mm is shown in Figure 5-11.

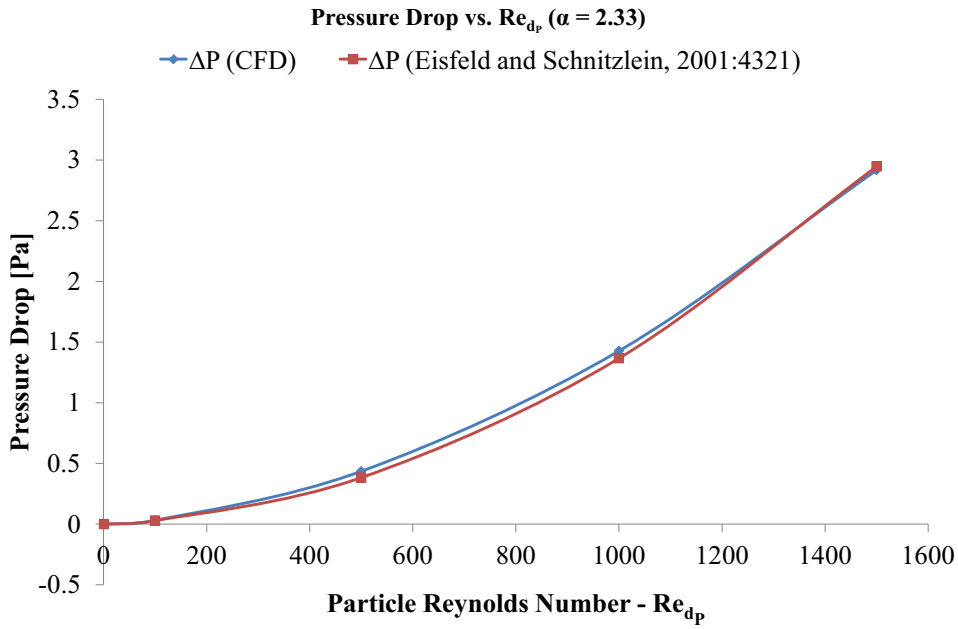

Figure 5-11. Pressure drop versus particle Reynolds number at $\alpha = 2.33$.

5.3.2.4 Velocity distribution

The channels formed in the packing structure at α = 2.33 are shown in Figure 5-12. The packing structure formed a channel in the centre region of the column. Channels were also formed near the wall.

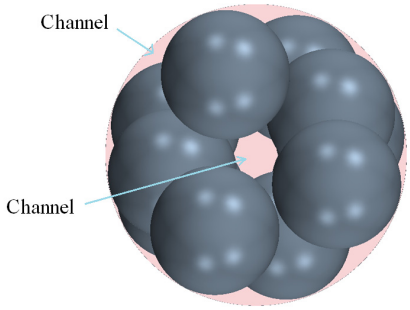

Figure 5-12. Channels formed at α = 2.33.

Similarly to α = 1.39 the maximum velocity occurred within the channels. Figure 5-13 shows the velocity distribution at Re_p = 1000. The channel formed in the centre of the column produced a large increase in velocity, similar increase in velocity was noted by Eppinger *et al.* (2011:324). A similar variation in velocity was found in the laminar, transition and turbulent regions.

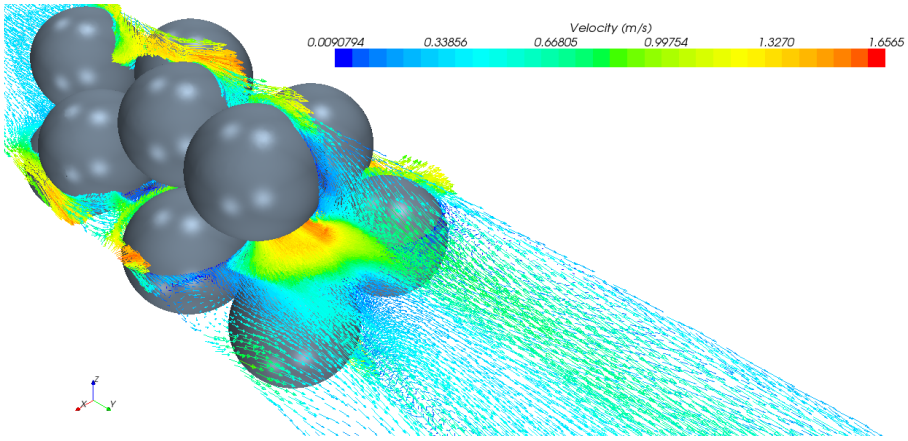

Figure 5-13. Velocity distribution at α = 2.33.

5.3.3 Flow at aspect ratio of 4.93

5.3.3.1 Simulation overview

Similar to the simulations at aspect ratios of 1.39 and 2.33 the simulation was set up using the method described in Section 3.4. The pressure drop through packed spheres at an aspect ratio of 4.93 was also modelled for steady state flow using air as an ideal gas. The inlet and outlet bound-

aries were specified at a static temperature of 26.85°C. A uniform inlet velocity was specified at the inlet boundary and atmospheric pressure of 101.325 kPa at the outlet.

The mesh conditions are given in Table 3-2 with a base size of 4 mm and sphere surface sizes defined at a target of 0.625 mm and maximum of 0.375 mm. Unstructured polyhedral cells were generated in the primary flow domain and structured prism cells at the contact regions.The thin mesher was used and 3617497 cells were generated. The realisable k - ε turbulence model was used for turbulent simulations.

The pressure drop and velocity distribution was analised for laminar, transition and turbulent flow and the particle Reynolds numbers simulated were; 1 - laminar, 100 - transition, 500, 1000, 1500 - turbulent.

5.3.3.2 Pressure drop

Similar to the results for aspect ratios of 1.39 and 2.33 the pressure drop was extracted over various lengths of the packing to determine the accuracy of the simulation. The ranges are shown in Figure 5-14.

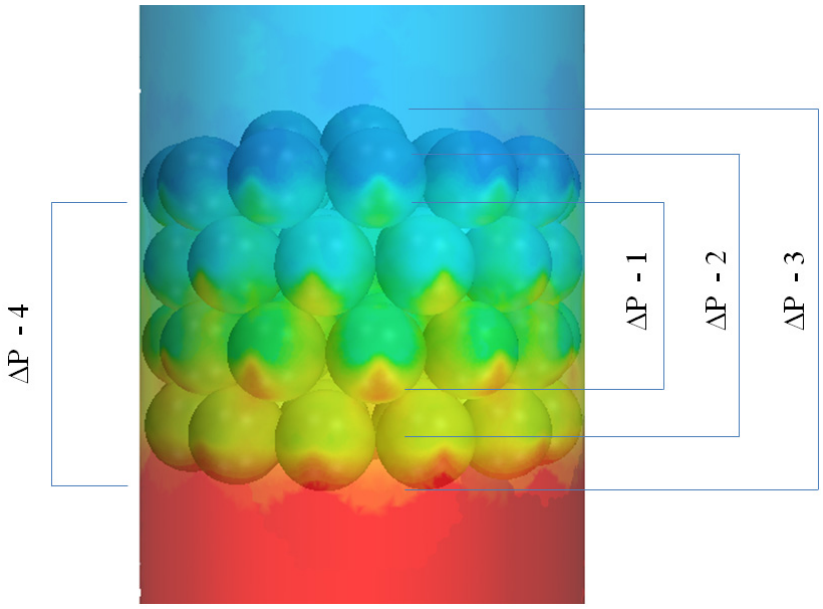

Figure 5-14. Pressure ranges extracted from CFD simulations, α = 4.93.

The average porosity $\bar{\varepsilon}$, used in the Eisfeld and Schnitzlein (2001:4321) correlation was obtained in the DEM simulation and calculated as 0.421 for an aspect ratio of 4.93. Particle Reynolds number Re_{dp} was varied to account for the flow regimes discussed previously. The column inner

diameter D and sphere diameter d_p are given in Table 5-5. The four pressure drop regions and their respective lengths are given in Table 5-8.

Table 5-8. Pressure drop ranges, α = 4.93.

Case	*Length [mm]*
ΔP - 1	44.3
ΔP - 2	72.2
ΔP - 3	101.1
ΔP - 4	72.2

5.3.3.3 Pressure drop results

The pressure drop over the laminar, transition and turbulent ranges are given in Figure 5-15. The Eisfeld and Schnitzlein (2001:4321) pressure drop correlation is valid for an aspect ratio of 4.93. The comparison between the simulated results and the correlation is evident from Figure 5-15. The simulated pressure drop showed acceptable agreement up to a particle Reynolds number of 1000, the correlation then over-predicted the pressure drop at a particle Reynolds number of 1500. The decrease in pressure drop at higher turbulence was noted by Reddy and Joshi (2008:444) due to the channeling near the wall. The combination of a relatively short packing height and increased turbulence could explain the deviation from the correlation. The normalised root mean square deviation over the pressure ranges given in Table 5-8 is 9.78%.

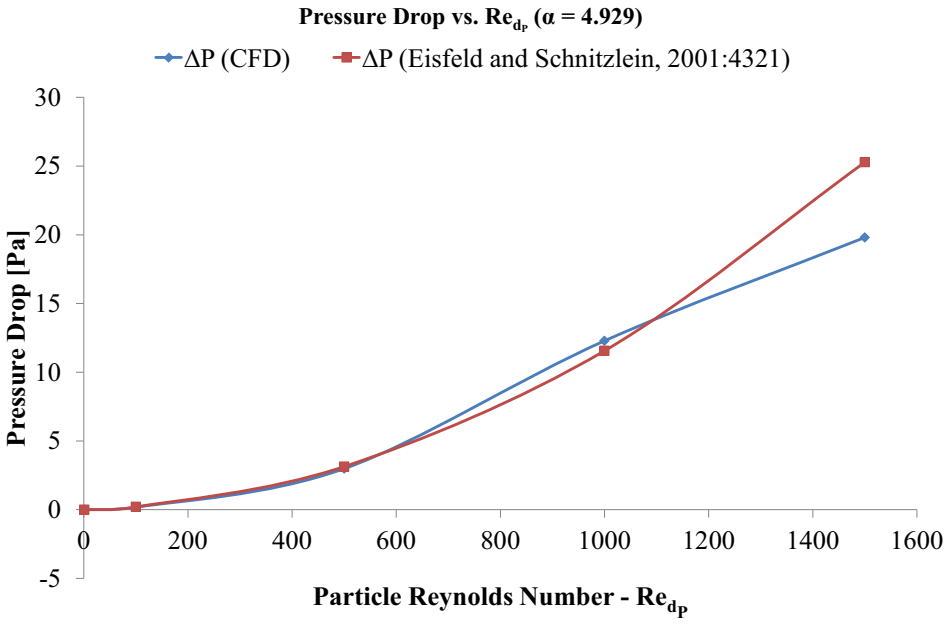

Figure 5-15. Pressure drop versus particle Reynolds number at α = 4.93.

Comparison between the simulated and correlated pressure drop at a length of 72.2 mm is shown in Figure 5-7. Additional studies can be performed in the future to determine the relation between packing height and Reynolds number.

5.3.3.4 Velocity distribution

No distinct channels were formed at α = 4.93 as shown in Figure 5-16. The porosity, however, showed an increase at the walls as discussed in Section 4.3.16.

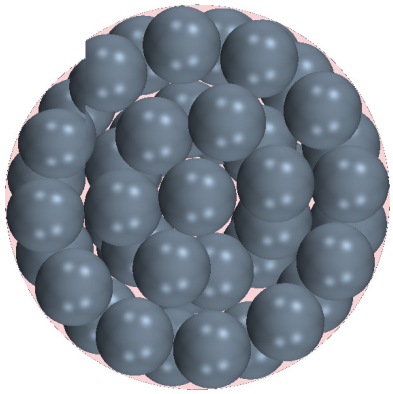

Figure 5-16. Channels formed at α = 4.93.

The maximum velocity occurred near the walls of the packing. The variation was similar to that described by White and Tien (1987:291) where an increase in porosity at the wall region distorts the velocity distribution causing higher velocities in the near-wall regions. Figure 5-17 shows the velocity distribution at Re_p = 1000. A similar variation in velocity was found in the laminar, transition and turbulent regions.

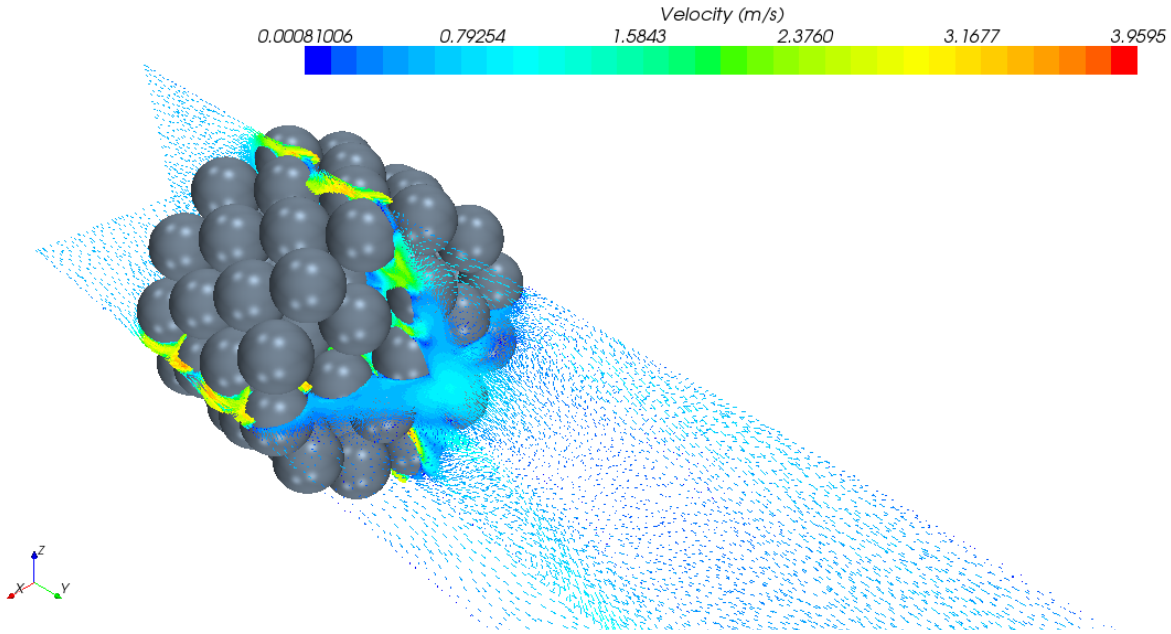

Figure 5-17. Velocity distribution at α = 4.93.

5.4 Conclusion

The CFD simulations and validation chapter summarised, described and validated the results obtained using the CFD method discussed in Chapter 3.

The study initially validated various methods of contact treatment and meshing. Six cases were performed, each with a different mesher and contact treatment. It was found that when performing the test at a particle Reynolds number of 1500 (Turbulent) the meshing models tested showed very little variation in pressure drop results. The contact treatment where spheres were decreased to 99% of their size produced the best quality meshes. However, variation in pressure drop was observed because the porosity of the model was changed. It was therefore concluded that the combination of 100% sphere size and the thin mesher was best suited to low aspect ratio packed beds, considering pressure drop was the primary result to be used from the simulations.

The study then went on to perform simulations on three of the low aspect packings generated using the DEM functionality of STAR-CCM+®. Specific aspect ratios were chosen where channels were formed at various sections of the packings. The bed length was also reduced for the largest of the aspect ratios to account for the exponential increase in cells generated during meshing. The short packing structure was studied with regard to pressure drop and it's applicability to the Reichelt's approach to account for walls in packed columns defined by Eisfeld and Schnitzlein (2001:4321). It was found that at a particle Reynolds number of 1500 the pressure drop deviated from the Eisfeld and Schnitzlein (2001:4321) correlation. A similar decrease in pressure drop was noted by Reddy and Joshi (2008:444) who observed a decrease in the pressure drop due to the channeling near the wall. Additional studies can be performed in the future to determine the relation between packing height and Reynolds number for low aspect ratio beds.

The flow distribution was modelled for three different aspect ratios. Laminar, transitional and turbulent flow regimes were compared with results from the literature concerning porosity and pressure drop. The results agreed with the Eisfeld and Schnitzlein (2001:4321) correlation when valid ranges were considered. Velocity distribution within the packed beds was also investigated. Each of the unique channels caused an increase in velocity in the specific regions.

The results obtained were accurate and provided insight into flow distribution through low aspect ratio packed beds. The method followed to simulate the flow distribution proved to be valid.

STAR-CCM+® provided a stable platform in which any column-to-sphere diameter ratio packing could be modelled with relative ease.

The study highlighted that when considering pressure drop through a packed column the meshing models tend to give similar results. Future recommendations would be to include heat transfer in the simulations and validate the applicability of the thin mesher defined with 2 prism layers.

As increased computing resources become more affordable the number of spheres to be meshed can be increased and the pressure drop over longer lengths can be simulated. The wall and bottoming effect can be taken into account and their effect on the pressure drop investigated. The CFD study showed that the current meshing techniques in STAR-CCM+® allow meshing of contact points and accurately predict velocity distribution and pressure drop through packed columns.

6 Conclusion

6.1 Study Conclusion

This study was aimed at performing the numerical analysis of the flow distribution within low aspect ratio packed columns using an explicit approach. The analysis investigated the ability of STAR-CCM+® to perform both the DEM and CFD simulations in a single platform. Validation of the bed packing was done by comparing the DEM generated beds with experimental data acquired in previous studies at the North-West University (NWU) and porosity variation correlations found in literature. Validation of the pressure drop was done by comparing the simulated pressure drop to correlations found in the literature.

The study firstly established from literature the applicability of DEM and CFD in terms of low aspect ratio packed columns and provided a description of previous research. The initial stages of the survey focused on the general analysis of low aspect ratio packed beds. The study found that multiple authors had investigated low aspect ratio packed beds. It was found that DEM allowed authors to generate mechanically stable randomly packed 3D beds and with the increase in computational power in recent years it was possible to effectively use DEM and CFD codes.

Influential factors at low aspect ratios were then investigated, the factors were: packing, DEM, porosity, CFD, and flow distribution. The critical aspects of each factor was highlighted in the literature survey. It was found that multiple reproducible packing arrangements were possible at low aspect ratios. It was also noted that within specific ranges the reproducibility of packing arrangements was lost. The DEM research confirmed that DEM is an appropriate tool for simulation of packed bed arrangements. The CFD literature study showed that flow distribution over low aspect ratio packings were well researched. The pressure drop study found that the most suitable pressure drop correlation was the correlation derived by Eisfeld and Schnitzlein (2001:4321) with the adapted parameters for friction coefficient of Reichelt's correlation. The velocity distribution literature survey found that an increase in porosity at the wall region distorts the velocity distribution causing higher velocities at the near-wall regions (flow-channelling).

The literature survey therefore provided a a fundamental understanding of previous research and highlighted the most influential factors in the analysis of packed beds. The study then went on to establish a method to simulate both DEM and CFD in STAR-CCM+®

The method chapter defined a methodology to accurately simulate sphere packing in a column using STAR-CCM+® and validate the results using experimental and correlated data. Similarly a methodology to accurately simulate flow distribution and pressure drop using STAR-CCM+® and validation of the results using correlated data was discussed. It was found that in addition to the experimental data obtained by Roslee (2009), the empirically derived formula by Cheng (2011:261) which describes the relationship between $\bar{\varepsilon}$ and the beds aspect ratio (D/d_p) was applicable to validate the packing.

The general setup and steps required to ensure accurate simulation of pressure drop through packed spherical particles in a column using CFD simulation in STAR-CCM+® was discussed and a methodology determined. The CAD model boundaries, mesh generation, contact treatment, mesh independency and turbulence models were discussed. The Realizable k - ε was found to be the most suitable of the RANS turbulence models. The pressure drop correlation derived by Eisfeld and Schnitzlein (2001:4321) with the adapted parameters for friction coefficient of Reichelt's correlation was used to validate the flow distribution.

The method chapter therefore provided methodology to set up and validate packing and flow distribution simulations in STAR-CCM+®. The study then progressed to establish a method to simulate both packing and flow distribution in STAR-CCM+®.

The packing simulations were performed for eight packed column aspect ratios. The results showed that for the first four aspect ratio packings (α = 1.39, 1.4, 1.55 and 2.33) a reproducible packing structure was formed. The DEM simulations and the experimental data with regard to axial variation in porosity showed similar variation and slight deviations which could be accounted for as measuring errors during the experimental data extraction. The DEM results for the first four simulations were therefore considered accurate. The larger aspect ratios (α = 2.65, 2.96, 4.42 and 4.93) produced random packing structures and the axial porosity variation showed a similar trends when comparing the DEM axial porosity variation results to the axial porosity variation found in the experimental data. The joint effect of the bottom and confining wall was observed at these aspect ratios. The DEM results for the last four simulations were therefore also considered accurate.

The overall porosity variations were compared with the results from the studies performed by Theuerkauf *et al*. (2006:98) and correlations by Dixon (1988:707) and Cheng (2011:261). The DEM results achieved by the authors showed similar variation in porosity at various aspect ratios. A similar trend was seen when the global porosity found in the DEM simulations were compared to the experimental results and global porosity derived from correlations.

The use of the discrete element method (DEM) to determine sphere positions for calculation of axial porosity distribution and overall porosity produced results which strongly correlated with experimental data and algorithms developed by Dixon (1988:707) and Cheng (2011:261). DEM could therefore be considered a fast and reliable tool to producing 3D structures of the packed beds for CFD simulations and other purposes.

The CFD simulations and validation chapter summarised, described and validated the results obtained using the CFD setup and validation discussed in the method chapter. The study initially validated various methods of contact treatment and meshing. Six cases were performed, each with a different mesher and contact treatment. It was found that when performing the test at a particle Reynolds number of 1500 (Turbulent) the meshing models tested showed very little variation in pressure drop results. The contact treatment where spheres were decreased to 99% of their size produced the best quality meshes. However, variation in pressure drop was observed because the porosity of the model was changed. It was therefore concluded that the combination of 100% sphere size and the thin mesher was best suited to low aspect ratio packed beds, considering pressure drop was the primary result to be used from the simulations.

The study then went on to perform simulations on three of the low aspect packings generated using the DEM functionality of STAR-CCM+®. Specific aspect ratios were chosen where channels formed at various sections of the packings. The bed length was also reduced for the largest of the aspect ratio to account for the exponential increase in cells generated during meshing. The short packing structures were validated with regard to pressure drop and their applicability to Reichelt's approach to account for walls in packed columns defined by Eisfeld and Schnitzlein (2001:4321). The Flow distribution was modelled for three different aspect ratios. Laminar, transitional and turbulent flow regimes were compared with results from the literature concerning porosity and pressure drop. The results agreed with the Eisfeld and Schnitzlein (2001:4321) correlation when valid ranges were considered. Velocity distribution within the packed beds was also investigated. Each of the unique channels caused an increase in velocity in the specific regions.

The results obtained were accurate and provided insight into flow distribution through low aspect ratio packed beds. The method followed to simulate the flow distribution proved to be correct. STAR-CCM+® provided a stable platform in which any column-to-sphere diameter ratio packing could be modelled with relative ease.

The combination of DEM to pack the columns and CFD to model the flow distribution proved to be an efficient and accurate method to model the flow distribution and associated phenomena through packed columns when considering an explicit approach. A methodology to simulate both packing and flow distribution in STAR-CCM+® was defined. The study can therefore conclude that STAR-CCM+® is an acceptable, accurate and reliable tool to simulate flow distribution within packed columns for uncomplicated explicit methods.

6.2 Recommendations for Future Work

The study highlighted that when considering pressure drop through a packed column the meshing models tend to give similar results. Future recommendations would be to include heat transfer in the simulations and validate the applicability of the thin mesher defined with 2 prism layers.

As increased computing resources become more affordable the number of spheres to be meshed can be increased and the pressure drop over longer lengths can be simulated. The wall and bottoming effect can taken into account and their effect on the pressure drop investigated. The CFD study showed that the current meshing techniques in STAR-CCM+® allow meshing of contact points and accurately predict velocity distribution and pressure drop through packed columns.

It was found that at a particle reynolds number of 1500 the pressure drop deviated from the Eisfeld and Schnitzlein (2001:4321) correlation for a packing at $\alpha = 4.93$. A similar decrease in pressure drop was noted by Reddy and Joshi (2008:444) who observed a decrease in the pressure drop due to the channeling near the wall. Additional studies can be performed in the future to determine the relation between packing height and Reynolds number for low aspect ratio beds.

Additional recommendations for future work would include the following:

- Experimental setup to further validate results found in CFD simulation at ranges not valid in the pressure drop correlation developed by Eisfeld and Schnitzlein (2001:4321).
- Modelling of heat transfer between the spheres and the gas.

- Perform an extensive mesh dependence study over multiple particle Reynolds numbers in the laminar, transition and turbulent ranges which include:
    - An extensive study on the velocity distribution found in channels at low aspect ratio, and their effect on heat transfer between the spheres and particles.
    - A detailed simulation of velocity distribution over laminar, transition and turbulent regions.
- Validate meshing methods used by other CFD software.
- Verification of STAR-CCM+® DEM model for single and multiple contact situations.

Bibliography

ATMAKIDIS, T. & KENIG, E.Y. 2009. CFD-based analysis of the wall effect on pressure drop in beds with moderate tube/particle diameter ratios in the laminar flow regime. *Chemical engineering journal*, 155:404-410.

AUGIER, F., IDOUX, F. & DELENNE, J.Y. 2010. Numerical simulations of transfer and transport properties inside packed beds of spherical particles. *Chemical engineering science,* 65:1055-1064.

BENENATI, R.F. & BROSILOW, C.R., 1962. Void fraction distribution in beds of spheres, *AIChE journal*, 8(3):359-361.

CALIS, H.P.A., NIJENHUIS, J., PAIKERT, B.C., DAUTZENBERG, F.M. & VAN DEN BLEEK, C.M. 2001. CFD modelling and experimental validation of pressure drop and flow profile in a novel structured catalytic reactor packing. *Chemical engineering science*, 56(4):1713-1720, Feb.

CARMAN, P.C. 1973. Fluid flow through granular beds. *Transactions of the institution of chemical engineers.* (London), 27:150-166.

CAULKIN, R., FAIRWEATHER, M., JIA, X., GOPINATHAN, N. & WILLIAMS, R.A. 2006. An investigation of packed columns using a digital packing algorithm. *Computers and chemical engineering,* 30:1178-1188.

CD-ADAPCO. 2010. User's Manual to STAR-CCM+® Version 6.04.014, New York, US.

CHENG, N. 2011. Wall effect on pressure drop in packed beds. *Powder technology*, 210:261-266.

CHENG, Z. & YUAN, W. 1997. Estimating radial velocity of fixed beds with low tube-to-particle diameter ratios. *AIChE journal*, 43(5):1319-1324.

CUNDALL, P.A. & STRACK, O.D.L. 1979. A discrete numerical model for granular assemblies. *Geotechnique*, 29:47-65.

DE KLERK, A. 2003. Voidage variation in packed beds at small column to particle diameter ratio, *AIChE journal*, 49(8):2022-2029.

DE RENZO, A. & DI MAIO, F.P. 2004. Comparison of contact-force models for the simulation of collisions in DEM-based granular flow codes. *Chemical engineering science*. 59:525-54.

DI FELICE, R. & GIBILARO, L.G. 2004. Wall effects for the pressure drop in fixed beds. *Chemical engineering science*, 59:3037-3040.

DIXON, A.G. 1988. Correlations for wall and particle shape effects on fixed bed bulk voidage. *Chemical engineering journal*, 66:705–708.

DIXON, A.G. & NIJEMEISLAND, M. 2001. CFD as a design tool for fixed bed reactors. *Industrial and engineering chemistry research*, 40:5246-5254.

DIXON, A.G., TASKIN, E.M., NIJEMEISLAND, M. & STITT, E.H. 2011. Systematic mesh development for 3D CFD simulation of fixed beds: Single sphere study, *Computers and chemical engineering*, 35:1171–1185.

DREIßIGACKER, V., MULLER-STEINHAGEN, H. & ZUNFT, S. 2010. Thermo-mechanical analysis of packed beds for large-scale storage of high temperature heat, *Heat mass transfer*, 46:1199–1207.

DU TOIT, C.G. 2008. Radial variation in porosity in annular packed beds. *Nuclear engineering and design*, 238:3073-3079.

EISFELD, B. & SCHNITZLEIN, K. 2001. The influence of confining walls on the pressure drop in packed beds. *Chemical engineering science*, 56:4321-4329.

EPPINGER, T., SEIDLER, K. & KRAUME, M. 2011. DEM-CFD simulations of fixed bed reactors with small tube to particle diameter ratios. *Chemical engineering journal*, 166:324–331.

ERGUN, S. 1952. Fluid flow through packed columns. *Chemical engineering progress*, 48(2):89-94.

FREUND, H., ZEISER, T., HUBER, F., KLEMM, E., BRENNER, G., DURST, F. & EMIG, G. 2003. Numerical simulations of single phase reacting flows in randomly packed fixed bed reactors and experimental validation. *Chemical engineering science*, 58:903-910.

GOODLING, J.S., VACHON, R.I., STELPFLUG, W.S. & YING, S.J. 1983. Radial porosity distribution in cylindrical beds packed with spheres. *Powder technology*, 35:23-29.

GOVINDARAO, V.M.H., RAMRAO, K.V.S. & RAO, A.V.S. 1992. Structural characteristics of packed beds at low aspect ratio. *Chemical engineering science*. 47(8):2105-2109.

GRANTON, L.C & FRASER, H.J. 1935. Systematic Packing of Spheres: With Particular Relation to Porosity and Permeability. *Journal of geology.* 43:785-909.

GRAY, W.A. 1968. The packing of solid particles, Chapman and Hall, London, 43 p.

GUARDO, A., COUSSIRAT, M., LARRAYOZ, M.A., RECASENS, F. & EGUSQUIZA, E. 2005. Influence of the turbulence model in CFD modelling of wall-to-fluid heat transfer in packed beds. *Chemical engineering science*, 60(6):1733-1742.

GUO, X. & DAI, R. 2010. Numerical simulation of flow and heat transfer in a random packed bed. *Particuology,* 8:293–299.

JAFARI, A., ZAMANHKHAN, P., MOUSAVI, S.M. & PIETARINEN, K. 2008. Modelling and CFD simulation of flow behavior and dispersivity through randomly packed bed reactors. *Chemical engineering journal*, 144:467-482.

JOHNSON, K.L. 1985. Contact Mechanics, Cambridge University Press, Cambridge, 80 p.

KODAM, M., BHARADWAJ, R.,CURTIS, J., HANCOCK, B. & WASSGREN, C. 2010. Cylindrical object contact detection for use in discrete element method simulations. Part I – Contact detection algorithms. *Chemical engineering science*, 65:5852–5862.

KOZICKI, J. & DONZE', F.V. 2009. YADE-OPEN DEM: an opensource software using a discrete element method to simulate granular material. *International journal for computer-aided engineering and software*, 26(7):786-805.

LEE, J., PARK, G., KIM, K. & LEE, W. 2007. Numerical treatment of pebble contact in the flow and heat transfer analysis of a pebble bed reactor core. *Nuclear engineering and design*, 237(22):2183-2196.

LIU, F.L., ZHANG, Z.P. & YU, A.B. 1999. Dynamic simulation of the centripetal packing of mono-sized spheres. *Physica A*, 268:433-453.

LOGTENBERG, S.A., NIJEMEISLAND, M. & DIXON, A.G. 1999. Computational fluid dynamics simulations of fluid flow and heat transfer at the wall-particle contact points in a fixed bed reactor. *Chemical engineering science*, 54(13-14):7-21.

MCLAUGHLIN, B., STAINSBY, R., DENNIER, A., MACINTOSH, S., WORSLEY, M., GRIEF, A. & VAN HEERDEN, E. 2008. Development of local heat transfer and pressure drop models for pebble bed high temperature gas-cooled reactor cores. (*In* Proceedings HTR2008: 4th International Topical Meeting on High Temperature Reactor Technology, Sept. 28 – Oct. 1, 2008. Washington DC, USA.)

MUELLER, G.E., 1992. Radial void fraction distribution in randomly packed fixed beds of uniformly sized spheres in cylindrical containers. *Powder Technology*, 72:69-275.

MUELLER, G.E. 1997. Numerical simulation of packed beds with monosized spheres in cylindrical containers. *Powder technology*, 92:179-183.

NIJEMEISLAND, M. & DIXON, A.G. 2001. Comparison of CFD simulation to experiment for convective heat transfer in a gas-solid fixed bed. *Chemical engineering science*, 84(1-3):231-246.

PRELLER, A. 2011. Verbal communication with the author. Potchefstroom. (Notes in possession of the author.)

REDDY, R.K. & JOSHI, J.B. 2008. CFD modeling of pressure drop and drag coefficient in fixed and expanded beds. *Chemical engineering research and design*, 86:444–453.

REDDY, R.K. & JOSHI, J.B. 2010. CFD modeling of pressure drop and drag coefficient in fixed beds: Wall effects. *Particuology,* 8(1):37-43.

REICHELT, W. 1972. Zur Berechung des Druckverlustes einphasig durchströmter Kugel - und Zylinderschüttungen. *Chemie Ingenieur Technik,* 44(18):1068-1071.

REYNEKE, H.J. 2009. Investigation into the velocity distribution through an annular packed bed. Potchefstroom: NWU. (Dissertation - M.Eng.)

ROBLEE, L.H.S., BAIRD, R.M. & TIERN, J.W. 1958. Radial porosity variations in packed beds. *AIChE journal*, 4:460–464.

ROMKES, S.J.P., DAUTZENBERG, F.M., VAN DEN BLEEK, C.M. & CALIS, H.P.A. 2003. CFD modelling and experimental validation of particle-to-fluid mass and heat transfer in a packed bed at very low channel to particle diameter ratio. *Chemical engineering journal*, 96:3-13.

ROSLEE, A. 2009. Analysis of the Variation in the Porosity of Packed Columns. Potchefstroom: NWU. (4^{th} year project.)

THEUERKAUF, J., WITT, P. & SCHWESIG, D. 2006. Analysis of particle porosity distribution in fixed beds using the discrete element method. *Powder technology*, 165:92-99.

VAN ANTWERPEN, W., DU TOIT, C.G. & ROUSSEAU, P.G. 2010. A review of correlations to model the packing structure and effective thermal conductivity in packed beds of mono-sized spherical particles. *Nuclear engineering and design*, 240(7):1803-1818.

VAN DER WALT, 2006. Pressure drop through a packed bed. Potchefstroom: NWU. (Dissertation - M.Eng.)

VERSTEEG, H.K. & MALALASEKERA, W. 1995. An introduction to computational fluid dynamics, the finite volume method. Addison Wesley: Harlow. 211 p.

VORTMEYER, D. & SCHUSTER, J. 1983. Evaluation of steady flow profiles in rectangular and circular beds by a variation method. *Chemical engineering science*, 38(10):1691-1699.

WANG-KEE IN, W.J. & HASSAN, Y.A. 2008. CFD simulation of a coolant flow and heat transfer in a pebble bed reactor. (*In* Proceedings HTR2008: 4th International Topical Meeting on High Temperature Reactor Technology, Sept. 28 – Oct. 1, 2008. Washington DC, USA.)

WHITE, S.M. & TIEN, C.L. 1987. Analysis of flow channelling near the wall in packed beds. *Wärme- und stoffübertragung, springer-verlag,* 21:291-296.

WINTERBERG, M. & TSOTSAS, E. 2000. Impact of tube-to-particle-diameter ratio on pressure drop in packed beds. *AIChE journal*, 46(5):1084-1088.

ZEISER, T., LAMMERS, P., KLEMM, E., LI, W., BERNSDORF, J. & BRENNER, G. 2001. CFD-calculation of flow, dispersion and reaction in a catalyst filled tube by the lattice Boltzmann method. *Chemical engineering science*, 56(4):1697-1704.

ZHO, R.P. & YU, A.D. 1995. The packing of spheres in a cylindrical container: the thickness effect. *Chemical engineering science*, 50(9):1504-1507.

ZHU, H.P., ZHOU, Z.Y., YANG, R.Y. & YU, A.B. 2007. Discrete particle simulation of particulate systems: theoretical developments. *Chemical engineering science*, 62:3378-3396.